Non-equilibrium dynamics in quantum and classical many-body spin systems: strong zero modes and large deviations

Loredana Mihaela Vasiloiu

Thesis submitted to The University of Nottingham
for the degree of Doctor of Philosophy

June, 2020

Abstract

The work presented in this thesis is divided into two main parts: strong zero modes in quantum spin chains with open boundaries and large deviations in classical spin systems. The results concerning the strong zero modes are presented in chapters 2 and 3, while chapter 4 contains the results about large deviations in systems of many, but independent, classical degrees of freedom. These two distinct classes of problems in spin chains are both about aspects of slow relaxation to equilibrium in many-body systems.

Nowadays slow dynamics and non-ergodicity in many-body quantum systems are receiving much attention due to their notable technological potential for storing and processing, for very long times, the quantum information encoded in boundary degrees of freedom. In the first part of the work presented in this thesis we mainly focus on quantum spin chains with open boundaries, which can display coherence times for edge spins, that diverge with the system size, as a consequence of the emergence, in the thermodynamic limit, of conserved local quantities, called strong zero modes. First, we discuss the fate of these coherence times when dynamics becomes dissipative. Understanding the behavior of these long correlation times in open quantum systems, undergoing Markovian (memoryless) dynamics, would allow for the possibility of exploiting the protected information encoded in the boundary spins for applications in quantum devices in realistic non-equilibrium settings. Second, we study one possible simple generalization of the transverse field Ising model to a class of ladder spin systems with plaquette interactions in the presence of a transverse field. Also for these systems one can explicitly construct the strong zero mode operators and understand the behavior of the consequential long coherence times for the edge degrees of freedom under isolated (unitary) dynamics. This is possible because the models we consider, while appearing complex superficially, can be brought to simple forms by exploiting an extensive number of conserved quantities they possess.

The results presented in chapters 2 and 3 are closely related, even if they focus on different models and investigate different aspects of their dynamics. Nevertheless, the underlying concept they are based on is the same one, that is, an eigenstate phase transition for the strong zero modes that has interesting consequences for the full energy spectrum.

In the second part of the thesis we focus on a different type of phase transitions. Here we address the issue of dynamical large deviation phase transitions from a disordered phase to an ordered one, in classical systems which consist in a collection of independent Ising spins evolving stochastically. Surprisingly, by reweighing trajectories accordingly to a certain type of time-integrated observable, even a system of independently evolving spins

can display some critical behavior, at the fluctuation level, in trajectory space in the large size and long time limit. By making use of the tilted generator techniques we study the statistics of two particular time-integrated observables. Their associated tilted generators have an exact Kramers-Wannier duality and they look like, up to a sign and an additive constant, some specific well known quantum Hamiltonians. In this sense, the dynamical large deviation phase transitions we observe in these classical stochastic systems translate in ground state quantum phase transitions taking place at the self dual point of the tilted generators we study.

Acknowledgements

I would like to thank my supervisor Prof. Juan P. Garrahan for giving me the great opportunity to start a PhD in condensed matter theory given my previous little background knowledge in this field and for his support throughout my entire PhD. During the years we have collaborated, I have learnt about many different topics and how to approach research projects. I also want to thank him for giving me the opportunity to work and collaborate also with other excellent scientists because this has represented for me a good chance for learning to effectively collaborate in a research team.

I would also like to thank one of my dearest collaborators, my friend Dr. Federico Carollo. I thank him for the many many hours of explanations and discussions about our research projects. I am extremely grateful for his huge support and his immense patience. His extraordinary always polite attitude made me feel safe in facing one of my biggest fears, that is, asking questions and this speeded up my learning process.

I am very grateful also to Dr. Matteo Marcuzzi and Dr. Tom Oakes for their very precious help, support, availability and their life and work advice. I would like to thank also Prof. Roberto Tateo and Dr. Andrea Cavaglià for their important support. I want to thank also my colleagues for all the serious and fun conversations we shared over the years: Neil, Chris, Gary, Jamie, Maike, Jemma, Filippo, Stefano, Kasia, Carlos and Ciarán.

I want to mention my close and old friends for always supporting me: Bruna, Arianna, Martina, Pier, Luca, Valeria, Gaia and Davide. I had the luck to make new friends during this path. I thank Eliana for all our discussions and all the amazing and special moments we shared at work but also outside work and when bouldering together. Many thanks to Caroline and Pete for bouldering with me and for their very useful climbing and life advice. I want to thank also Elisabetta, Lara and Yoran.

Everything during this path would have been more difficult and complicated without the support of my partner Tommaso. I am incredibly grateful for his patience and for listening to me talking for hours about my work even while living thousands of kilometres far apart from each other and for letting me test my talks on him. Many thanks to my family and Tommaso's family. Last but not least, I am extremely grateful to my bassethound Iubi. Thanks to her stubbornness I have been forced to take many walks that revealed to be relaxing and healthy and to learn that life has also other priorities other than physics, that are, according to her, she. Thanks to her always relaxed, happy and carefree personality and to her love I have learnt to reweigh life and doctoral problems.

Contents

Introduction **6**

1 Background material **8**
1.1 Transverse Field Ising Model (TFIM) 8
1.1.1 Exact spectrum of TFIM with periodic boundary conditions 10
1.1.2 Duality in the TFIM 13
1.2 Lindbladians and open quantum systems 14
1.3 Large deviations in classical problems 17
1.3.1 An example of large deviation results 18
1.3.2 Large deviation theory as mathematical language of equilibrium statistical mechanics 20
1.3.3 Stochastic Dynamics and Large Deviations 21

2 Enhancing correlation times for edge spins through dissipation **25**
2.1 Introduction 25
2.2 Strong zero modes in the TFIM 28
2.3 Weak bond in the ring geometry for the TFIM 29
2.4 Dissipative dynamics in the open chain TFIM and enhancement of correlation times 30
2.5 Dissipative strong zero maps 35
2.6 Strong Zero Map in an interacting system 36
2.7 Discussion 37

3 Strong zero modes in a class of generalised Ising spin ladders with plaquette interactions **38**
3.1 Introduction 38
3.2 M-leg spin-1/2 ladder 40
3.3 Strong zero modes in M-leg ladders 41
3.3.1 Pairing due to the SZM 43
3.3.2 Derivation of the SZM for the ladder system 44
3.4 Norm of Ψ and relation to phase transitions 46
3.5 Quasi-random Ising chains from the ladder model 47
3.5.1 Block decomposition of the ladder Hamiltonian for M odd 49

3.5.2 Block decomposition of the ladder Hamiltonian for M even 50
3.6 Long coherence times of boundary spins 51
3.7 Discussion 57

4 Trajectory phase transitions in non-interacting spin systems 58
4.1 Introduction 58
4.2 Model and Observables 60
4.3 Duality of the Quantum Triangular Plaquette Model 64
4.4 Large deviations of the bond order parameter 67
4.5 Large deviations of the triangular plaquette order parameter 68
4.5.1 Sampling LDs with transition path sampling 68
4.5.2 Improvement to TPS trajectory proposal and acceptance 70
4.5.3 Trajectory umbrella sampling and choice of alternative dynamics . . 71
4.5.4 First order transition in triangular plaquette order 72
4.6 Discussion 73

Conclusions 75

Appendix A Markovian quantum master equation 77

Appendix B Examples for the Clebsch−Gordan decomposition series 82

Appendix C Probability for the random transverse field 83

Appendix D Mapping from 1d TFIM to 2D classical Ising model 84

Bibliography 87

Introduction

In this thesis we focus on the theoretical investigation into novel aspects of nonequilibrium dynamics in classical and quantum many-body spin systems. A central problem addressed by this work, of current fundamental and practical relevance, is that of relaxation to stationarity. Combining approaches from statistical and condensed matter physics we investigate, in the first part of this thesis, the breaking of ergodicity and some of its witness measures, such as strong zero modes, in the dynamics of closed and open quantum systems; this establishes connections to the nonequilibrium dynamics of highly excited states. In the second part of the thesis we focus on the statistical mechanics approach, adapted and based on dynamical large deviation methods, for studies of trajectory ensembles. Among its many applications, in particular this approach allows to investigate the existence of dynamical phase transitions in nonequilibrium processes.

The first chapter of this thesis is a general introduction to the main topics explored throughout the thesis such as the transverse field Ising model, Lindblad formulation for open quantum systems and large deviation theory.

In the second chapter we present novel results concerning the fate of coherence times for edge spins of many-body quantum systems in the presence of dissipation and we show how, in principle, the latter can enhance characteristic correlation times beyond those of purely unitary cases. Long coherence times, or long relaxation time-scales, can arise in several different scenarios, for instance many-body localisation, prethermalisation or metastability, but in this thesis we will study many-body quantum spin chains with open boundaries which can display coherence times for edge spins that diverge exponentially with system size. These long times arise as a consequence of the presence of almost conserved operators, the so-called strong zero modes. Thus, this phenomenon provides a useful platform for storing and protecting the information encoded in the many-body quantum states for very long times with possible applications in future quantum technologies. However, in actual applications, these effects, so far only established in isolated unitary systems, must face the presence of thermal environments affecting the many-body quantum time-evolution; while in general these induce decoherence and loss of information, we show that particularly simple environments can actually increase the edge spin correlation times by orders of magnitude as compared to the unitary case. Our research is mainly focused on the transverse field Ising model but we show how our findings are expected to apply also to interacting spin chains and we further generalize the notion of strong zero modes to the case of Markovian dissipative quantum dynamics.

In the third chapter we present novel exact results about the observation of long coherence times for edge spins in a class of spin-1/2 ladder models with plaquette interactions, which generalize the transverse field quantum Ising model to a quasi two-dimensional model. Also for this class of models the long coherence times appear as a direct consequence of the existence of a strong zero mode, i.e. an operator which commutes with the Hamiltonian up to exponentially small corrections in the size of the system. We explicitly construct this operator for the quantum ladder models in terms of almost Majorana fermionic operators. However, it is also possible to exploit an extensive set of symmetries to break up the complex ladder Hamiltonian into the direct sum of several, more tractable, Ising models with quasi-random transverse field. The realization of the transverse field profile is determined, in each of the symmetry sector, by the choice of the values of the conserved quantum numbers. On one hand, this mapping is of interest as it provides a further example in which quasi-randomness can emerge in clean quantum models from the presence of an extensive number of conserved quantities. On the other, it can actually be used to properly understand the behavior of the infinite temperature autocorrelator, measuring the coherence times of the edge spins in the infinite temperature state, for the original disorder-free ladder model. Like in other models, long edge-spin coherence times are to be expected in the parameter regime where the full ladder model exhibits a strong zero mode; surprisingly, however, it can also happen that, even if the full ladder does not support a strong zero mode, many symmetry sectors of the Hamiltonian do and therefore long correlation times can still be displayed.

In the fourth chapter we present counterintuitive results about rare emergent collective behavior in non-interacting spin systems. We show indeed how it is possible to observe surprisingly large fluctuations towards ordered behavior in a system of many independent degrees of freedom evolving stochastically. To formalize this statement, we make use of large deviation theory where these large fluctuations present themselves in the form of dynamical phase transitions. Specifically, we consider a set of non-interacting spins undergoing single spin-flip dynamics at infinite temperature. We study in detail two examples of time-integrated plaquette observables. To unravel their statistics, we make use of tilted generator techniques. For our observables, these generators have an exact and explicit Kramers-Wannier (spin-plaquette) duality. We use this duality to locate the critical point at which the dynamical phase transitions occur. In the first case, the plaquette operator measures the degree of ordering between consecutive spins and is thus introducing a virtual one-dimensional geometry. The corresponding dynamical order parameter presents Ising critical behavior. In the second case, the plaquette observable considers spins as if they were arranged in a two-dimensional triangular lattice. In this case, the corresponding dynamical order parameter undergoes a discontinuous (first-order) transition; we provide numerical evidence for this by implementing an efficient trajectory sampling scheme which exploits the non-interacting nature of the spin dynamics. These results shed light on new aspects of dynamical transitions in trajectory ensembles. In particular, they go beyond the conventional paradigm of observing these phase transitions only in interacting many-body dynamics.

Chapter 1

Background material

This introductory chapter presents the main topics on which is based the research work addressed in this thesis and is organised in the following way: in the first part we describe the transverse field Ising chain since this model, and its properties, are recurrent throughout all the problems presented in this thesis; in the second part, we describe the Lindblad formulation for open quantum systems that is used in chapter 2, and in the third part, we present a simple and short introduction to the large deviation formalism used in chapter 4.

1.1 Transverse Field Ising Model (TFIM)

In this section we describe the transverse field Ising model and its most important features since we will study this model from several perspectives and we will make use of its properties across all chapters of this thesis.

The one-dimensional transverse field Ising model [1, 2] of size L with open boundary conditions is described by the quantum mechanical Hamiltonian

$$H_{\text{TFIM}} = -J \sum_{i=1}^{L-1} \sigma_i^z \sigma_{i+1}^z - h \sum_{i=1}^{L} \sigma_i^x \,, \tag{1.1}$$

where σ_i^β, with $\beta = x, y, z$, are the Pauli matrices acting at site i, the coupling constant J describes the magnetic interaction between consecutive spins and h is the transverse magnetic field acting in the x direction. Each spin has two possible orientations that are described by an up state $|\uparrow\rangle_i$, indicating the spin has a positive magnetisation, and by a down state $|\downarrow\rangle_i$, indicating a negative local magnetisation. The magnetisation operator for each spin is the Pauli matrix σ_i^z, the up state corresponding to the eigenvalue $+1$, $\sigma_i^z |\uparrow\rangle_i = |\uparrow\rangle_i$, whereas the down state corresponds to the eigenvalue -1, $\sigma_i^z |\downarrow\rangle_i = -|\downarrow\rangle_i$. The 2^L-dimensional Hilbert space is therefore $\mathbb{C}^{2^{\otimes L}}$, where $\mathbb{C}^2$ is the space spanned by the two states $(|\uparrow\rangle_i, |\downarrow\rangle_i)$ on each site i. The Pauli matrices σ_i^β represent the quantum degrees of freedom and act non trivially only on the spin states at site i, that is, $\sigma_i^a = \mathbf{1} \otimes \mathbf{1} \otimes \ldots \otimes \mathbf{1} \otimes \sigma^{\mathbf{a}} \otimes \mathbf{1} \otimes \ldots \otimes \mathbf{1}$ and $\left[\sigma_i^a, \sigma_j^b\right] = 2i\delta_{i,j}\epsilon_{abc}\,\sigma_j^c$.

The transverse field Ising model Hamiltonian (1.1) describes a chain of length L of two-level systems with nearest neighbour interaction in the presence of an external transverse magnetic field h. By definition, quantum phase transitions are identified by the points of nonanalyticity in the ground state energy functions, thus, we are interested in studying the ground state energy of this Hamiltonian as a function of the couplings h and J. The ground state of the transverse field Ising model Hamiltonian depends on the ratio h/J, therefore we can identify two different cases: the regime where $h/J \ll 1$, known as the ferromagnetic or ordered phase, and the quantum paramagnetic phase where $h/J \gg 1$. It is known that for this model the ground state energy has only one critical point at $h = J$ where the Hamiltonian exhibits a second order quantum phase transition at zero temperature $T = 0$ between these two distinct phases.

In the $h/J \gg 1$ phase, the term describing the effects of the transverse field dominates the nearest neighbour interaction term. At $J = 0$, the ground state is the tensor product of the state of each individual spin $|\rightarrow\rangle_i$

$$|0\rangle = \prod_i |\rightarrow\rangle_i \,, \tag{1.2}$$

where

$$\begin{aligned} |\rightarrow\rangle_i &= \frac{|\uparrow\rangle_i + |\downarrow\rangle_i}{\sqrt{2}} \,, \quad \sigma_i^x \,|\rightarrow\rangle_i = +\sigma_i^x \,, \\ |\leftarrow\rangle_i &= \frac{|\uparrow\rangle_i - |\downarrow\rangle_i}{\sqrt{2}} \,, \quad \sigma_i^x \,|\leftarrow\rangle_i = -\sigma_i^x \,, \end{aligned} \tag{1.3}$$

are the two eigenstates of the first Pauli matrix σ_i^x associated with the eigenvalues ± 1. In this limit the ground state is a polarised state, with all spins orientated in the $+x$ direction, known as a quantum paramagnet state. In the case of very small, but not zero, values of the interaction coupling J, most of the spins will point in the $+x$ direction.

In the $h/J \ll 1$ phase, the first term on the right side of equation (1.1) dominates, and in particular, at $h = 0$, the spins have either all positive or all negative magnetization. In this case, the Hamiltonian is diagonal in the basis of the eigenstates of σ_i^z and there are two degenerate ground states

$$|\uparrow\rangle = \prod_i |\uparrow\rangle_i \quad \text{or} \quad |\downarrow\rangle = \prod_i |\downarrow\rangle_i \,, \tag{1.4}$$

where all spins point respectively in the $+z$ or $-z$ direction.

The parity operator defined as

$$P = \prod_i \sigma_i^x \,, \tag{1.5}$$

is the generator of an exact global $\mathbb{Z}_2$ symmetry of the transverse field Ising model Hamiltonian. This symmetry, which in the ordered phase, maps one ground state onto the other, is spontaneously broken as the system will choose only one of the two states (1.4) as its ground state. For very small values of the transverse magnetic field h there will still exist degeneracy of the ground state where in one state most spins, but not all spins, will be

pointing in the $+z$ direction while in the other state most of the spins will point in the $-z$ direction.

For these two opposite limits of the ratio h/J, the properties of the respective ground states are qualitatively different reflecting the fact that the ground state energy can not be everywhere a smooth function of the couplings h and J. Indeed in the following section 1.1.1 we will see that $h = J$ is the critical point of the ground state energy function. For simplicity and without loss of generality, from now on we will mainly focus on the case where $J > 0$, which correspond to a ferromagnetic coupling, rather than on the antiferromagetic exchange characterized by $J < 0$. We will also consider the transverse magnetic field strength to be non-negative, i.e., $h > 0$.

1.1.1 Exact spectrum of TFIM with periodic boundary conditions

In this section we outline the main points of the formalism used to diagonalise the transverse field Ising model Hamiltonian with periodic boundary conditions. The exact spectrum of the Ising chain in a transverse field is obtained by first performing the Jordan-Wigner transformation, that maps spin-1/2 operators in spinless fermions, and by successively performing the Bogoliubov transformation, that maps the Fermi operators, violating the fermion conservation number, into a set of fermionic operators that have a definite fermion number. The Jordan-Wigner transformation is a non-local transformation that depends on the boundary conditions. In this section we will focus on periodic boundary conditions [1–4], that is, we use the identification $\sigma^z_{L+1} = \sigma^z_1$, meaning that we add a term, connecting the first and last spins, to the Hamiltonian of equation (1.1) which now becomes

$$H_{\text{TFIM}} = -J \sum_{i=1}^{L} \sigma_i^z \sigma_{i+1}^z - h \sum_{i=1}^{L} \sigma_i^x \,. \tag{1.6}$$

The exact spectrum of the transverse field Ising model Hamiltonian can be obtained straightforwardly also for open and antiperiodic boundary conditions as shown in [5, 6].

We start from the transverse field Ising model Hamiltonian of equation (1.6) and by performing an unitary canonical transformation, that consists in rotating the spin axes of $\pi/2$ around the y-axis, we change coordinates

$$\sigma_i^x \to -\sigma_i^z, \qquad \sigma_i^z \to \sigma_i^x \,, \tag{1.7}$$

so that we now rewrite the Hamiltonian as

$$H_{\text{TFIM}} = -J \sum_{i=1}^{L} \sigma_i^x \sigma_{i+1}^x + h \sum_{i=1}^{L} \sigma_i^z \,. \tag{1.8}$$

This Hamiltonian can be expressed in terms of raising σ_i^+ and lowering σ_i^- operators defined at each site i as

$$\begin{aligned} \sigma_i^+ &= \frac{1}{2} \left(\sigma_i^x + i\sigma_i^y \right) \,, \\ \sigma_i^- &= \frac{1}{2} \left(\sigma_i^x - i\sigma_i^y \right) \,, \end{aligned} \tag{1.9}$$

with

$$\begin{aligned}\sigma_i^x &= \sigma_i^+ + \sigma_i^- \,, \\ \sigma_i^z &= \sigma_i^+\sigma_i^- - \sigma_i^-\sigma_i^+ \,.\end{aligned} \tag{1.10}$$

These operators are referred to as hard-core bosons as they satisfy fermionic anticommutation relations on the same site

$$\{\sigma_i^\pm, \sigma_i^\pm\} = 0\,, \quad \{\sigma_i^\pm, \sigma_i^\mp\} = 1\,, \tag{1.11}$$

while they satisfy bosonic commutation relations on different sites

$$\left[\sigma_i^\pm, \sigma_j^\pm\right] = 0\,, \quad \left[\sigma_i^\pm, \sigma_j^\mp\right] = 0 \quad \forall i \neq j\,. \tag{1.12}$$

The transverse field Ising model Hamiltonian in terms of the ladder operators reads

$$H_{\mathrm{TFIM}} = -J\sum_{i=1}^{L}\left(\sigma_i^+ + \sigma_i^-\right)\left(\sigma_{i+1}^+ + \sigma_{i+1}^-\right) + 2h\sum_{i=1}^{L}\sigma_i^+\sigma_i^- - hL\,. \tag{1.13}$$

By performing the conventional Jordan-Wigner transformation, that brings spin-1/2 operators into spin-less fermionic operators for many-sites problems,

$$\begin{aligned}c_i &= \prod_{j=1}^{i-1}\exp\left(i\pi\sigma_j^+\sigma_j^-\right)\sigma_i^-, \\ c_i^\dagger &= \prod_{j=1}^{i-1}\exp\left(-i\pi\sigma_j^+\sigma_j^-\right)\sigma_i^+\,,\end{aligned} \tag{1.14}$$

with inverse

$$\begin{aligned}\sigma_i^- &= \exp\left(-i\pi\sum_{j=1}^{i-1}c_j^\dagger c_j\right)c_i, \\ \sigma_i^+ &= \exp\left(i\pi\sum_{j=1}^{i-1}c_j^\dagger c_j\right)c_i^\dagger\,,\end{aligned} \tag{1.15}$$

the Hamiltonian can be rewritten in the form

$$H_{\mathrm{TFIM}} = -J\sum_{i=1}^{L}\left(c_i^\dagger c_{i+1} - c_i c_{i+1}^\dagger + c_i^\dagger c_{i+1}^\dagger - c_i c_{i+1}\right) + 2h\sum_{i=1}^{L}c_i^\dagger c_i - hL\,, \tag{1.16}$$

where c_i and $c_i^\dagger$ are respectively Fermi annihilation and creation operators that now satisfy proper anticommutation relations

$$\{c_i, c_j^\dagger\} = \delta_{i,j}\,, \quad \{c_i, c_j\} = 0\,, \quad \{c_i^\dagger, c_j^\dagger\} = 0\,, \quad \forall i \neq j\,. \tag{1.17}$$

The Hamiltonian of equation (1.16) is quadratic in Jordan-Wigner fermions and therefore it can be diagonalised exactly using standard methods [2–4]. The last term in equation (1.16) is a constant energy shift which we will neglect from now on. We will also neglect the term proportional to $-J(\exp(i\pi\sum_i^L c_i^\dagger c_i)(c_L^\dagger c_1 + c_L^\dagger c_1^\dagger) + \exp(-i\pi\sum_i^L c_i^\dagger c_i)(c_L c_1^\dagger + c_L c_1))$ due to the periodic boundary conditions. This latter correction term can be ignored as it becomes negligible in the thermodynamic limit of infinite size systems.

We introduce the Fourier transformation to the momentum space

$$\begin{aligned} a_k &= \frac{1}{\sqrt{L}}\sum_j c_j\, e^{-ikr_j}\,, \\ a_k^\dagger &= \frac{1}{\sqrt{L}}\sum_j c_j^\dagger\, e^{ikr_j}\,, \end{aligned} \tag{1.18}$$

with inverse

$$\begin{aligned} c_j &= \frac{1}{\sqrt{L}}\sum_k a_k\, e^{ikr_j}\,, \\ c_j^\dagger &= \frac{1}{\sqrt{L}}\sum_j a_k^\dagger\, e^{-ikr_j}\,. \end{aligned} \tag{1.19}$$

Substituting these transformed operators in equation (1.16) we obtain

$$\begin{aligned} H_{\text{TFIM}} &= 2\sum_k -iJ\sin(k)\left[a_k^\dagger a_{-k}^\dagger - a_{-k}a_k\right] + (h - J\cos(k))\left[a_k^\dagger a_k - a_{-k}a_{-k}^\dagger\right] \\ &= 2\sum_k \begin{pmatrix} a_k^\dagger & a_{-k}\end{pmatrix}\begin{pmatrix} h - J\cos(k) & -iJ\sin(k) \\ iJ\sin(k) & -h + J\cos(k)\end{pmatrix}\begin{pmatrix} a_k \\ a_{-k}^\dagger\end{pmatrix}\,, \end{aligned} \tag{1.20}$$

where the wave numbers $k = m\pi/L$, with m an odd number in the interval $0 \le m \le 2L-1$, satisfy the periodic boundary conditions [6].

We now perform the Bogoliubov transformation

$$\begin{pmatrix} a_k \\ a_{-k}^\dagger\end{pmatrix} = \begin{pmatrix} \cos(\phi_k) & i\sin(\phi_k) \\ i\sin(\phi_k) & \cos(\phi_k)\end{pmatrix}\begin{pmatrix} b_k \\ b_{-k}^\dagger\end{pmatrix}\,, \tag{1.21}$$

that maps the pair $(a_k, a_{-k}^\dagger)$ into a new pair of fermionic operators $(b_k, b_{-k}^\dagger)$. This is an unitary transformation where the angle ϕ_k is determined by the relation

$$\tan(2\phi_k) = \frac{\sin k}{h/J - \cos k}\,. \tag{1.22}$$

Using this canonical transformation we can express the transverse field Ising model Hamiltonian (1.20) in terms of the new set of fermionic operator $(b_k, b_{-k}^\dagger)$ and obtain the final form

$$H_{\text{TFIM}} = -J\sum_k \left[\left(1 - \frac{h}{J}\right)^2 + 4\frac{h}{J}\sin^2\left(\frac{k}{2}\right)\right]^{1/2}\left(b_k^\dagger b_k - b_{-k}b_{-k}^\dagger\right)\,, \tag{1.23}$$

where the ground state energy for periodic boundary conditions is

$$E_0(J,h) = -J \sum_{\substack{m=0 \\ m\,\text{odd}}}^{2L-1} \left[\left(1 - \frac{h}{J}\right)^2 + 4\frac{h}{J}\sin^2\left(\frac{m\pi}{2L}\right) \right]^{1/2} . \tag{1.24}$$

In the ground state of the Hamiltonian (1.23) all fermionic states are empty, and in order to create excited states, single-particle states must be occupied. In such a case the gap between the excited states and the ground state is

$$\Delta E = E_k(J,h) - E_0(J,h) = 2J \left[\left(1 - \frac{h}{J}\right)^2 + 4\frac{h}{J}\sin^2\left(\frac{k}{2}\right) \right]^{1/2} , \tag{1.25}$$

with the minimum energy gap, obtained for the first excited state with $k = 0$

$$\Delta E = 2J\,|1 - h/J| \, . \tag{1.26}$$

This energy gap closes at $h = J$ that is the critical point of the one dimensional spin-1/2 transverse field Ising model at which the second order zero temperature quantum phase transition takes place in the limit $L \to \infty$.

1.1.2 Duality in the TFIM

The classical two-dimensional Ising model has a Kramers-Wannier duality [7, 8]; the strong coupling expansion of the partition function on a graph coincides with the weak coupling expansion on the dual graph, that is, any phenomenon taking place at high temperature is transformed into an analogous low temperature phenomenon. Due to the mapping between the two-dimensional classical model and the one dimensional quantum Ising model (see appendix D), it is expected that the existence of this duality symmetry would have consequences also for the transverse field Ising model Hamiltonian. In general duality symmetries are very informative as they help to make estimate of the value of the critical field at which a phase transition might occur thus they help to locate the critical points.

The duality transformation in the quantum case is defined in the following way [2]

$$\begin{aligned} \tau_i^x &= \sigma_i^z \sigma_{i+1}^z \, , \\ \tau_i^z &= \prod_{k=1}^{i} \sigma_k^x \, , \end{aligned} \tag{1.27}$$

where the operators τ_i^β, with $\beta = x, y, z$, are defined on the dual lattice and they satisfy the same algebra as the Pauli operators σ_i^β belonging to the primal lattice

$$(\tau_i^\alpha)^2 = \mathbf{1} \, , \quad \{\tau_i^\alpha, \tau_i^\beta\} = 0 \, , \quad \left[\tau_i^\alpha, \tau_j^\beta\right] = 2i\delta_{i,j}\epsilon_{\alpha\beta\gamma}\,\tau_j^\gamma \, , \quad \forall j \neq i \, . \tag{1.28}$$

This non-local transformation maps sites on the original lattice onto bonds on the dual lattice and sites on the dual lattice into links on the original lattice. The dual lattice is obtained by putting a node at the center of each cell in the original lattice, thus, for this model a dual site is place halfway between two sites on the original lattice.

Using the duality symmetry (1.27) we can rewrite the transverse field Ising model Hamiltonian

$$\begin{aligned} H_{\text{TFIM}}(J,h) &= -J\sum_{i=1}^{L}\sigma_i^z\sigma_{i+1}^z - h\sum_{i=1}^{L}\sigma_i^x \\ &= -J\left(\sum_{i=1}^{L}\tau_i^x - \frac{h}{J}\sum_{i=1}^{L}\tau_i^z\tau_{i+1}^z\right) \\ &= JH_{\text{TFIM}}(h/J,1)\,, \end{aligned} \tag{1.29}$$

implying that the ground state energy of the system satisfies the relation

$$E_0(J,h) = JE_0(h/J,1)\ . \tag{1.30}$$

Similarly to what happens in the classical case, the duality transformation involved in the quantum model relates the ferromagnetic and paramagnetic phases and suggests that the critical point at which the quantum phase transition occurs is the self dual point $J = h$.

1.2 Lindbladians and open quantum systems

In this section we discuss, in a short and schematic manner, the derivation of the Lindblad master equation describing the non-unitary and irreversible evolution of Markovian quantum open systems [9–14]. In physics being able to exhaustively describe the time evolution of systems is of fundamental importance for deciphering their properties. In particular, the study of the dynamics of open quantum systems has a wide range of applications including those in quantum optics, quantum information, chemical physics, condensed matter and statistical physics [11, 14–16].

We consider an isolated multipartite quantum system undergoing unitary dynamics. This closed system is composed by a subsystem, that we are interested in studying and which is described by a time-independent Hamiltonian H_S, and, the rest, identified as the external environment E of the subsystem S and characterized by a Hamiltonian H_E. In general, the subsystem S and the environment E interact with each other, this interaction being described by a Hamiltonian H_{SE}.

The Hilbert space $\mathcal{H}$ of the whole system is the tensor product of the Hilbert spaces of the subsystem $\mathcal{H}_S$ and of the environment $\mathcal{H}_E$

$$\mathcal{H} = \mathcal{H}_S \otimes \mathcal{H}_E\,, \tag{1.31}$$

with dimension equal to the product of the dimensions of $\mathcal{H}_S$ and $\mathcal{H}_E$,

$$\dim\mathcal{H} = \dim\mathcal{H}_S \cdot \dim\mathcal{H}_E\,. \tag{1.32}$$

The whole system undergoes a unitary evolution governed by the total Hamiltonian

$$H_{\text{tot}} = H_S + H_E + H_{SE}\,, \tag{1.33}$$

with equation of motion, known as the Liouville-von Neumann equation, for the global density matrix operator ρ_{tot}

$$\frac{d}{dt}\rho_{\text{tot}} = -i\,[H_{\text{tot}}, \rho_{\text{tot}}]\ , \tag{1.34}$$

where we set the Planck constant $\hbar$ equal to 1.

It is convenient to consider the interaction picture where the time evolution of the operators in the Hilbert space $\mathcal{H}$ is generated only by the system and the environment Hamiltonian $H_S + H_E$ and not by the Hamiltonian of the whole system H_{tot} as it happens in the Heisenberg picture. We are looking for approximate solutions, through a perturbative approach, for the above equation of motion and the interaction picture helps us to better describe the dymanics of the system. In this interaction picture, the corresponding Liouville von-Neumann equation, describing the time evolution of the total density matrix, assumes the form

$$\frac{d}{dt}\rho(t) = -i\,[H(t), \rho(t)]\ , \tag{1.35}$$

where the interaction picture Hamiltonian operator,

$$H(t) = U^\dagger H_{SE} U\,, \tag{1.36}$$

and the interaction picture density matrix operator,

$$\rho(t) = U^\dagger \rho_{\text{tot}} U\,, \tag{1.37}$$

are obtained from their corresponding Schrödinger picture operators, H_{SE} and ρ_{tot}, by means of an unitary trasformation with evolution operator

$$U = e^{-i(H_S + H_E)t}\,. \tag{1.38}$$

Formally integrating both terms of equation (1.35) we obtain

$$\rho(t) = \rho(0) - i\int_0^t [H(s), \rho(s)]\,ds\,. \tag{1.39}$$

Substituting this equivalent integral form in equation (1.35) yields to

$$\frac{d}{dt}\rho(t) = -i\,[H(t), \rho(0)] - \int_0^t \Big[H(t), [H(s), \rho(s)]\Big]\,ds\,. \tag{1.40}$$

At this point we perform a first approximation which is known as the Born approximation. In the setting of this approximation we assume that the system (S) - environment (E) coupling is weak and that the environment is large, so that the environment is only slightly affected by changes taking place in the system. In formulae this translates as

$$\rho(t) \approx \rho_S(t) \otimes \rho_E(0)\,, \tag{1.41}$$

meaning that the density matrix of the total system at time t, $\rho(t)$, can be expressed as the direct product of the density matrix describing the system S at time t, $\rho_S(t)$, with the density matrix of the environment that is really never changing since the latter is always in the equilibrium thermal state that we denote with $\rho_E(0)$. In other words, we assume that the environment state is decoupled from the system state, thus, we have

$$\frac{d}{dt}\rho(t) = -i\left[H(t), \rho_S(0)\otimes\rho_E(0)\right] - \int_0^t \Big[H(t), \left[H(s), \rho_S(s)\otimes\rho_E(0)\right]\Big] ds\,. \tag{1.42}$$

We are interested in studying the time evolution of the open quantum system S and to that end we eliminate the degrees of freedom related to the external environment E by considering the reduced density matrix

$$\rho_S = tr_E \rho\,. \tag{1.43}$$

This reduced density matrix, obtained as the partial trace taken over the environment degrees of freedom, contains the full statistical information one needs for studying and describing observables O belonging to the system S, as the expectation value of these observables is defined as

$$\langle O\rangle = tr_S\left(O\rho_S\right)\,. \tag{1.44}$$

That being said, we perform the partial trace and we get

$$\frac{d}{dt}\rho_S(t) = -\int_0^t tr_E\Big[H(t), \left[H(s), \rho_S(s)\otimes\rho_E(0)\right]\Big] ds\,, \tag{1.45}$$

where we assumed that

$$tr_E\left[H(t), \rho_S(0)\otimes\rho_E(0)\right] = 0\,, \tag{1.46}$$

since H_{SE}, in $H(t) = U^\dagger H_{SE} U$, can be always defined such that equation (1.46) holds.

The continuation of the description of the standard procedure for deriving from equation (1.45) the quantum master equation in Lindblad form can be found in appendix A and it follows that of [9, 14]. Here we briefly outline the next approximations within this approach. The second approximation, in the microscopic derivation of the Lindblad generator starting from the Hamiltonian dynamics, is the Markov approximation. In this approximation it is assumed that characteristic decay times τ_E of correlation functions in the external environment E take place on shorter timescales with respect to the relaxation time of the system τ_S (A.4). As a result of taking this approximation, the evolution of the state of the system does not depend anymore on the initial state. Next, in the rotating wave approximation all the non-secular terms can be neglected ensuring that the Redfield equation, that is, the quantum master equation obtained after taking the Born-Markov approximation, does preserve positivity of the density matrix (A.14). This set of assumptions and approximations eventually leads to the quantum master equation

$$\frac{d}{dt}\rho_S(t) = \mathcal{L}\rho_S(t)\,, \tag{1.47}$$

with Lindblad generator [*cf.* (A.23)]

$$\mathcal{L}\rho_S(t) = -i\,[H, \rho_S(t)] + \sum_\alpha \left(L_\alpha \rho_S(t) L_\alpha^\dagger - \frac{1}{2}\{L_\alpha^\dagger L_\alpha, \rho_S(t)\} \right), \tag{1.48}$$

where the operators L_α are referred to as jump operators and $H = H_S + H_{LS}$ [*cf.* (A.20), (A.23)]. The first term on the right side of the equation describes the coherent part of the evolution, whereas the terms in the sum represent the dissipator of the master equation which encodes the consequences of the existence of a large external environment weakly interacting with the system.

In chapter 2 we assume that the above derivation of the Markovian quantum master equation can be done for the quantum systems we investigate. Thus, we use the structure of the Lindblad generator (1.48) by writing Hamiltonians H and jump operators L_α specific to the systems and to the settings we study [*cf.* (2.1), (2.8), (2.9), (2.17)].

1.3 Large deviations in classical problems

In recent years there has been a growing interest in understanding and controlling dynamical large fluctuations as they play an essential role in characterizing the dynamical behavior of equilibrium and out of equilibrium classical and quantum systems. Such exciting intellectual effort has a lot of applications in many branches of science including topics such as glassy systems, multifractals, chemical reactions, transport phenomena, protein folding, exclusion processes, disordered media, stochastic models of gene expression, chaotic systems, atmospheric and climate models and finance (detailed references can be found in [17–21]).

Large deviation theory deals with the exponential decay of probabilities of observing rare events in stochastic processes in a certain scaling limit. The scaling limit can be that of long observation times over which a stochastic system is studied, a large number of degrees of freedom characterizing the stochastic process under investigation, as well as, a small noise perturbing a system with stochastic dynamics [21, 22].

In this section we discuss a very simple, but yet very explicative, example of large deviation results that will give an immediate intuition of what large deviation theory is about. There are several, but strictly related, different points of view, depending on the mathematical or physical background contexts and applications, of describing what is the theory that studies large deviations [21]. In this thesis we will focus on the physical point of view which argues that large deviation theory is the rigorous mathematical language of statistical mechanics, thus, we will study the large deviation formalism through a statistical mechanics approach where we will investigate ensembles of trajectories of the dynamics in the context of the thermodynamics method developed by Ruelle, Lanford, Ellis and Oono [21, 23, 24].

1.3.1 An example of large deviation results

The basic example of large deviation theory that we consider in this section consists in tossing N coins. These represent N independent and identically distributed random variables following a Bernoulli distribution where, for each of the N coins, we associate the number 1 to heads and the number 0 to tails. When flipping a single coin, the probability to obtain head or tail is $\frac{1}{2}$, with associated variance $\sigma^2 = \frac{1}{4}$, meaning that each coin can take the value 0 or 1 with equal probability. When tossing N coins, we can define a sequence $p = (p_1, p_2, \ldots, p_N)$ where each component p_i, with $i = 1, 2, \ldots, N$, represents a coin and can assume the value 0 or 1.

In particular, we are interested in studying the fraction of 1's enclosed in the sequence p and defined as the sum of the random variables p_i,

$$R_N = \frac{1}{N} \sum_{i=1}^{N} p_i \,, \tag{1.49}$$

in the limit of a large number of coins. The first thing that comes to someone's mind is to apply the law of large numbers and the central limit theorem, and as expected, the result is that, when tossing a large number of coins, on average, half of coins will display their head side and the remaining half will display their tail side.

What we are interested in studying is not this well known behaviour but rather investigating the probability of finding a certain atypical fraction of heads in the vector p, different from the standard fraction $\frac{1}{2}$, as for example, the probability of having a very large or very small fraction of 1's or even the probability of having only 1's in the sequence p. The limitation of the central limit theorem is that, it describes well only the fluctuations around the average, whereas we are interested in studying the probability of observing rare events far away from the mean, as for example having all the components of the vector p equal to 1's or 0's.

In this specific simple case under investigation, we can perform the exact combinatorial analysis where the probability $\pi(R_N = r)$ that the fration of heads R_N assumes a value r, with r a rational number that can take one of the values in the set $\{0, \frac{1}{N}, \frac{2}{N}, \frac{3}{N}, \ldots, \frac{N-1}{N}, 1\}$, has the form

$$\pi(R_N = r) = \frac{1}{2^N} \frac{N!}{(rN)!(N - rN)!} \,. \tag{1.50}$$

For large N we can perform a scaled analysis by taking the Stirling approximation $N! \approx N^N e^{-N}$ that leads to the following exponential form for the probability distribution

$$\pi(R_N = r) \asymp e^{-NG(r)} \,, \tag{1.51}$$

with

$$G(r) = \log 2 + r \log r + (1 - r) \log (1 - r) \,. \tag{1.52}$$

Every time a probability distribution takes the form of that of equation (1.51), we say that it follows a large deviation principle, with $G(r)$ being the large deviation function.

One important feature of the large deviation function $G(r)$, describing the whole range of fluctuations, is that its form is different, except around the mean, from the parabolic shape $G(r) \approx \frac{(r-\mu)^2}{2\sigma^2}$, where μ represents the mean and σ^2 the variance, predicted by the central limit theorem for independent and identically random variables distributed according to a Gaussian distribution and describing fluctuations only of the mean. In this sense we can say that large deviation theory is an improvement of the law of large numbers and of the central limit theorem since it describes the probability of large fluctuations and not only the probability of small fluctuations around the average. The large deviation function $G(r)$ of equation (1.52) is positive and convex for all the values of r in the set $\{0, \frac{1}{N}, \frac{2}{N}, \frac{3}{N}, \ldots, \frac{N-1}{N}, 1\}$, with an unique zero, as one would expect, at $r = 1/2$. The exponential form of equation (1.51) means that the probability of observing a fraction of 1's in the sequence p different from the typical one, so for $r \neq 1/2$, will decay exponentially fast for increasing the number N of coins and for large N, the only sequence with a not zero probability to be observed, is the one associated to the zero of the function $G(r)$ located at $r = 1/2$, that is, half of the entries of p are 1's and half 0's.

In equation (1.51) the symbol $\asymp$ represents the asymptotic logarithmic equality meaning that the dominant behavior of the density probability $\pi(R_N = r)$ is a decaying exponential in N and the rate of decay is controlled by the large deviation function $G(r)$ which is a not everywhere zero function. The equivalent and more precise way (but still not enough precise, for a strictly more precise mathematical definition *cf.* (37-40) in [21]) of referring to the large deviation principle is by considering the limit

$$\lim_{N\to\infty} -\frac{1}{N} \log \pi(R_N = r) = G(r)\,. \tag{1.53}$$

If this limit exists, then the probability $\pi(R_N = r)$ of the random variable R_N satisfies a large deviation principle with $G(r)$ being the large deviation function which in this context we refer as the rate function. This definition of the large deviation principle clarifies the use of the approximation used in equation (1.51). The exact probability distribution can be expressed as

$$\pi(R_N = r) = e^{-NG(r)+o(N)}\,, \tag{1.54}$$

where $o(N)$ contains correction terms which are sub-linear in N, that is,

$$\lim_{N\to\infty} -\frac{1}{N} \log \pi(R_N = r) = G(r) - \lim_{N\to\infty} \frac{o(N)}{N} = G(r)\,, \tag{1.55}$$

meaning that the limit of equation (1.53) is the appropriate needed limit to consider for preserving the exponential scaling law of $\pi(R_N = r)$ in equation (1.51).

For this specific example of N random bits, which describes a very simple model, it is possible to perform the above exact combinatorial calculations but in general, in many stochastic processes, the statistics of certain stochastic observables one would like to study are not known and in these cases one has to perform simulations. In general, when performing a simulation and considering a certain scaling limit, for example that of a large number of coins if we refer to the above example, it is very difficult to obtain the large

deviation form presented in equation (1.51), as for increasing N the probability decays exponentially fast with N, so in these cases one has to tackle the problem of numerically evaluating the large deviation probabilities and of obtaining the large deviation form by implementing, appropriate and efficient, importance sampling algorithms.

1.3.2 Large deviation theory as mathematical language of equilibrium statistical mechanics

Large deviation functions are everywhere in physics, in particular large deviation theory is the mathematical language of equilibrium in statistical mechanics. From this point of view, the entropy functions and the variational principles, that is, maximum entropy principle of microcanonical ensembles and minimum free energy principle of canonical ensembles, encountered in the study of thermodynamic systems in equilibrium, based on the statistical method and on the language of the Gibbs ensembles, correspond in the large deviation theory to special rate functions and contraction principles. Furthermore, from the large deviation techniques can be derived the equivalence between the microcanonical and canonical ensembles in the thermodynamic limit [25] and the appearance of the Legendre-Fenchel transform connecting the canonical free energy and the microcanonical entropy [21].

In the Gibbs ensembles theory, the macroscopic states of matter are determined by the properties and by the motion of their microscopic constituents. An isolated macroscopic system is characterized by a large number of elementary components, its volume N and the total energy E. Fixing the value of these quantities allows one to identify a macrostate of the system. At the microscopic level there are many distinct states, called microstates, that correspond to the same macrostate.

The microcanonical ensemble is the set of all microstates with fixed energy E and volume N which describes the properties of a isolated system in equilibrium. One important consequence of the Liouville theorem, asserting that the density of the accessible microstates of a system is constant, is that one can compute explicitly the number of microstates which is proportional to the volume of the state space

$$\text{Number of microstates} \equiv \Omega(E, N)\,. \tag{1.56}$$

The link between the entropy $S(E)$, a thermodynamic property of the system, and the number of microstates $\Omega(E, N)$, a microscopic feature of the system, is defined by the Planck equation

$$S(E) = k \log \Omega(E, N)\,, \tag{1.57}$$

where k is the Boltzmann constant (see [25] for a precise mathematical definition of the statistical weight $\Omega(E, N)$).

In the large size limit, the counting factor $\Omega(E, N)$ follows a large deviation form as the one of equation (1.51), with large deviation function equal to the entropy density $s(E)$

$$\Omega(E, N) \asymp e^{Ns(E)/k}\,, \tag{1.58}$$

where the symbol $\asymp$ implies the limit presented in equation (1.53). Since $\log \Omega(E,N)$ is an increasing function of $\Omega(E,N)$ as the system evolves towards equilibrium, this is equivalent of saying that, the equilibrium macrostate is the one maximizing the entropy.

The canonical ensemble describes a macroscopic system with, fluctuating and not uniquely determined energy, and fixed temperature T, in equilibrium with a thermal environment. In this case we can define the canonical partition function as the Laplace transform of parameter $\beta = 1/kT$ of the fuction $\Omega(E,N)$

$$Z(\beta,N) = \sum_E \Omega(E,N) e^{-\beta E} \,. \tag{1.59}$$

Unlike the microcanonical ensemble where all microstates have equal probability to be occupied, in the canonical ensemble, the microstates are characterized by different energies so they have different probabilities of occupation and the partition function indicates the probability of occupation of a microstate depending on its energy.

In the large size limit the partition function follows a large deviation principle with large deviation function which is equal to the Helmoltz free energy density $f(\beta) = F(\beta)/N$

$$Z(\beta,N) \asymp e^{-\beta N f(\beta)} \,. \tag{1.60}$$

It is precisely this large deviation structure of the equilibrium statistical mechanics, e.g. equations (1.58) and (1.60), that is responsible for obtaining the Legendre-Fenchel transform connecting the free energy density $f(\beta)$ and the entropy density $s(u)$

$$s(u) = \inf_\beta \left[\beta u - f(\beta)\right] \,, \tag{1.61}$$

with $u = E/N$ and where "inf" stands for "infimum of".

In general we are interested in studying out of equilibrium systems, such as transport phenomena, glassy systems and open quantum settings, and since in these cases we do not have a complete theory of nonequilibrium statistical mechanics to apply, large deviation techniques can be utilised in order to study the properties of nonequilibrium systems. In these cases, spatio-temporal correlations emerge and the interesting behavior of the dynamics of the nonequilirium systems under investigation is not anymore in the configurations as in the thermodynamic case but in the trajectories. For this reason, a thermodynamics of trajectories base on large deviation techniques has been developed and is the one we are going to exploit in the cases we study in chapter 4.

1.3.3 Stochastic Dynamics and Large Deviations

In this section we establish our notation and review the basics of dynamical large deviation methods. In chapter 4 we focus on classical stochastic systems with continuous-time Markovian dynamics. Our notation is similar to that of, for example, Refs. [19, 26–28]. The state of the system is described by a vector $|P_t\rangle$ collecting the probabilities $P_t(C)$ of observing the state in a given configuration C at time t

$$|P_t\rangle = \sum_C P_t(C)\,|C\rangle \,. \tag{1.62}$$

In classical stochastic dynamics such a vector evolves according to a master equation (ME)

$$\partial_t |P_t\rangle = \mathbb{W} |P_t\rangle \ . \tag{1.63}$$

The classical stochastic generator $\mathbb{W}$ contains information about transition probabilities and the escape rate from a given configuration. Explicitly it reads,

$$\mathbb{W} = \sum_{C,C' \neq C} W(C \to C') \, |C'\rangle \langle C| - \sum_{C} R(C) \, |C\rangle \langle C| \ , \tag{1.64}$$

where $W(C \to C')$ is the transition rate from C to C' and $R(C) = \sum_{C' \neq C} W(C \to C')$ is the escape rate from C. The dynamics encoded in the ME (1.63) is realised by means of stochastic trajectories. Starting from configuration C, the system survives in this state for a random time Δt, which is distributed exponentially according to $S(\Delta t) = R(C) e^{-R(C)\Delta t}$, and then jumps into a new configuration according to the rates $W(C \to C')$.

As such, a trajectory of total time t consists in a sequence of configurations, $\omega_t = (C_0 \to C_{t_1} \to C_{t_2} \to \cdots \to C_{t_n})$, and waiting times for jumps between them, where $0 < t_1 < t_2 < t_3 < \cdots < t_n < t$ are the times at which the change of configuration occurs, and C_0 is the initial configuration. Between the time of the last jump t_n, and the final time t of the trajectory, the configuration remains unchanged (i.e., "survives" in C_{t_n}). The evolution of the probability state vector $|P_t\rangle$ can be recovered by averaging over all stochastic trajectories.

To investigate the emergence of ordered dynamical phases and of strong spatio-temporal correlations it is necessary to investigate the full probability of time-integrated observables [20–22, 28]. We represent observables as vectors,

$$\langle O| = \sum_{C} O(C) \langle C| \, , \tag{1.65}$$

where $O(C)$ is the value of the observable in configuration C. Given that classical observables are diagonal in the configuration basis, this is equivalent to representing observables as matrices $\hat{O}$ and multiplying on the left by the flat state

$$\langle -| = \sum_{C} \langle C| \, , \tag{1.66}$$

so that $\langle O| = \langle -|\hat{O}$.

We consider dynamical observables defined as time-integral of configuration operators over a trajectory

$$\mathcal{O}[\omega_t] = \int_0^t dt' \langle O|C_{t'}\rangle \, , \tag{1.67}$$

where $C_{t'}$ is the configuration of the state at time t' in a stochastic realisation ω_t. Note that while O is a static observable (a function only of the configuration), $\mathcal{O}$ is a dynamical observable, a functional of the trajectory and extensive in time (and in space if O is space-additive).

For each realisation of the process, i.e. for each trajectory ω_t, there is associated a value of the time-integrated observable, $\mathcal{O}[\omega_t]$. Its probability distribution can thus be written as

$$\pi_t(\mathcal{O}) = \sum_{\omega_t} \mathcal{P}(\omega_t)\delta\left(\mathcal{O}[\omega_t] - \mathcal{O}\right) , \tag{1.68}$$

where $\mathcal{P}(\omega_t)$ is the probability of trajectory ω_t to occur. For long times this probability distribution obeys a large deviation (LD) principle [20–22, 28]

$$\pi_t(\mathcal{O}) \asymp e^{-t\varphi(\mathcal{O}/t)} . \tag{1.69}$$

The so-called large rate function $\varphi(o)$, which is the analog of an entropy density in the ensemble of trajectories, is a function of the intensive order parameter $o = \mathcal{O}/t$ and gives information about the exponential decay of the probability of observing a large deviation far away from the typical value of o. Indeed, this function is positive $\varphi(o) \geq 0$, and equal to zero only at the typical outcome of the observable.

The moment generating function (MGF) for the observable, $Z_t(s)$, defined as

$$Z_t(s) = \sum_{\mathcal{O}} \pi_t(\mathcal{O}) e^{s\mathcal{O}} , \tag{1.70}$$

also obeys a large principle for large times [20–22, 28]

$$Z_t(s) \asymp e^{t\,\theta(s)}, \tag{1.71}$$

where $\theta(s)$ is the scaled cumulant generating function (SCGF). Its derivatives evaluated at $s = 0$ give the cumulants of $\mathcal{O}$ scaled by time. The large deviation function $\theta(s)$ is the analog of a free energy density for the ensemble of trajectories and s is a parameter conjugate to the observable $\mathcal{O}$. This parameter has a role akin to the temperature in this dynamical large deviation setting and it can be seen as a parameter modifying the original probability of the observables. Tuning this parameter allows one to explore the tails of the distribution $\pi_t(\mathcal{O})$.

The SCGF $\theta(s)$ contains the full statistical information about the observable $\mathcal{O}$, indeed the $n-$th scaled cumulant of the observable is

$$\frac{\langle\langle \mathcal{O}^n \rangle\rangle}{t} = \frac{\partial^n}{\partial s^n}\theta(s)\bigg|_{s=0} , \tag{1.72}$$

where $\langle\langle \cdot \rangle\rangle$ indicates cumulant. Interesting phase behaviours in trajectory space are encoded in the analytic properties of the SCGF and its singularities are indicative of dynamical phase transitions. The rate function $\varphi(o)$ and the SCGF $\theta(s)$ are related by a Legendre-Fenchel transform [20–22, 28]

$$\theta(s) = \sup_o \left[o\, s - \varphi(o)\right] . \tag{1.73}$$

For finite s, the SCGF $\theta(s)$ encodes information about large fluctuations of the stochastic dynamics. More precisely, for a given s, $\theta(s)$ provides a way to investigate the trajectories of the process giving an atypical time-average value of $\langle o \rangle_s$ [29] identified by the relation

$$\langle o \rangle_s = \theta'(s) \,. \tag{1.74}$$

The SCGF $\theta(s)$ can be obtained by means of tilted operators techniques [17, 20–22, 28, 30, 31]. In particular, it is the largest eigenvalue associated with a deformation of the original stochastic generator $\mathbb{W}$, which for observables of the form (1.67) reads,

$$\mathbb{W}_s = \sum_{C,C' \neq C} W(C \to C') \, |C'\rangle \, \langle C| - \sum_{C} \left[R(C) - s \, O(C) \right] |C\rangle \, \langle C| \,. \tag{1.75}$$

In chapter 4 we make use of the notions mentioned in this section in order to investigate the presence of collective dynamical phase transitions, from a disordered phase to an ordered phase, for a set of stochastic independently evolving spins.

Chapter 2

Enhancing correlation times for edge spins through dissipation

This chapter is the first of two chapters that together make up the first part of the thesis on strong zero modes. Spin chains with open boundaries, such as the transverse field Ising model, can display coherence times for edge spins that diverge with the system size as a consequence of almost conserved operators, the so-called strong zero modes. In this chapter, we discuss the fate of these coherence times when the system is perturbed in two different ways. First, we consider the effects of a unitary coupling connecting the ends of the chain; when the coupling is weak and non-interacting, we observe stable long-lived harmonic oscillations between the strong zero modes. Second, and more interestingly, we consider the case when dynamics becomes dissipative. While in general dissipation induces decoherence and loss of information, here we show that particularly simple environments can actually enhance correlation times beyond those of the original unitary case. This allows us to generalise the notion of strong zero modes to irreversible Markovian time-evolutions, thus defining conditions for dissipative strong zero maps. Our results show how dissipation could, in principle, play a useful role in protocols for storing information in quantum devices. The work discussed in this chapter appeared in the publication:

"Enhancing correlation times for edge spins through dissipation"
L. M. Vasiloiu, F. Carollo and J. P. Garrahan
Physical Review B **98**, 094308 (2018).

2.1 Introduction

Recent results have demonstrated the possibility of observing in many-body quantum chains with open boundary conditions coherence times for edge spins that diverge exponentially with the size of the system [32–37]. One of the interests in this phenomenon stems from the possibility of storing and protecting the information encoded in quantum states for very long times, with possible applications in future quantum technologies [38–40]. From this perspective, for the applicability of long coherence times for boundary degrees of

freedom - so far only established in isolated (unitary) quantum systems [32,33] - the effect of the inevitable interaction of the system of interest with the surrounding environment must be considered. This is the problem we address in this chapter.

Acting as a source of dissipation and noise, the interaction of a system with an environment usually leads to suppression of truly quantum features in the system and to the emergence of classical-like behavior. However, in some instances it has been shown that engineered system-environment couplings can actually enhance or even generate quantum correlations, such as entanglement [41–50]. While robustness of coherence times for edge spins has been extensively studied in the presence of interactions or of integrability-breaking terms and also in the presence of disorder in the Hamiltonian [32,33,51], less is known about their behavior under irreversible open quantum dynamics [9, 10, 12, 13, 40, 52–54]. In particular, it is not clear whether under Markovian (memory-less) dynamics these long edge time-correlations can be observed and general conditions for their existence are not known. Understanding the behavior of these time-correlations in open quantum systems would allow for the possibility of exploiting the protected information encoded in edge spins for applications in quantum devices also in realistic non-equilibrium settings.

Long coherence times of edge spins are due to the presence of almost conserved operators - the so-called strong zero modes (SZM) [32–37]. The simplest example is that of the transverse field Ising model (TFIM) with free boundaries where the SZMs operators can be written down explicitly in compact form [32, 34]. For finite sized systems, the SZMs are coupled by the dynamics but their evolution happens on very slow time-scales, so that initial information stored in the edge spins is preserved for times which are exponential in the system size [32].

In this chapter we consider the effect of two different perturbations away from the optimal conditions for the dynamical protection of the SZMs, which we analyze separately. One can think of two possible scenarios. The first one, illustrated in Fig. 2.1(a), consists of connecting the two ends of an open chain via a unitary perturbation. Figure 2.1(b) illustrates our main result in this case: when the Hamiltonian perturbation is non-interacting (in a way we specify in the following section) we observe macroscopic coherent oscillations between the two SZMs, occurring on faster time-scales than those of the TFIM with free boundaries [cf. Fig. 2.1(c)], as the two ends are, in this case, directly connected.

More interestingly, we then address the case in which the system undergoes a dissipative Markovian dynamics induced by the presence of an external environment weakly interacting with it. Not only we show that Markovian quantum dynamics can sustain finite yet long correlation times, but also that suitably engineered - but still relatively simple - environments can increase coherence times by orders of magnitude with respect to original TFIM scenario. Figure 2.1(c) illustrates this result. In fact, these correlation times diverge with system size with a faster exponential rate in the dissipative case than in the purely coherent case of the TFIM with free boundaries.

Indeed, as we will show, specific type of dissipations can induce fast decoherence effects affecting solely one of the two localized operators: the coherent slow oscillations of the TFIM are suppressed but the information stored in one of the two edges is protected for much longer time-scales than the original unitary ones. In particular, even a small

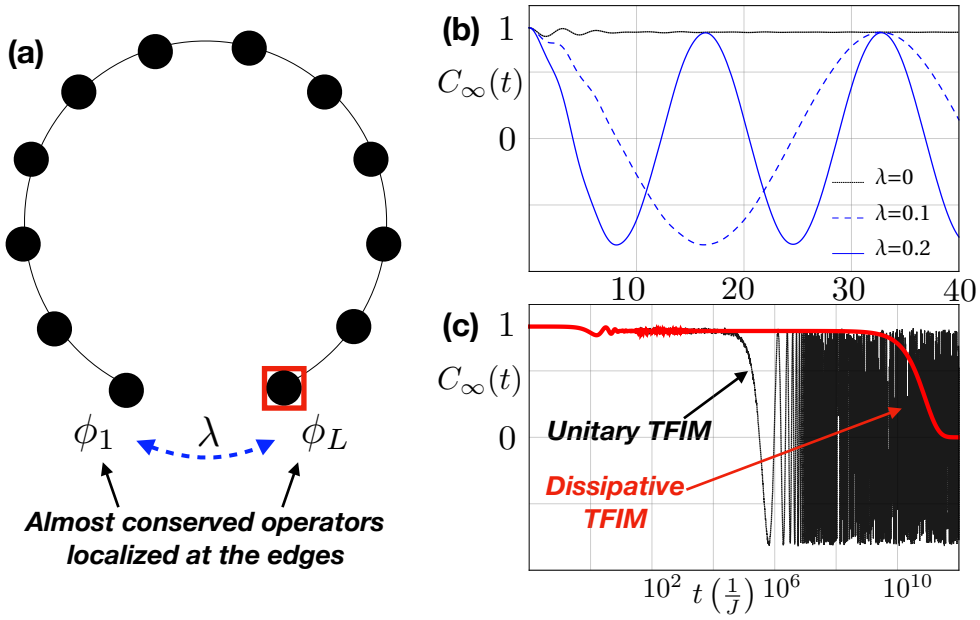


Figure 2.1: **(a)** Pictorial representation of a quantum spin chain featuring almost conserved operators, (ϕ_1, ϕ_L), localized at the two edges, perturbed either by weakly closing the chain (blue arrow) or by dephasing one edge (red box). **(b)** $L = 50$, $h = 0.2\,J$: Behavior in time of the infinite temperature time-correlations of the z-magnetization of the first spin $C_\infty(t)$, given by Eq. (2.7), when the edges of the original free boundary TFIM are joined through a non-interacting Hamiltonian perturbation ($\lambda \neq 0$). Coherent oscillations between the two strong zero modes take place on faster time-scales than those of the free boundary case ($\lambda = 0$). **(c)** $L = 8$, $h = 0.2\,J$: In the presence of dephasing ($\Gamma = 1$, $\alpha = 1/8$) acting only on one edge of the free boundary TFIM ($\lambda = 0$) oscillations between the strong zero modes are suppressed; however the correlation time for the spin at the edge is doubled in order of magnitude with respect to the original TFIM with free boundaries. In the plot time is represented on a log-scale.

perturbation, such as dephasing on the last site of the chain, can double in order of magnitude the correlation time for the first spin in the TFIM with free boundary conditions [see Fig. 2.1(c)]. While for finite systems these correlations will eventually decay, in the thermodynamic limit they can persist for infinitely long times also in the presence of dissipation.

We mainly focus on the TFIM [1, 2, 5, 6] allowing for numerical diagonalization of large system size and amenable analytical considerations; nonetheless, we expect our findings to be very general and we show how they apply also for a dissipative interacting spin chain featuring almost conserved operators - the XYZ chain [33, 55].

Finally, we introduce the conditions for the existence of strong zero maps, which generalize the notion of SZMs to irreversible Markovian quantum dynamics. These are obtained exploiting the possible presence of symmetry sectors in the dynamical generator of the open quantum dynamics [56, 57].

2.2 Strong zero modes in the TFIM

The simplest many-body system where the emergence of long correlation times for the edge spins can be observed is the TFIM (see section 1.1 for a general description of the model) with free boundary conditions [1, 5, 6]. It consists of a chain of two-level systems described by the Hamiltonian (here and in what follows we set $\hbar = 1$)

$$H = -J \sum_{i=1}^{L-1} \sigma_i^z \sigma_{i+1}^z - h \sum_{i=1}^{L} \sigma_i^x \,, \tag{2.1}$$

where σ_i^β, with $\beta = x, y, z$, represents the β Pauli matrix corresponding to the i-th site. The parameter J embodies the strength of magnetic interactions between neighboring sites, while h is a transverse magnetic field in the x direction. This Hamiltonian describes non-interacting fermions. Indeed, by introducing the Majorana operators

$$\gamma_i^A = \sigma_i^z \prod_{k=1}^{i-1} \sigma_k^x, \quad \gamma_i^B = \sigma_i^y \prod_{k=1}^{i-1} \sigma_k^x \,, \tag{2.2}$$

such that $\{\gamma_i^X, \gamma_j^Y\} = 2\delta_{X,Y}\delta_{i,j}$, the Hamiltonian can be written as

$$H = -iJ \sum_{i=1}^{L-1} \gamma_i^B \gamma_{i+1}^A - ih \sum_{i=1}^{L} \gamma_i^A \gamma_i^B. \tag{2.3}$$

Introducing the parity operator [*cf.* (1.5)]

$$P = \prod_{i=1}^{L} \sigma_i^x, \tag{2.4}$$

it is immediate to check that $[H, P] = 0$, implying that the eigenvectors of the Hamiltonian, as well as its eigenvalues, can be divided into even and odd sectors. Interestingly, in the magnetically ordered phase $|h| < |J|$, the even and odd parts of the Hamiltonian spectrum become identical exponentially fast in the system size L. This can be shown by introducing the so-called SZMs [32–37]

$$\phi_1 = \mathcal{C} \sum_{i=1}^{L} \left(\frac{h}{J}\right)^{i-1} \gamma_i^A, \quad \phi_L = \mathcal{C} \sum_{i=1}^{L} \left(\frac{h}{J}\right)^{L-i} \gamma_i^B \tag{2.5}$$

where the constant $\mathcal{C}^2 = [1 - (h/J)^2]/[1 - (h/J)^{2L}]$ normalizes the operators in such a way that $\phi_{1/L}^2 = \mathbf{1}$. First of all, one notices that ϕ_1 and ϕ_L anticommute with the parity operator P, and almost commute with the Hamiltonian H,

$$[H, \phi_{1/L}] = \pm 2i\mathcal{C}J \, (h/J)^L \, \gamma_{L/1}^{B/A}, \tag{2.6}$$

i.e., these commutators decay exponentially with system size. Therefore, with $|\psi_i\rangle$ being an even (odd) eigenvector of the Hamiltonian associated to the eigenvalue ϵ_i, one has that $\phi_1|\psi_i\rangle$ is a vector which is odd (even) under parity transformation. Then, because $\|[H,\phi_1]\| \approx 0$ for large L, one has

$$H\phi_1|\psi_i\rangle \approx \epsilon_i\, \phi_1|\psi_i\rangle\,,$$

showing that ϵ_i becomes, in the thermodynamic limit, an eigenvalue associated to both an even and an odd eigenvector. These two vectors are mapped one onto the other by the action of the SZM.

To state these properties more concisely, a SZM is an operator that almost commutes with the dynamical generator of the system, $[H,\phi_1] \approx \beta_L$, where the norm of the correction operator, $\|\beta_L\| < e^{-cL}$, with c a positive constant, is exponentially decaying with the size L of the system. In addition, the SZM is an operator that also anticommutes with the generator of a spin-flip symmetry, $\{P,\phi_1\} = 0$, where $[H,P] = 0$, and has finite norm, $\phi_1^2 = \mathbf{1}$.

The above mentioned properties of the Hamiltonian have remarkable practical consequences: since the SZM operators are localized at the two ends of the chain when $|h| \ll |J|$, the information in the boundary sites can be stored for times which are exponentially long in the system size [32]. Even more interestingly, this can actually be observed at high-temperatures as witnessed by the (infinite temperature) time-correlations

$$C_\infty(t) := \frac{1}{2^L}\mathrm{Tr}\left(\mathrm{e}^{-iHt}\sigma_1^z \mathrm{e}^{iHt}\sigma_1^z\right)\,, \tag{2.7}$$

as we now explain.

2.3 Weak bond in the ring geometry for the TFIM

While the nice properties discussed in the previous section are completely lost when considering the same model in the ring geometry (i.e. the system is made translationally invariant through periodic boundary conditions), a question one may ask is what occurs in intermediate regimes that interpolate between the free boundary case with its long coherence times, and the ring geometry where they are absent. To this aim we introduce a Hamiltonian perturbation H_b to the free boundaries TFIM Hamiltonian of Eq. (2.1), consisting of a term directly coupling the ends of the chain, as illustrated in Fig. 2.1(a); the unitary time-evolution is then governed by $\hat{H} = H + \lambda H_\mathrm{b}$. First, we consider a non-interacting perturbation $H_\mathrm{b} = -iJ\gamma_L^B\gamma_1^A$: in this situation, for small λ, as we display in Fig. 2.1(b), the time-correlations $C_\infty(t)$ manifest stable macroscopic oscillations. This feature emerges from the fact that the Hamiltonian perturbation connects harmonically the modes $\phi_{1/L}$, now with a finite (i.e. not decreasing with the system size) frequency that is isolated from the region of the spectrum that becomes dense in the large L limit, [see Fig. 2.2].

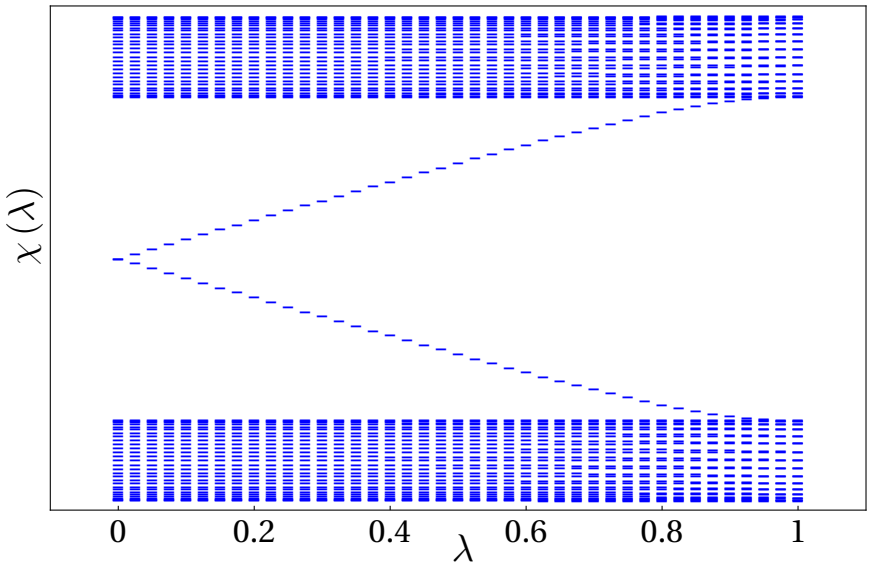


Figure 2.2: Eigenvalues $\chi(\lambda)$ of the dual of the Liouvillian map, defined by $\mathcal{L}_0^*[X] := i[\hat{H}, X]$, as a function of λ for a non-interacting perturbation $H_b = -iJ\gamma_L^B\gamma_1^A$ ($J = 1, h = 0.2$ and $L = 30$). Here the observables X are linear in Majorana fermions $\gamma_i^{A/B}$. For small λ we observe two finite frequencies $\omega_\lambda = \pm 2\lambda J$, that are isolated from the region of the spectrum that becomes dense as $L \to \infty$, which are responsable for the stable macroscopic oscillations of the time correlation function $C_\infty(t)$ between the two strong zero modes as displayed in Fig. 2.1(b). As λ approaches 1, the frequencies ω_λ enter in the continuous region of the spectrum and the coherent oscillations fade away.

Thus, while correlations of all other modes are rapidly washed out by destructive interference, the two SZMs display stable long-lived oscillations with frequency $\omega_\lambda = 2\lambda J$. When $\lambda \approx 1$, ω_λ enters in the continuous region of the spectrum and the stable oscillations fade away. Completely different is the scenario in which boundary sites of the Ising chain are connected through the Hamiltonian $H_\mathrm{b} = -J\sigma_L^z\sigma_1^z$; in this case, the first-order perturbation correction vanishes and thus the modification to the evolution comes as a second-order map determining a decay of the correlation function $C_\infty(t)$ [see Fig. 2.3].

2.4 Dissipative dynamics in the open chain TFIM and enhancement of correlation times

The results of the previous section concern instances of unitary quantum dynamics, thus describing a system which is perfectly isolated from its thermal surrounding. This situation is an idealized one and, in order to account for more realistic settings, one needs to consider open quantum evolutions [9, 10, 12, 13, 52]. For simplicity, we will consider in this section the case of an environment weakly interacting with the system. Usually, such

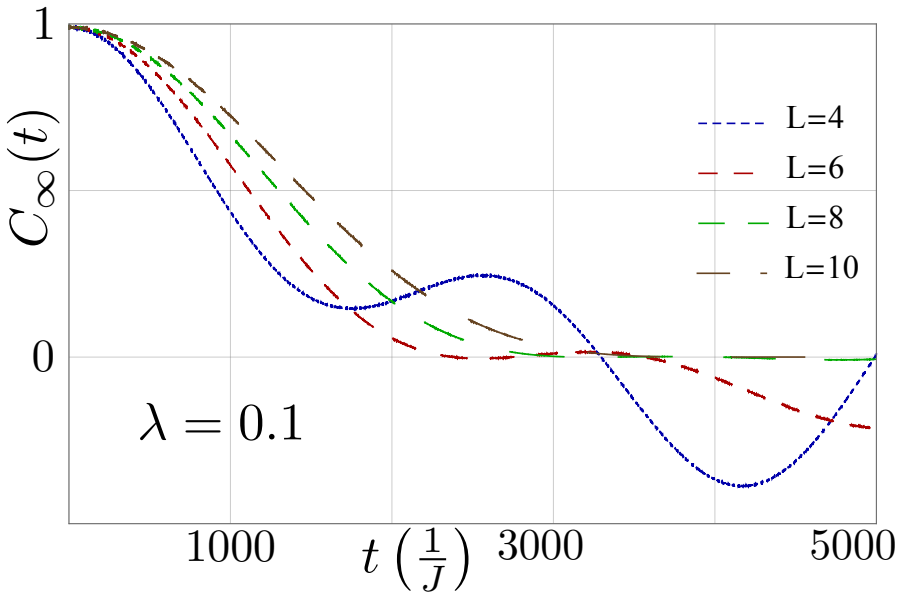


Figure 2.3: Behavior of the time correlation function $C_\infty(t)$ in the unitary case ($h = 0.1\,J$) when joining the edges of the chain through the Hamiltonian $H_\mathrm{b} = -J\sigma_L^z\sigma_1^z$ with a small perturbative parameter $\lambda = 0.1$. In this case, we see that $C_\infty(t)$ decays instead of undergoing macroscopic oscillations as shown in Fig. 2.1(b). For increasing system sizes the characteristic time of this decay increases, however it does not show an exponential dependence on L.

interaction leads to loss of quantum coherence and of quantum correlations. However, as we now discuss, certain open quantum dynamics can still feature long correlation times for edge spins as a consequence of the existence of SZMs.

In the following we will consider a dissipative perturbation of the original free boundary TFIM, and not anymore the Hamiltonian perturbation of the previous section (namely, in what follows $\lambda = 0$).

In the Markovian regime, the irreversible evolution of system observables is generated by $\dot{X}_t = \mathcal{L}^*[X_t]$ where $\mathcal{L}^*$ is the dual of the Lindbladian map $\mathcal{L}$ [9,10,12], which generates the dynamics of the state of the system, ρ, through $\dot{\rho} = \mathcal{L}[\rho]$ (see section 1.2). The dual map has the following structure

$$\mathcal{L}^*[X] := i[H, X] + \sum_k \left(L_k^\dagger X L_k - \frac{1}{2}\left\{ L_k^\dagger L_k, X \right\} \right) . \tag{2.8}$$

In the generator above, the first term represents the coherent part of the dynamics while the terms in the sum encode noisy effects due to the environment. We now assume that the presence of the environment induces decoherence in the spin chain, which can be described by Lindblad operators

$$L_i = \sqrt{\Gamma_i}\sigma_i^z, \tag{2.9}$$

with Γ_i being the dephasing rate at site i. As one would expect, when dephasing acts uniformly on the whole system, $\Gamma_i = \Gamma$, the spin-chain cannot sustain correlation times

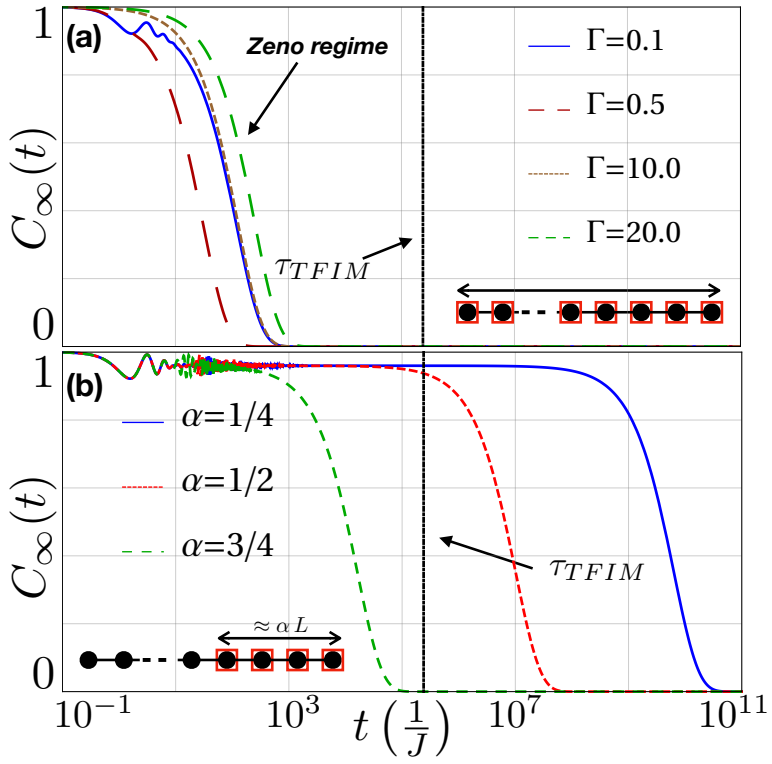


Figure 2.4: Transverse field Ising model with free boundaries ($\lambda = 0$) subject to dephasing on a fraction α of the chain starting from the last site. In both panels, we specify the characteristic time-scale of the edge correlation in the original TFIM, $\tau_{TFIM} \propto (J/h)^L$ [*cf.* (18) in [32]], where τ_{TFIM} is the first instance when $C_\infty(t) = 1/\mathrm{e}$ in the unperturbed TFIM with free boundaries. **(a)** For $\alpha = 1$ the infinite temperature time-correlation $C_\infty(t)$ decays much faster than in the original TFIM case (the plot is for $h = 0.2\,J$, $L = 8$ and different Γ). When $\Gamma \gg 1$ the time-scales of the decay of $C_\infty(t)$ are dominated by the Zeno effect and the presence or not of a strong zero mode is irrelevant. **(b)** In the presence of dissipation only on a small portion of the chain, $\alpha < 1$, we observe that $C_\infty(t)$ can decay later than in the unitary TFIM with free boundaries (data shown for the same parameters J, h and L as in **(a)** with $\Gamma = 1$ and different α.)

that grow with system size [see Fig. 2.4(a)]. Nevertheless, with Γ small, the presence of SZMs of the coherent case, leads to correlations times for the boundary spins which, while finite, are longer than those where SZMs are not present (for instance when $h = J$). When $\Gamma \gg 1$ the physics changes, and time-correlations increase irrespective of the presence or the absence of SZMs in the unitary case. This corresponds to a quantum Zeno regime, with characteristic decay time given by $\tau_z \approx \Gamma/(2h^2)$, which can be obtained straightforwardly from second-order perturbation theory.

A very different scenario emerges when one considers dissipation only on a fraction α of the chain starting from the rightmost site,

$$\begin{cases} \Gamma_i = 0 & i < L(1-\alpha) \\ \Gamma_i = \Gamma & i \geq L(1-\alpha) \end{cases} \tag{2.10}$$

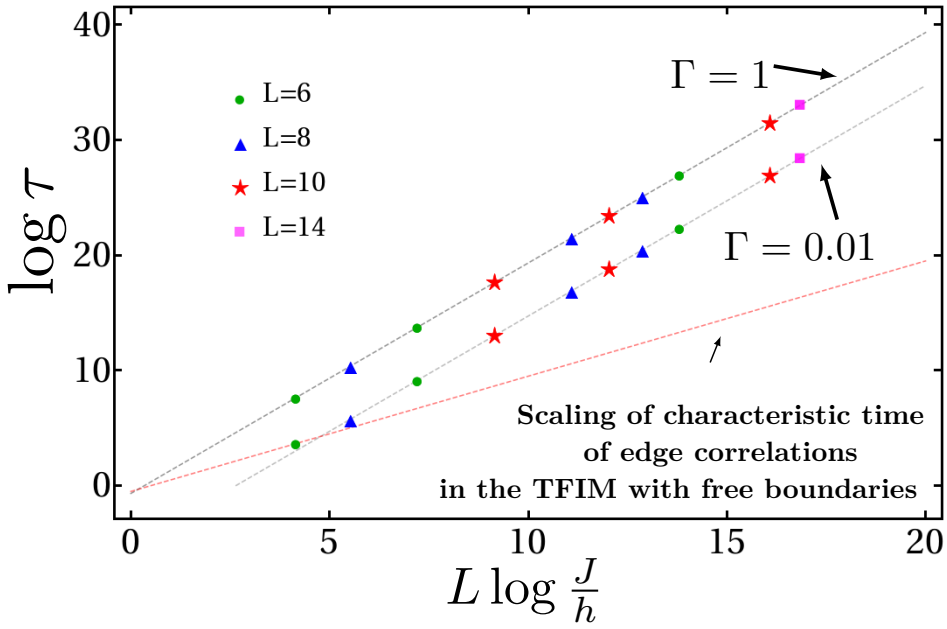


Figure 2.5: Behavior of the logarithm of the characteristic time of the correlation functions $C_\infty(t)$ as a function of $x = L\log(J/h)$. In the unitary case of the TFIM with free boundaries the scaling is characterized by slope equal to one ($\log\tau \approx x$). Remarkably, the presence of dephasing affecting the last site of the chain, enhances the scaling of $\log\tau$ which clearly shows, in this case, a behavior $\log\tau \approx 2x$, meaning that correlation time is doubled in order of magnitude with respect to the TFIM case. In the plot we fix $J = 1$ and explore different values of L, h and Γ.

as illustrated in Fig. 2.4(b). Also in this dissipative case we see that characteristic decay times for $C_\infty(t)$ are exponentially large with the size of the system. This is a surprising result suggesting that SZMs and infinitely long time-correlations can be observed in open quantum dynamics.

However, there is a much more interesting effect that we can observe: not only, as we already pointed out, SZMs can exist in dissipative settings, but, strikingly, the characteristic decay time of time-correlations associated to their existence can be enhanced by the presence of an external environment. This is clearly displayed in Fig. 2.4(b): decreasing the portion of the chain affected by dephasing - which we denote by $\alpha \in [0, 1]$, *cf.* (2.10) - we can see that the time-correlations $C_\infty(t)$ stay almost invariant for larger times and, interestingly, for certain values of α these can be much greater than the characteristic time $\tau_{TFIM} \propto (J/h)^L$ [*cf.* (18) in [32]], where τ_{TFIM} is the first instance when $C_\infty(t) = 1/\mathrm{e}$ in the unperturbed TFIM with free boundaries.

In order to understand this feature we consider the extreme case in which only the last site of the chain is subject to dephasing. Notice that this represents, in the large L limit, a perturbation to the unitary time-evolution of the TFIM with free boundaries which is infinitely far apart from the SZM ϕ_1 which is instead localized around the first edge. In this scenario, considering a small transverse field h, the effective "slow" dynamics of the

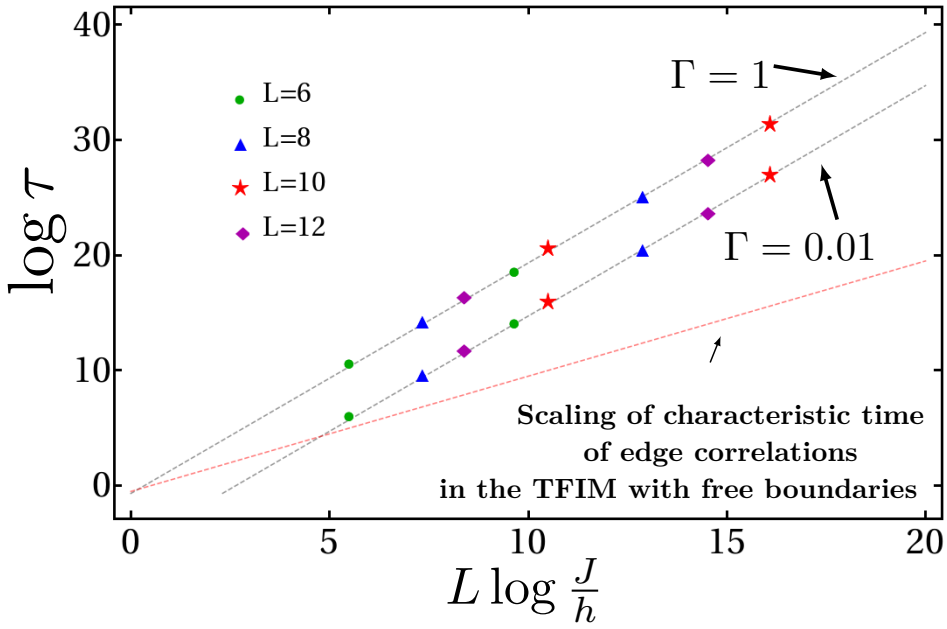


Figure 2.6: Behavior of the logarithm of the characteristic time of the correlation functions $C_\infty(t)$ as a function of $x = L\log(J/h)$. In the unitary case the scaling is characterized by slope equal to one ($\log\tau \approx x$). Remarkably, the presence of dephasing affecting uniformly the whole chain described by Lindblad operators $L_k = -i\sqrt{\Gamma}\sigma_k^z\sigma_{k+1}^y$, enhances the scaling of $\log\tau$ which clearly shows, in this case, a behavior $\log\tau \approx 2x$, meaning that correlation time is doubled in order of magnitude with respect to the unitary case. In the plot we fix $J = 1$ and explore different values of L, h and Γ.

SZMs is given, at the largest order in h, by the following system of differential equations

$$\frac{d}{dt}\begin{pmatrix}\phi_1\\ \phi_L\end{pmatrix} = \begin{pmatrix}0 & -2J\left(\frac{h}{J}\right)^L\\ 2J\left(\frac{h}{J}\right)^L & -2\Gamma\end{pmatrix}\begin{pmatrix}\phi_1\\ \phi_L\end{pmatrix}. \tag{2.11}$$

Computing the eigenvalues of the matrix in the above equation one finds $\Delta_\pm = -\Gamma \pm \sqrt{\Gamma^2 - 4J^2\,(h/J)^{2L}}$; for increasing L one always reaches a regime where $\Gamma \gg (h/J)^L$ and thus we can expand the square root in order to obtain a prediction for the characteristic decay time

$$\log\tau \approx \log\frac{\Gamma}{2J^2} + 2L\log\frac{J}{h}. \tag{2.12}$$

Noticing that for the case of the unperturbed TFIM with free boundaries one expects $\log\tau_{TFIM} \propto L\log(J/h)$, we immediately see how Eq. (2.12) predicts, for the dissipative perturbation under investigation, a characteristic time for the edge correlation function $C_\infty(t)$ which is doubled in order of magnitude with respect to the unperturbed evolution. In Fig. 2.5 we show how the prediction in Eq. (2.12) is confirmed by numerical results.

While it is remarkable that a small modification of the dynamics affecting a site far apart from the first edge can have such a strong effect on $C_\infty(t)$, the same scaling of the

correlation times can also be found for a dissipative dynamics affecting the whole chain and described by jump operators given by $\sigma^z_k\sigma^y_{k+1}$ for $k = 1, 2, \dots L-1$ [see Fig. 2.6]. We also notice that different types of unitary perturbation on the rightmost site of the chain, such as an extra transverse field proportional to $\sigma^{(L)}_x$ or a longitudinal field proportional to $\sigma^{(L)}_z$, can sustain and even enhance the time-correlations of the original TFIM with free boundaries. It is however surprising that such an enhancement can also be achieved by means of specific dissipative perturbations, both extremely localized or extended through the whole chain.

2.5 Dissipative strong zero maps

In this section we now proceed to a formal definition of SZMs in dissipative contexts. This is achieved by promoting the notion of SZM from an operator acting on vectors to that of a map acting on operators. Let us consider a Lindblad generator $\mathcal{L}$ as in equation (2.8) and assume that it commutes with a map implementing a discrete symmetry transformation on the system operators. Given the generator S of the symmetry, the map can be written as $\pi_s[X] = SXS$; thus if the operator X is even under this transformation one has $\pi_s[X] = X$, while if it is odd one has $\pi_s[X] = -X$. The fact that the Lindblad operator commutes with the transformation $\mathcal{L}^* \circ \pi_s = \pi_s \circ \mathcal{L}^*$ means that one can divide eigenmatrices and eigenvalues of $\mathcal{L}$ into even and odd sectors.

If there exists a map Ψ such that

1. commutes, up to exponentially small corrections in system size, with the Lindblad generator
$$\mathcal{L}^* \circ \Psi[X] \approx \Psi \circ \mathcal{L}^*[X]\,, \qquad \forall X\,, \tag{2.13}$$
2. anti-commutes with the parity transformation
$$\Psi \circ \pi_s = -\pi_s \circ \Psi\,, \tag{2.14}$$

then we can show that the even part of the spectrum of the Lindblad operator $\mathcal{L}$ is exponentially (in system size) close to the odd part. Indeed, considering X_+ to be an even eigenmatrix of $\mathcal{L}$, namely

$$\pi_s(X_+) = X_+\,, \qquad \mathcal{L}^*[X_+] = \epsilon_+ X_+\,, \tag{2.15}$$

one has that $\Psi[X_+]$ is an odd operator under the transformation, $\pi_s \circ \Psi[X_+] = -\Psi[X_+]$, and, because of the almost commutation of Ψ with $\mathcal{L}$, also

$$\mathcal{L}^*\Big[\Psi[X_+]\Big] \approx \Psi\Big[\mathcal{L}^*[X_+]\Big] = \epsilon_+ \Psi[X_+]\,.$$

This shows that $\Psi[X_+]$ is, in the thermodynamic limit, an odd eigenmatrix of $\mathcal{L}$ with eigenvalue ϵ_+, meaning that the odd and even parts of the spectrum of the Lindblad operator are indeed paired. In order for the above derivation to be meaningful it is important

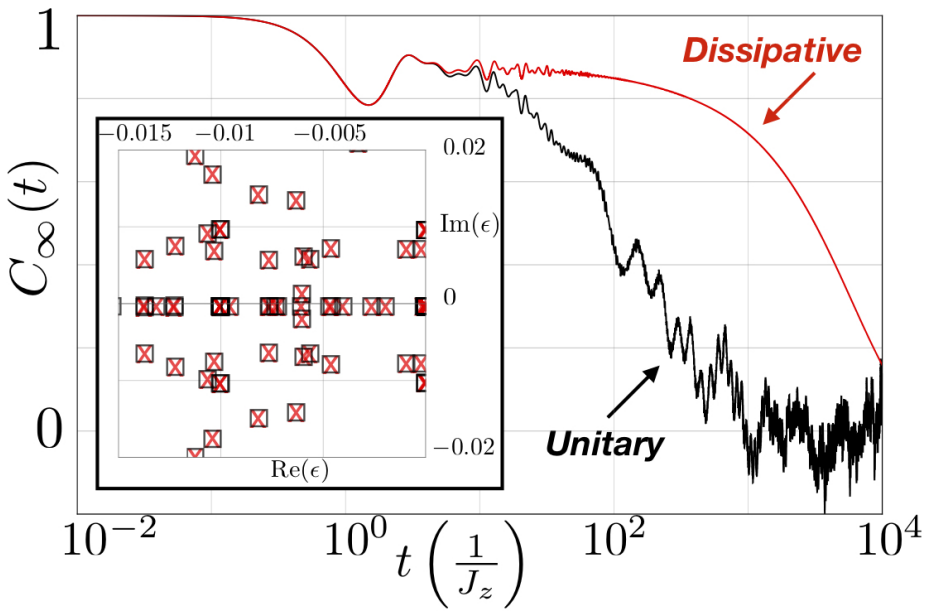


Figure 2.7: Time correlation function $C_\infty(t)$ for the XYZ chain ($L = 8$) with $J_x = 0.2$, $J_y = 0.3$, $J_z = 1$ in the unitary case as well as with dephasing $\Gamma = 1$ on the right boundary. Also for this interacting Hamiltonian we see that the presence of dephasing enhances the characteristic correlation time for the first spin. In the inset, we display a portion of the complex spectrum of the Lindbladian superoperator for the XYZ chain ($L = 6$) with $J_x = J_y = 0.1$ and $J_z = 1$: crosses represent eigenvalues from the odd sector while squares are from the even one. We found the largest distance between corresponding eigenvalues in the two sectors to be of order 10^{-4}.

that $\|\Psi[X]\| = \|X\|$, $\forall X$ or, at least, that the norm $\|\Psi[X]\|$ is neither zero nor divergent for all operators X. As a consequence of this pairing, with dissipative quantum dynamics (and not just coherent dynamics), correlation times of system observables which diverge exponentially with system size can be observed at infinite temperature.

For example, considering the operator $\Psi[\mathbf{1}]$ where $\mathbf{1}$ is the identity, one has

$$\begin{aligned}\frac{1}{2^L}\mathrm{Tr}\left(e^{t\mathcal{L}^*}\left[\left(\Psi[\mathbf{1}]\right)^\dagger\right]\Psi[\mathbf{1}]\right) &\approx \frac{1}{2^L}\mathrm{Tr}\left(\left(\Psi\left[e^{t\mathcal{L}^*}[\mathbf{1}]\right]\right)^\dagger\Psi[\mathbf{1}]\right)\\ &= \frac{1}{2^L}\mathrm{Tr}\left(\left(\Psi[\mathbf{1}]\right)^\dagger\Psi[\mathbf{1}]\right). \end{aligned} \tag{2.16}$$

In the examples of the previous section, the strong zero map is given by $\Psi[X] = \phi_{1/L}X$ or equivalently by $\Psi[X] = X\phi_{1/L}$, and $S = P$.

2.6 Strong Zero Map in an interacting system

The construction of the dissipative strong zero maps (DSZMs) of the previous section is generic and does not depend on the specific model, once the conditions listed in the previous

section are met. So far, however, we have only discussed the case of the TFIM which is in effect a system of non-interacting fermions. To show the more general applicability, we now study the case of an XYZ chain with open boundaries which, in contrast to the TFIM, corresponds to an interacting system.

The Hamiltonian we consider is

$$H_{XYZ} = \sum_{k=1}^{L-1} \sum_{\beta=x,y,z} J_\beta \sigma_k^\beta \sigma_{k+1}^\beta \,, \tag{2.17}$$

with couplings J_β which in principle can be different for the three components $\beta = x, y, z$. Furthermore, we consider dissipative dynamics, Eq. (2.8), with dephasing acting on the last site of the lattice, that is, with jump operators (2.9) with $\Gamma_i = \Gamma \delta_{i,L}$.

Figure 2.7 shows the comparison between the boundary correlation function $C_\infty(t)$ for the case where dynamics is unitary generated by Eq. (2.17) and the case where there is dephasing on the last site. From Ref. [33] we know that in the unitary case, the existence of a SZM in the XYZ model, ϕ_{XYZ}, gives rise to long coherence time (see black curve in Fig. 2.7), for analogous reasons to what occurs in the TFIM case. From the explicit expression of ϕ_{XYZ} given in [33], we know that this operator anti-commutes with the parity operator P (which is also a symmetry of the Lindblad generator), and almost commutes with the Lindblad generator. Thus, the conditions listed in the previous section are met and the map $\Psi_{XYZ}[X] = \phi_{XYZ} X$ is, also in this case, a good DSZM. The corresponding correlator in the dissipative case is shown as the red curve in Fig. 2.7. Due to the existence of a DSZM, as in the TFIM case (cf. Fig. 2.4), we expect the existence of long correlation times, as it is indeed shown in Fig. 2.7. We further notice that also in this case the characteristic life-time of the autocorrelator for the first edge spin is actually enhanced due to dissipation at the opposite edge. The inset to Fig. 2.7 shows moreover that the complex spectrum of the Lindbladian is paired (approximately for the finite system shown, but the splitting will vanish exponentially in system size) between even and odd eigenstates of $\mathcal{L}$.

2.7 Discussion

In this chapter we have considered the stability of strong zero modes in quantum chains with open boundaries. Our central result is that local dissipation can significantly enhance the correlation time of boundary spins. On the one hand this is surprising, as dissipation often acts to suppress memory of initial states as it tends to open up relaxation channels beyond those existing in its absence. We find that for both the non-interacting transverse field Ising model and for the interacting XYZ model, dephasing at one end of an open chain increases the correlation time of spins at the opposite end. This observation led us to define disspative strong zero maps, corresponding to superoperators that play the role in the case of dissipative (and Markovian) dynamics of the strong zero mode operators present in the unitary case.

Chapter 3

Strong zero modes in a class of generalised Ising spin ladders with plaquette interactions

This chapter is the second of two chapters that together make up the first part of the thesis on strong zero modes. In this chapter we study a class of spin-1/2 quantum ladder models with generalised plaquette interactions in the presence of a transverse field. We show that in certain parameter regimes these models have strong zero modes responsible for the long relaxation times of edge spins. By exploiting an infinite set of symmetries in these systems, we show how their Hamiltonians can be represented, in each symmetry sector, by a transverse field Ising chain. Due to the presence of an extensive number of conserved quantities, even if the original system has no disorder, most of these symmetry sectors feature a quasi-random transverse field profile. This representation of the ladder system in terms of a disordered Ising chain allows to explain the features of the edge autocorrelation function of the original system. Furthermore, we find what appears to be a novel mechanism for slow decorrelation: even in parameter regimes where the full ladder model does not possess an obvious strong zero mode, some of the initial information stored in the edge spins can be preserved for long times as a consequence of the existence of strong zero modes within individual symmetry sectors. The work discussed in this chapter appeared in the publication:

"Strong zero modes in a class of generalized Ising spin ladders with plaquette interactions"
L. M. Vasiloiu, F. Carollo, M. Marcuzzi and J. P. Garrahan
Physical Review B **100**, 024309 (2019).

3.1 Introduction

Many-body quantum systems can display slow relaxation and long correlation times due to collective dynamical effects. Slow dynamics and non-ergodicity in quantum systems is receiving much attention nowadays both from the experimental and the theoret-

ical side within physics. From a practical perspective, the existence of long time-scales in the dynamics is of interest as it can be related to the possibility of maintaining long coherence times for localised degrees of freedom in many-body systems, with the technological potential for storing and processing quantum information encoded in many-body states [35,38–40,58,59]. On the other hand, the behavior displayed by these systems is connected with topics of fundamental interest in physics such as prethermalization [37,60–62], phase transitions [33] and the existence of topological phases of matter [34,36,63].

Long relaxation time-scales can arise in a variety of physical scenarios. Concrete examples include many-body systems in the presence of disorder leading to many-body localisation [64–74] and metastability in open quantum systems [75–77]. In this thesis we focus on another area where long timescales emerge, quantum systems with free boundaries with so-called strong zero modes (SZMs) [32–37]. Namely, a SZM is an operator which commutes with the dynamical generator up to exponentially small corrections in the system size, the paradigmatic example [32] being the one-dimensional transverse field Ising model (TFIM) with free boundaries [1,5]: in the ferromagnetic phase, one can explicitly construct the SZM operators in an iterative manner and express them as a sum of Majorana fermions [32]. The existence of a SZM operator implies the slow relaxation of certain boundary modes, for example giving rise of coherence times that grow exponentially in system size for edge spins in the TFIM [32,34]. SZMs can also be related to a slow logarithmic-in-time growth of the entanglement entropy [78]. More recently, the possibility of observing SZMs in open settings has also been discussed [40, 54], which connects to the more general question of protection of coherences from dissipation [53, 56, 57]. For instance, as seen in chapter 2, properly engineered dissipation can increase edge coherence times in spin chains with open boundaries beyond those of the non-dissipative case.

In this chapter we consider SZMs in a simple generalisation of the TFIM. We consider a class of ladder spin systems with plaquette interactions. Figure 3.1 describes the class of models we study. The arrangement for an "M-leg ladder" is that of M parallel chains of length L with a qubit on each site. The interactions are along the z direction involving the product of all sites within one rung of the ladder and the ones on the rung immediately next to it, see the shaded regions in Fig. 3.1 (details are given in section 3.2). The system is also subject to a magnetic field on each site in the transverse direction.

In section 3.3 we show how to explicitly construct the SZMs in these systems. As we shall see, similarly to what happens in other models [32,33], the normalisation of the SZMs diverges as the strength of the transverse field approaches a critical value for which the ladder models display a quantum phase transition. We then tackle the same class of systems from a different perspective: we identify an extensive set of symmetries of the ladder Hamiltonians which allows us to block-diagonalise them, with each symmetry sector described by a one-dimensional TFIM. Due to the presence of the symmetries, most sectors in general will manifest quasi-randomness in the transverse field. This is another example of how a clean system can mimic the presence of spatial disorder in the Hamiltonian due to a large set of conserved quantities, *cf.* Refs. [79, 80]. We exploit this quasi-random picture to explain the behavior of the autocorrelations of the edge spins in the infinite temperature state. In addition, the block structure of the Hamiltonian—together with the

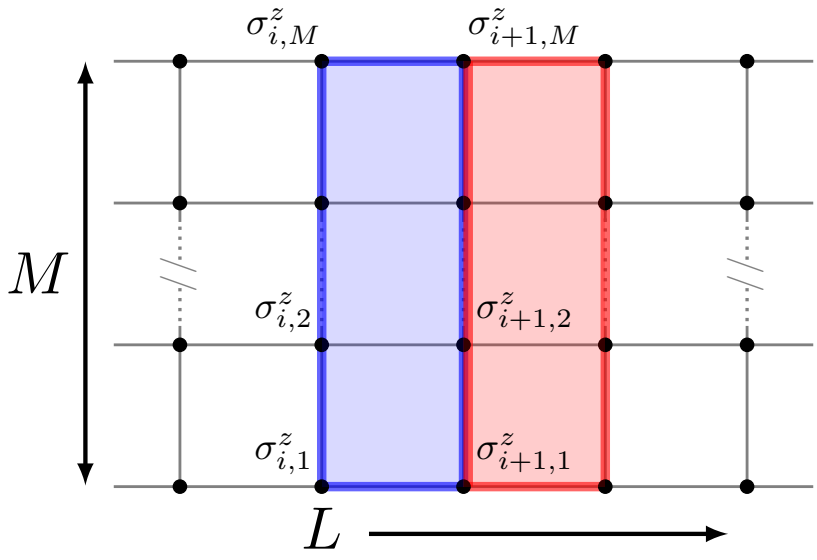


Figure 3.1: Quantum M-leg ladder model with plaquette interactions. Spins $\sigma^\mu_{i,k}$, located at the vertices of an $L \times M$ lattice ($i = 1, \ldots, L; k = 1, \ldots, M$), are subject to a transverse field in the x direction. Interactions (along the z direction) between spins are given by the product of all spin operators $\sigma^z_{i,k}$ in two neighbouring rungs of the ladder. Concretely, each plaquette is associated with $2M$ spins and the interaction is given by the product $\prod_{k=1}^{M} \sigma^z_{i,\,k}\, \sigma^z_{i+1,\,k}$. Two such plaquette interactions are shown as the shaded areas in the sketch.

quasi-randomness of the effective transverse field in the various sectors—makes apparent how it is possible to observe the existence of SZMs only in certain symmetry sectors. Interestingly, in certain parameter regimes this can lead to the long coherence times for the edge spins even when the full system does not possess a SZM. This appears to be a novel mechanism for obtaining long correlation times.

3.2 M-leg spin-1/2 ladder

In this section we define the class of models we study. We consider spin systems which consist of a lattice of M parallel chains of L sites each, arranged in such a way that the i-th sites of all the chains lie on a segment which is perpendicular to the chains themselves, *cf.* Fig. 3.1. Each site of this lattice carries a spin-1/2 degree of freedom, and we use the notation $\sigma^\mu_{i,k}$ for the local Pauli matrix in the direction μ acting on the i-th site of the k-th chain.

As stated in the introduction 3.1 of this chapter, the Hamiltonian of the system is a generalisation of the TFIM Hamiltonian (1.1) which we define in the following way

$$H = -J \sum_{i=1}^{L-1} Z_i Z_{i+1} \; - h \sum_{i=1}^{L} S^x_i, \tag{3.1}$$

with

$$Z_i = \prod_{k=1}^{M} \sigma^z_{i,k}, \tag{3.2}$$

and

$$S^\mu_i = \sum_{k=1}^{M} \sigma^\mu_{i,k}, \tag{3.3}$$

where the field strength h and coupling strength J are non-negative. The term proportional to h represents the uniform transverse magnetic field, while the terms in the first sum appearing in Eq. (3.1) represent longitudinal magnetic plaquette interactions between neighboring rungs of the ladder—as illustrated in Fig. 3.1. Notice that the TFIM is recovered when $M = 1$.

For the whole M-leg ladder model we can define a parity operator

$$\mathcal{F} = \prod_{i=1}^{L} \prod_{k=1}^{M} \sigma^x_{i,\,k}, \tag{3.4}$$

which implements a discrete $\mathbb{Z}_2$ spin-flip symmetry. When $M > 1$, however, one can also decompose such a parity operator into the product of single chain parity operators

$$\mathcal{F}_k = \prod_{i=1}^{L} \sigma^x_{i,\,k}, \tag{3.5}$$

with $\mathcal{F} = \prod_k \mathcal{F}_k$.

One can easily check that

$$[H, \mathcal{F}_k] = 0 \quad \forall k, \tag{3.6}$$

so that

$$[H, \mathcal{F}] = 0. \tag{3.7}$$

This implies that an eigenstate $|\varphi\rangle$ of H can be chosen to be a simultaneous eigenvector of all the $\mathcal{F}_k$,

$$\mathcal{F}_k|\varphi\rangle = \beta_k|\varphi\rangle\,, \text{with}\, \beta_k = \pm 1\,,$$

and we can decompose the Hilbert space into parity sectors $\mathbb{P}_{\vec{\beta}}$, with $\vec{\beta} = (\beta_1, \beta_2, \ldots, \beta_M)$, which are mapped onto themselves by the action of the system Hamiltonian.

3.3 Strong zero modes in M-leg ladders

After having introduced the class of models we consider in section 3.2, we will now proceed to show that they feature, in certain parameter ranges, SZMs. We first review the definition of a SZM [32–34], and then explicitly construct the SZMs for the M-leg ladders.

A SZM Ψ is an operator which almost commutes with the Hamiltonian, $\|[H, \Psi]\| \approx \epsilon_L$, with a correction term ϵ_L which is exponentially decaying with the size L of the system.

Usually, such an operator is also required to anticommute with a parity operator P, commuting with the Hamiltonian $[P, H] = 0$. When this is the case, the SZM is an operator that maps an eigenstate of the Hamiltonian in one of the two parity sectors into an eigenstate in the other sector. The two mapped states are split in energy by ϵ_L, and since this mapping occurs across the energy spectrum this guarantees the existence of long coherence times.

For general M-leg ladder models, however, due to the presence of a larger number of parity sectors, $\mathbb{P}_{\vec{\beta}}$, the situation is more subtle. Indeed, as we show below, SZM operators for this class of systems obey

$$\{\Psi, \mathcal{F}_k\} = 0\,, \forall\, k\,. \tag{3.8}$$

In terms of the parity operator for the whole system, $\mathcal{F}$, one then has

$$\begin{cases} [\Psi, \mathcal{F}] = 0 & M \text{ even} \\ \\ \{\Psi, \mathcal{F}\} = 0 & M \text{ odd}\,. \end{cases} \tag{3.9}$$

While the commutation/anticommutation relations of the SZM with $\mathcal{F}$ are not of help to understand the action of the SZM on eigenstates of the Hamiltonian, the properties expressed in Eq. (3.8) can be used to show that it connects eigenstates and eigenvalues of the Hamiltonian in the parity sector $\mathbb{P}_{\vec{\beta}}$ with those of $\mathbb{P}_{-\vec{\beta}}$. To show this, lets assume $|\varphi\rangle$ to be an eigenvector of the Hamiltonian associated to an eigenvalue λ_φ belonging to the parity sector $\mathbb{P}_{\vec{\beta}}$. One then has that the vector $\Psi|\varphi\rangle$ is an eigenvector of the Hamiltonian:

$$H\Psi|\varphi\rangle = \lambda_\varphi \Psi|\varphi\rangle + O(\epsilon_L)\,, \tag{3.10}$$

where we have used the fact that the SZM commutes with the Hamiltonian up to terms of order ϵ_L exponentially small in system size. In addition, exploiting the anticommutation relations of the SZM with the parities $\mathcal{F}_k$ one has that

$$\mathcal{F}_k \Psi\,|\varphi\rangle = -\beta_k \Psi\,|\varphi\rangle\ , \forall k\,,$$

showing indeed that $\Psi\,|\varphi\rangle \in \mathbb{P}_{-\vec{\beta}}$. Summarizing, this means that for large system sizes the spectrum of the Hamiltonian H gets paired up between corresponding parity sectors $\mathbb{P}_{\vec{\beta}} \leftrightarrow \mathbb{P}_{-\vec{\beta}}$. For explicit examples we refer to section 3.3.1.

After having discussed the consequences of the existence of the SZM on the spectral properties of the ladder Hamiltonian we now provide its explicit form, from which we can recover the properties described in the previous discussion. As in the case of the TFIM [32], for general M-leg ladder models the SZM can be written as a sum of operators

$$\Psi = \sum_{j=1}^{L} \psi_j\,, \tag{3.11}$$

where the ψ_j are given by

$$\psi_j = \left(\frac{h}{J}\right)^{j-1} \prod_{i=1}^{j-1} S_i^x\, Z_j\,. \tag{3.12}$$

Notice that the terms ψ_j appearing in the SZM are almost Majorana operators for $M \neq 1$: while they anticommute, $\{\psi_j, \psi_i\} = 0$ for $i \neq j$, for $i = j$ the anticommutator is not a multiple of the identity (yet commutes with any other term ψ_k).

The first and most important property to be shown is that this operator Ψ almost commutes with the Hamiltonian. To do this we note that the Hamiltonian can be split in two parts: one describing the magnetic interaction between spins around plaquettes, $H_0 \propto \sum_j Z_j Z_{j+1}$, and the other describing the effects of the transverse magnetic field $H_1 \propto \sum_j S_j^x$. Thus, we can write the commutator of the Hamiltonian with the SZM in the following way

$$\begin{aligned}[H, \Psi] &= \sum_{j=1}^{L} \left([H_0, \psi_j] + [H_1, \psi_j]\right) \\ &= \sum_{j=1}^{L-1} (A_{j+1} + B_j) + B_L,\end{aligned} \tag{3.13}$$

where we introduced the quantities $[H_0, \Psi_j] = A_j$ and $[H_1, \Psi_j] = B_j$, and used $[H_0, \Psi_1] = A_1 = 0$. We show in section 3.3.2 that this is a telescoping series, namely $A_{j+1} + B_j = 0, \forall j$, therefore the only contribution to the commutator comes from the term B_L with norm $\|B_L\| \approx 2J\alpha^L$, where $\alpha = Mh/J$. This thus proves that the operator defined in Eq. (3.11) almost commutes with the Hamiltonian up to a factor that scales as α^L. When $\alpha < 1$ the correction to the commutator becomes exponentially small with system size.

The almost commutation of the SZM with the ladder Hamiltonian can be used to show the slow relaxation of coherences for the edge spins. Indeed, when $\alpha < 1$, one can notice from Eq. (3.12) that the SZM is highly localised around the first rung of the ladder. In particular, when $h \ll J$, one has that the SZM is $\Psi \approx Z_1$ up to corrections of order h: thus exploiting the fact that this SZM almost commutes with the Hamiltonian one can show (in the same way as it happens for the TFIM [32]) that the infinite temperature autocorrelation function

$$C_\infty(t) := \frac{1}{2^{ML}} \operatorname{Tr}\left(Z_1(t) Z_1\right) \approx 1\,, \tag{3.14}$$

up to times of the order $\tau \approx \alpha^{-L}$. We will discuss the behaviour of the autocorrelation in detail in the section 3.6.

3.3.1 Pairing due to the SZM

In this section we provide some examples regarding the pairing of the spectrum due to the existence of SZMs. For $M = 1$ we recover the usual one dimensional TFIM, where the SZM Ψ (*cf.* Eq. (2.5)) anticommutes with the parity operator $\mathcal{F}$ (3.4) (*cf.* Eq. (2.4)) and it maps the spectrum in the odd sector to that in the even sector up to corrections exponentially small in system size [32]. If $|\varphi_+\rangle$ is an eigenvector of the Hamiltonian associated with the eigenvalue λ_+ belonging to the parity sector $\mathbb{P}_+$ then one can show that $\Psi|\varphi_+\rangle$ is

an eigenvector of the Hamiltonian associated with an eigenvalue λ_-, exponentially close in system size to λ_+, belonging to the parity sector $\mathbb{P}_-$

$$H\left|\varphi_+\right\rangle = \lambda_+\left|\varphi_+\right\rangle, \quad H\Psi\left|\varphi_+\right\rangle \approx \lambda_+\Psi\left|\varphi_+\right\rangle,$$

$$\mathcal{F}\left|\varphi_+\right\rangle = \left|\varphi_+\right\rangle, \quad \mathcal{F}\Psi\left|\varphi_+\right\rangle = -\Psi\left|\varphi_+\right\rangle .$$

For $M = 2$ the Hamiltonian commutes with the single chain parity operators $\mathcal{F}_1$ and $\mathcal{F}_2$ meaning that we can organize its eigenstates in four sectors $\mathbb{P}_{++}, \mathbb{P}_{+-}, \mathbb{P}_{-+}, \mathbb{P}_{--}$. Given an eigenstate of the Hamiltonian $\left|\varphi_{\beta_1,\beta_2}\right\rangle$ belonging to a parity sector $\mathbb{P}_{\beta_1,\beta_2}$ with $\beta_i = \pm$, and corresponding to an eigenvalue $\lambda_{\beta_1,\beta_2}$, one can show that the SZM Ψ is mapping this vector onto an eigenstate of the Hamiltonian belonging to the parity sector $\mathbb{P}_{-\beta_1,-\beta_2}$. Indeed, exploiting the anticommutation relations of the SZM with $\mathcal{F}_i$ we have that

$$\begin{aligned} \mathcal{F}_1\Psi\left|\varphi_{\beta_1,\beta_2}\right\rangle &= -\beta_1\Psi\left|\varphi_{\beta_1,\beta_2}\right\rangle , \\ \mathcal{F}_2\Psi\left|\varphi_{\beta_1,\beta_2}\right\rangle &= -\beta_2\Psi\left|\varphi_{\beta_1,\beta_2}\right\rangle , \end{aligned} \tag{3.15}$$

and because of the almost commutation relation of the SZM with the Hamiltonian we have that $H\Psi\left|\varphi_{\beta_1,\beta_2}\right\rangle \approx \lambda_{\beta_1,\beta_2}\Psi\left|\varphi_{\beta_1,\beta_2}\right\rangle$. The latter relation shows that $\lambda_{\beta_1,\beta_2}$ is exponentially close to an eigenvalue in the parity sector $\mathbb{P}_{-\beta_1,-\beta_2}$.

When $M > 2$ the number of parity sectors increases as 2^M but with the same steps illustrated above one can show that the SZM pairs the spectrum of H in the sector $\mathbb{P}_{\vec{\beta}}$ with that in $\mathbb{P}_{-\vec{\beta}}$.

3.3.2 Derivation of the SZM for the ladder system

In this section we first derive the compact expression of the SZM for the ladder model following the iterative procedure used in [32, 33] and then we show that the correction term to the commutator of the SZM with the system Hamiltonian is exponentially small in system size.

In order to obtain a compact expression for the SZM we start by noticing that the Hamiltonian can be split in two parts

$$H_0 = -J\sum_{i=1}^{L-1}\prod_{k=1}^{M}\sigma^z_{i,k}\,\sigma^z_{i+1,k}\,, \tag{3.16}$$

and

$$H_1 = -h\sum_{i=1}^{L}\sum_{k=1}^{M}\sigma^x_{i,k}\,, \tag{3.17}$$

such that $H = H_0 + H_1$. We set the zeroth order contribution to the SZM to be $\Psi_1 = \prod_{k=1}^{M} \sigma^z_{1,k}$ since it commutes with H_0, $[H_0, \Psi_1] = 0$. Ψ_1 does not commute with H_1 though

$$[H_1, \Psi_1] = 2ih\Bigg(\sigma^y_{1,1} \prod_{k=2}^{M} \sigma^z_{1,k} + \sigma^y_{1,2} \prod_{k=1,k\neq 2}^{M} \sigma^z_{1,k} + \sigma^y_{1,3} \prod_{k=1,k\neq 3}^{M} \sigma^z_{1,k}\Bigg),$$

therefore we need to find a correction of order h to the SZM that cancels $[H_1, \Psi_1]$ when commuted with H_0; $\Psi_2 = (h/J)\left(\sum_{k=1}^{M} \sigma^x_{1,k}\right) \prod_{k=1}^{M} \sigma^z_{2,k}$ works fine since

$$[H_0, \Psi_2] = -\left[H_1, \Psi_1\right].$$

Now the commutator of Ψ_2 with H_1 will generate a contribution of order h^2 which can be canceled by a third correction to the SZM of order h^2. Following this pattern it is easy to show that if the SZM has the following compact form

$$\Psi = \sum_{j=1}^{L} \left(\frac{h}{J}\right)^{j-1} \prod_{i=1}^{j-1} \left(\sum_{k=1}^{M} \sigma^x_{i,k}\right) \prod_{k=1}^{M} \sigma^z_{j,k}\,, \tag{3.18}$$

then the norm of the error term to the commutator decays exponentially with system size, namely $\| [H, \Psi] \| \approx \alpha^L$ where $\alpha = Mh/J$.
In order to prove this last statement and the form of Eq. (3.18) we write the commutator, as mentioned in the main text, as a telescoping series

$$[H, \Psi] = \sum_{j=1}^{L-1} (A_{j+1} + B_j) + B_L\,, \tag{3.19}$$

and we now show that $A_{j+1} = -B_j, \forall j$, meaning that the only contribution to the commutator comes from the term B_L. We start by evaluating the term $B_j = [H_1, \Psi_j]$. Using the fact that Pauli matrices on different sites act on different spin states we can see that the only non zero contribute to this commutator is the one when $\sigma^x_{i,k}$ and $\sigma^z_{j,n}$ act on the same site, that is $i = j$

$$B_j = [H_1, \Psi_j] = -J \left(\frac{h}{J}\right)^{j} \prod_{l=1}^{j-1} \left(\sum_{n=1}^{M} \sigma^x_{l,n}\right) \times \left[\sum_{k=1}^{M} \sigma^x_{j,\,k}\,, \prod_{n=1}^{M} \sigma^z_{j,n}\right].$$

On the other hand when we evaluate the term $A_{j+1} = [H_0, \Psi_{j+1}]$, we observe that all the plaquette terms of H_0 commute with Ψ_{j+1} except the $j-$th plaquette

$$A_{j+1} = [H_0, \Psi_{j+1}] = -J \left(\frac{h}{J}\right)^j \left[\prod_{k=1}^{M} \sigma^z_{j,k}, \prod_{l=1}^{j} \sum_{n=1}^{M} \sigma^x_{l,n}\right]$$
$$= -J \left(\frac{h}{J}\right)^j \prod_{l=1}^{j-1} \left(\sum_{n=1}^{M} \sigma^x_{l,n}\right)$$
$$\times \left[\prod_{k=1}^{M} \sigma^z_{j,k}, \sum_{n=1}^{M} \sigma^x_{j,n}\right]$$

therefore

$$A_{j+1} + B_j = 0, \forall j.$$

To show that the norm of B_L decays exponentially with system size we note that, from all the terms of H_1, only the one at site (j,k) gives non zero contribute

$$[H_1, \Psi_j] = \left[-h \sum_{k=1}^{M} \sigma^x_{j,k}, \Psi_j\right]$$

and knowing that $\| [A,B] \| \leq 2\|A\|\|B\|$ and $\|\Psi_j\| \leq (h/J)^{j-1} M^{j-1}$ we get

$$\|B_L\| = \| [H, \Psi] \| = \| [H_1, \Psi_L] \| \approx 2J\alpha^L ,$$

with $\alpha = Mh/J$.

3.4 Norm of Ψ and relation to phase transitions

An important property for the SZM is that it must be normalisable. Indeed, if this were not true it would not be possible to give a meaning to the manipulations described in the previous section. In this section we prove the conditions under which the SZM operator has finite norm, i.e., the sum in Eq. (3.11) converges. We will also show that the point at which the norm of the SZM becomes unbounded, the ground state of the system undergoes an Ising-type phase transition. This seems to provide further evidence of the relation between existence of SZM and the occurrence of phase transitions in quantum Hamiltonian systems [33].

To compute the norm of the SZM, *cf.* Eq. (3.11), we make use of the anticommutation relations, $\{\psi_i, \psi_j\} = 0$, $\forall i \neq j$, and we express the square of the SZM as $\Psi^2 = \sum_{i=1}^{L} \psi_i^2$, with

$$\psi_i^2 = \left(\frac{h}{J}\right)^{2(i-1)} \prod_{k=1}^{i-1} (S^x_k)^2 .$$

Since all terms in Ψ^2 commute among themselves we can compute the norm as

$$\|\Psi\| = \sqrt{\|\Psi^2\|} = \left(\frac{1-\alpha^{2L}}{1-\alpha^2}\right)^{1/2} . \tag{3.20}$$

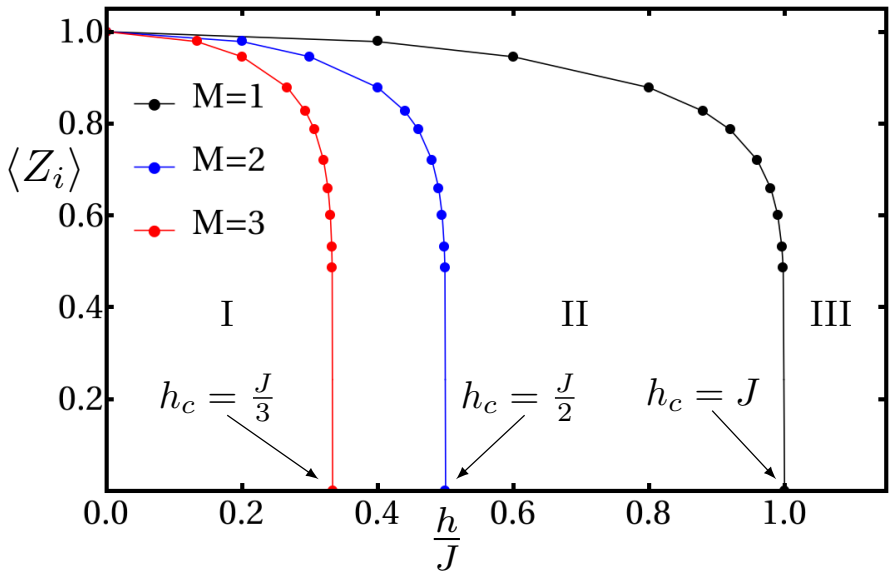


Figure 3.2: Phase transition in the ladder model for different values of M. The order parameter is the expectation value in the ground state of the product of the magnetization operators along the z direction for the single rungs of the ladder, $\langle Z_i \rangle$. When $M = 1$ (TFIM case) the transition occurs at $h_c = J$. For general values of M the transition is shifted to $h_c = J/M$. We show here results for $M = 1, 2, 3$ obtained by means of infinite time-evolving block decimation algorithms [81–84].

From the above equation it is clear that the SZM is normalisable for $\alpha < 1$. On the other hand, one can show that the ladder model undergoes a quantum phase transition when the transverse field approaches the critical value $h_c = J/M$, corresponding to $\alpha = 1$.

The order parameter for an M-leg ladder system is the expectation value in the ground state of the product of operators along the z direction for a rung of the ladder, $\langle Z_i \rangle$ (which generalises the order parameter of the TFIM). In Fig. 3.2 we plot the order parameter as a function of magnetic field for different values of M: we see that the point at which the eigenstates pairing due to the SZM disappears is the same value of the transverse field for which the quantum phase transition in the ground state of the Hamiltonian takes place [33].

3.5 Quasi-random Ising chains from the ladder model

In this section we show how the Hamiltonian for the ladder model can be decomposed into a direct sum of Ising Hamiltonians with a transverse field that can mimic the presence of randomness in the chain. In order to achieve this, in the spirit of [79], we characterize an extensive set of conserved quantities which we can then use to decompose the Hamiltonian in the various blocks identified by the conserved charges.

The first step thus consists in finding the above mentioned symmetries of the Hamiltonian. This can be achieved by directly inspecting the operator $S_i^2 = (S_i^x)^2 + (S_i^y)^2 + (S_i^z)^2$, proportional to the total angular momentum in each rung of the ladder, and also the square

of the magnetization along the x direction $(S_i^x)^2$. One can check that

$$\begin{aligned} \left[S_i^2, H\right] &= 0\,, \quad \forall i\,, \\ \left[(S_i^x)^2, H\right] &= 0\,, \quad \forall i\,. \end{aligned} \tag{3.21}$$

The existence of these conserved quantities allows us to represent the original ladder Hamiltonian in a simultaneous eigenbasis of S_i^2 and $(S_i^x)^2$ in the various symmetry sectors identified by the quantum numbers of S_i^2 and $(S_i^x)^2$.

We thus need to identify these values and to understand the action of the Hamiltonian on their eigenstates. From the definition of S_i^x and S_i^2 it is clear that we are dealing with the coupling of M spin-1/2 systems along each vertical column characterized by the index i. Therefore, the possible eigenvalues s_i^2 of S_i^2 are

$$s_i^2 = 4\ell(\ell+1), \tag{3.22}$$

where the factor 4 comes from the fact that we have defined S_i^2 in terms of Pauli matrices and not in terms of spin operators. Moreover $\ell_{\min} \leq \ell \leq \ell_{\max}$, where $\ell_{\max} = M/2$, while $\ell_{\min} = 0$ if M is even and $\ell_{\min} = 1/2$ if M is odd. For a fixed irreducible representation of the total angular momentum where $S_i^2 = 4\ell(\ell+1)$ one can also recover the possible quantum numbers of $(S_i^x)^2$ noticing that the eigenvalues of the magnetization along the x direction, s_i^x, belong to the set $[-2\ell, -2\ell+2, \ldots, 2\ell-2, 2\ell]$.

Thus, in the sector identified by the choice $(s_i^2, (s_i^x)^2)$ for the conserved quantum numbers, the ith rung of the ladder can be represented by means of a two-level system with states $|+\rangle$, $|-\rangle$ defined such that

$$S_i^2|\pm\rangle = s_i^2|\pm\rangle\,, \qquad S_i^x|\pm\rangle = \pm s_i^x|\pm\rangle\,, \tag{3.23}$$

if $s_i^x \neq 0$. In turn, when $s_i^x = 0$ (only possible for M even) the dimension of the irreducible representation of the angular momentum is one and the rung is described by a single state $|0\rangle$, such that $S_i^x|0\rangle = 0$.

In order to complete the mapping from the ladder to the chain, we need to understand the action of Z_i in the reduced space for the rung i identified by a choice of the conserved numbers. From the fact that Z_i anticommutes with S_i^x, one easily gets

$$Z_i|\pm\rangle = |\mp\rangle\,,$$

while, if $s_i^x = 0$ then $Z_i|0\rangle = \pm|0\rangle$, where the sign depends on the symmetric/antisymmetric property of the singlet $|0\rangle$. These considerations thus point to the fact that for a choice of the conserved quantum numbers $(s_i^2, (s_i^x)^2)$ the single rung operators are mapped onto

$$\begin{aligned} S_i^x = s_i^x\,\tau_i^x,\ Z_i = \tau_i^z \qquad & \text{if } s_i^x \neq 0\ ; \\ S_i^x = 0,\ Z_i = \pm 1 \qquad & \text{if } s_i^x = 0\ , \end{aligned} \tag{3.24}$$

where τ_i^μ are auxiliary Pauli matrices.

The last thing that one needs to clarify in order to show how the ladder Hamiltonian can be reduced to an Ising model one with quasirandom potential, is the multiplicity of the different values of the Hamiltonian quantum numbers. Such an information can be recovered from the Clebsch−Gordan decomposition series [85]. Indeed, we need to iteratively compose M spin-1/2 systems and to consider all the irreducible representations arising from this procedure; the above mentioned series takes into account the fact that, each time a spin-1/2 system is added to an irreducible representation, we obtain two irreducible representations, one with dimension increased by one and the other with dimension decreased by one with respect to the original representation.

The Clebsch−Gordan series is the following

$$\mathbf{2}^{\otimes M} = \bigoplus_{k=0}^{\lfloor \frac{M}{2} \rfloor} \left(\frac{M+1-2k}{M+1} \binom{M+1}{k} \right) (\boldsymbol{M+1-2k}) \,,$$

where $\lfloor \frac{M}{2} \rfloor$ is the integer floor function and $\binom{x}{y}$ is the binomial coefficient; it shows the dimension of the irreducible representations in the Clebsch−Gordan reduction of S_i^2 (boldface factor on the right side of the above equation) together with their multiplicity given by the first factor in the direct sum.

The dimension of the representation and the value $s_i^2 = 4\ell(\ell+1)$ are connected through the relation $\ell = (M-2k)/2$; therefore we can say that the eigenvalue $s_i^2 = 4\ell(\ell+1)$ of S_i^2 appears with a multiplicity κ_ℓ

$$\kappa_\ell = \frac{2\ell+1}{M+1} \binom{M+1}{\frac{M-2\ell}{2}} .$$

We can also recover all possible values of $|s_i^x|$: these are in the form $|s_i^x| = M-2k$, with $0 \leq k \leq \lfloor \frac{M}{2} \rfloor$ and can appear with a multiplicity ν_{M-2k} that can be derived from the multiplicity of the irreducible representations in the following way

$$\nu_{M-2k} = \sum_{m=0}^{k} \frac{M+1-2m}{M+1} \binom{M+1}{m} ; \tag{3.25}$$

namely, to find how many times the value $M-2k$ can appear for $|s_i^x|$, we need to count all possible irreducible representations containing that specific value. An explicit example is provided in the appendix B.

In the next subsections we use these findings to map the Hamiltonian of the system into an Ising-like Hamiltonian for a generic symmetry sector identified by fixing the quantum numbers s_i^2 and $(s_i^x)^2$ for all rungs in the ladder. The two cases, M odd and M even, present a substantial difference so that we will treat them separately.

3.5.1 Block decomposition of the ladder Hamiltonian for M odd

When the number of spins on each rung M is odd, for any choice of the conserved quantities S_i^2 and $(S_i^x)^2$, columns in the ladder behave like two-level systems, *cf.* Eq. (3.24).

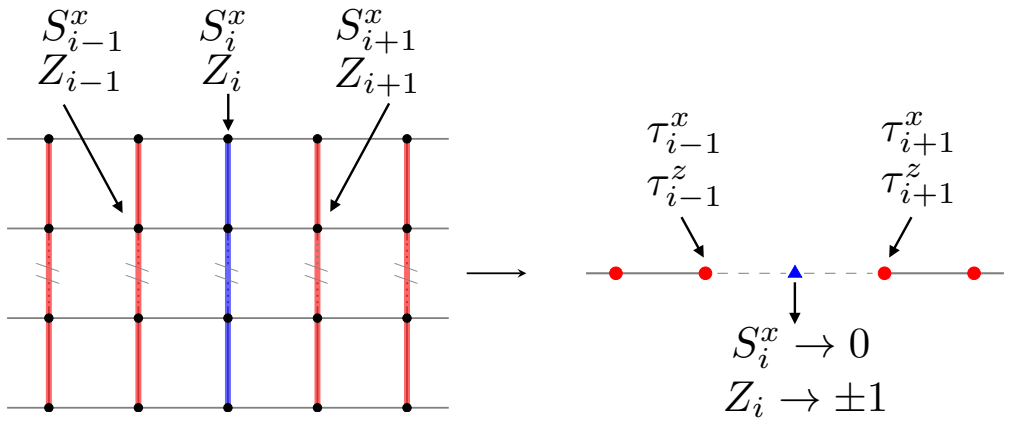


Figure 3.3: Mapping of the ladder model for even M with $(S^x_i)^2 = 0$ in one rung. The representative operators, appearing in the Hamiltonian, for each rung are Z_i and S^x_i; when $(S^x_i)^2 \neq 0$ (red color) these operators are mapped into operators proportional to Pauli matrices τ^z_i and τ^x_i. On the other hand, when $(S^x_i)^2 = 0$ (blue color) then one has the mapping $S^x_i \to 0$ and $Z_i \to \pm 1$. The Hamiltonian in this sector is simply recovered by substituting the operators Z_i and S^x_i with the appropriate quantities, see Eq. (3.28).

Therefore, by fixing for each rung i a choice of the values $(s^2_i, (s^x_i)^2)$, the ladder Hamiltonian can be mapped onto an Ising-like Hamiltonian

$$\tilde{H} = -J \sum_{i=1}^{L-1} \tau^z_i \tau^z_{i+1} - \sum_{i=1}^{L} h_i \tau^x_i, \tag{3.26}$$

where τ^μ_i are the Pauli matrices at site i, and h_i is a transverse magnetic field that has now become site dependent, according to the choice made for $(s^x_i)^2$. Specifically, one has $h_i = h\,|s^x_i|$.

This means that if one randomly selects the values of the conserved quantities for the whole ladder (out of the available possibilities), the resulting Hamiltonian will be an Ising one with uniform coupling constant J and with a transverse magnetic field that in general looks random in space. The values of h_i are distributed independently on each site, and the probabilities follow from the multiplicities of the different values

$$P[h_i = h\,(M - 2k)] = \frac{\nu_{M-2k}}{\sum_{k=0}^{\lfloor \frac{M}{2} \rfloor} \nu_{M-2k}}\,. \tag{3.27}$$

For an explicit example we refer to appendix C.

3.5.2 Block decomposition of the ladder Hamiltonian for M even

When the number of spins M on each rung is even, the situation is slightly more complicated than the one for M odd. While also for this case, fixing for each rung the values $(s^2_i, (s^x_i)^2)$, the ladder Hamiltonian is formally mapped onto an Ising Hamiltonian

[*cf.* Eq. (3.26)], unlike the M odd case, now the site dependent transverse magnetic field h_i can assume also the value 0, when $s_i^x = 0$. Moreover, also Z_i needs to be treated with some extra care: this operator can be mapped onto a Pauli matrix at site i, τ_i^z, when $s_i^x \neq 0$, whereas it is mapped into ± 1 when $s_i^x = 0$; the sign must be consistent with the symmetric or antisymmetric property of the state of the rung with zero magnetization along the x direction. Apart from this, the probability of obtaining a given value of $(s_i^x)^2$ when randomly choosing a sector for the ith rung is still described by Eq. (3.27).

To better understand how the mapping works in this case we now discuss a simple example: let us consider the case where the value $(s_i^x)^2$ is zero only at one site, namely $s_i^x = 0$, and $s_j^x \neq 0 \; \forall j \neq i$. The ladder Hamiltonian is thus mapped onto the following Hamiltonian, see Fig. 3.3,

$$\begin{aligned} \tilde{H} = & - J \sum_{j=1}^{i-2} \tau_j^z \tau_{j+1}^z - J \sum_{j=i+1}^{L-1} \tau_j^z \tau_{j+1}^z - \sum_{j=1}^{i-1} h_j \tau_j^x \\ & - \sum_{j=i+1}^{L} h_j \tau_j^x \pm \left(J \tau_{i-1}^z + J \tau_{i+1}^z \right) . \end{aligned} \tag{3.28}$$

It is clear here that the transverse field for the site i is turned off, and the sign in front of the last term in the above equation is determined by the symmetry property of the state associated to the zero eigenvalue of S_i^x: an antisymmetric state will result in a minus sign while a symmetric one will lead to a plus. Eq. (3.28) also shows that, in this sector, the ladder system is broken up into two separate chains that are disconnected by the i-th site.

Notice that, contrary to the odd case where all sectors have the same dimension 2^L (corresponding indeed to the dimension of a TFIM) in the M even case, the dimension of each sector varies. This can be understood by looking at relations (3.24): whenever one has $(s_i^x)^2 = 0$ on a rung then the dimension of the sector is reduced of a factor 2. As an example in a sector with exactly n rungs assuming a zero value of the magnetization along the x direction, the dimension is 2^{L-n}.

3.6 Long coherence times of boundary spins

In the previous section we have shown how the ladder Hamiltonian assumes a block diagonal form and how, in each of these blocks, it can be represented as an Ising-like Hamiltonian with values of the transverse field that depend on the conserved quantum numbers identifying the chosen sector. In addition, we have characterized the probabilities associated with these different values of the transverse field in the case in which a set of conserved quantities for each rung of the chain is randomly picked; practically speaking a random selection of a set of these conserved quantum numbers can mimic the presence of disorder in the transverse field profile of an open boundary Ising model, with probabilities for the single site fields h_i given by relation (3.27).

Even in the case of inhomogeneous transverse field, as for ordered Ising models, it is possible to construct a SZM operator $\tilde{\Psi}$; one way to proceed is to apply the usual iterative

procedure [32–34]. On the other hand it is also possible to obtain the representation of SZM for the chosen set of conserved quantities directly from Eq. (3.11) exploiting the same relations in Eq. (3.24) used to obtain the Hamiltonian.

Collecting all fixed choices for the quantum numbers $(s_i^2, (s_i^x)^2)$ into a vector $\vec{\omega}$ which now uniquely identifies the symmetry sector of the Hamiltonian, we can write the SZM $\Psi_{\vec{\omega}}$ in the sector as

$$\Psi_{\vec{\omega}} = \sum_{j=1}^{L} \tau_j^z \prod_{k=1}^{j-1} \frac{h_k}{J} \tau_k^x \,. \tag{3.29}$$

We can now make two interesting observations: first, we notice that the condition for the existence of this SZM is less restrictive than the condition implied by Eq. (3.20) for the existence of the SZM in the ladder. Indeed, in this sector one just needs

$$\mathcal{N}_{\vec{\omega}}^2 = \sum_{j=1}^{\infty} \prod_{k=1}^{j-1} \left(\frac{h_k}{J} \right)^2 < \infty$$

which can be true even if $\alpha = Mh/J \geq 1$, namely, the norm of the SZM $\Psi_{\vec{\omega}}$ in the sector is finite even if the norm of the SZM of Eq. (3.11) diverges. One can thus have sectors where a SZM can be defined even if the full system cannot support one. This is illustrated in Fig. 3.2: the region labelled I corresponds to $\alpha < 1$ where the overall system has a SZM; the region labelled II corresponds to $\alpha > 1$ but where some sectors have normalisable SZM operators (3.29); region III is where no sector has SZMs.

The second observation concerns only M even. In this case, the value of $(s_i^x)^2$ can be zero for some rungs of the ladder and this results in the presence of a SZM even in a finite system, *i.e.*, the operator strictly commutes with the Hamiltonian without taking the thermodynamic limit. For instance, if the the first rung of the ladder with $(s_i^x)^2 = 0$ is the m-th one, then, since $S_m^x \to 0$ in this sector, the exact SZM is still given by relation (3.29), but with the sum over the rungs that runs only up to the m-th term. In addition, looking at the term B_L of equation (3.13) the substitution $S_m^x \to 0$ also indicates that the SZM must exactly commute with the Hamiltonian, see section 3.3.2.

These considerations also suggest the general behavior that should be displayed by the infinite temperature autocorrelation function (3.14). Indeed, we can think of the autocorrelator as given by the sum of contributions from all different sectors:

$$C_\infty(t) = \frac{1}{\eta} \sum_{\forall \vec{\omega}} \frac{1}{\dim_{\vec{\omega}}} \mathrm{Tr} \left(e^{it\tilde{H}_{\vec{\omega}}} \tau_1^z e^{-it\tilde{H}_{\vec{\omega}}} \tau_1^z \right) , \tag{3.30}$$

where $\eta = (\sum_{k=0}^{\lfloor \frac{M}{2} \rfloor} \nu_{M-2k})^L$ is the total number of symmetry sectors in which the ladder Hamiltonian can be represented as an Ising-like Hamiltonian, while $\dim_{\vec{\omega}}$ is the dimension of the sector.

Exploiting a perturbative argument where one considers $\alpha \ll 1$, similarly to what is done in [86], we can observe that in each sector the expected behavior of the autocorrelator

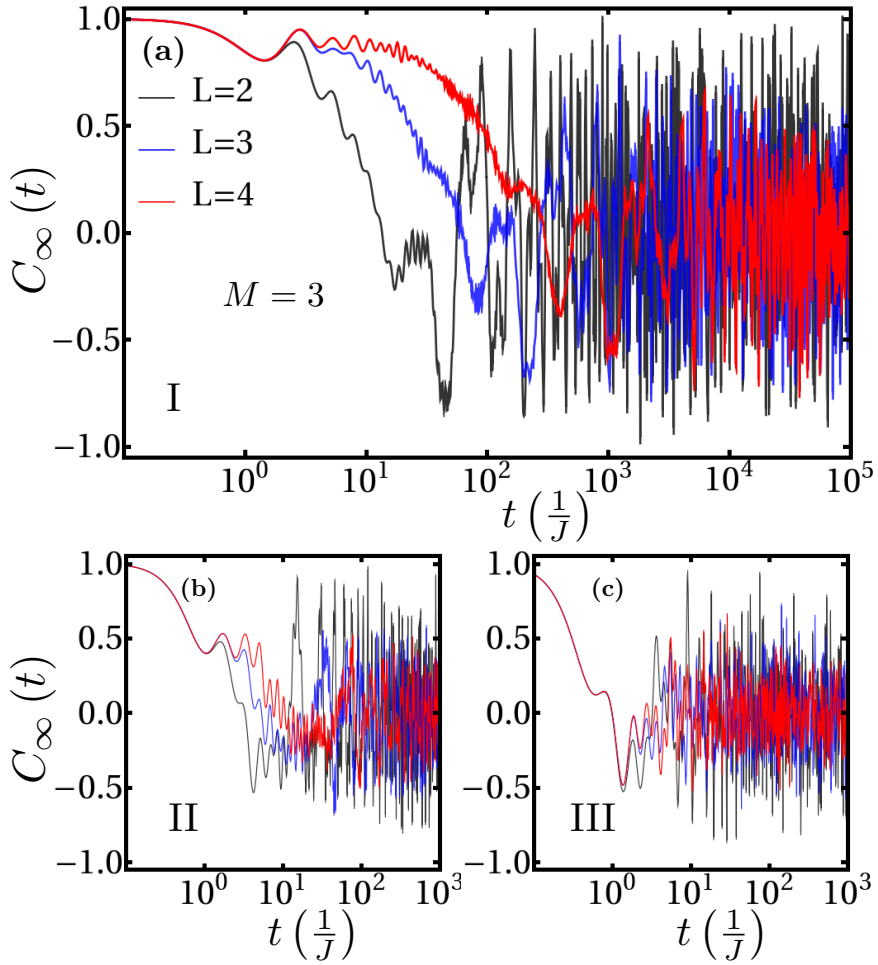


Figure 3.4: Infinite temperature edge autocorrelation from exact diagonalization for M odd. **(a)** Here we have taken $J = 1$ and $h = 0.2$ and compared the behavior of the infinite temperature time correlation functions for the edge spin operator Z_1 [*cf.* Eq. (3.14)] in the ladder model with $M = 3$ for different system sizes. Increasing the length L of the ladder we see how the correlation time increases exponentially. At later times we expect these to approach a zero value with chaotic oscillations that should be damped for larger and larger system sizes. **(b)** For $J = 1$, $h = 0.5$ and same L as in **(a)** the infinite temperature time correlators decay at earlier times compared with those in **(a)** since in this regime only some sectors of the ladder Hamiltonian possess a SZM [*cf.* Fig. 3.2]. **(c)** When $J = 1$ and $h = 1.1$ there is no sector featuring the presence of a SZM and this results in an almost immediate decay of the correlation functions (data shown for the same values of L as in **(a)**). Sectors I, II, III, correspond to those of Fig. 3.2. In the plot time is represented on a log-scale.

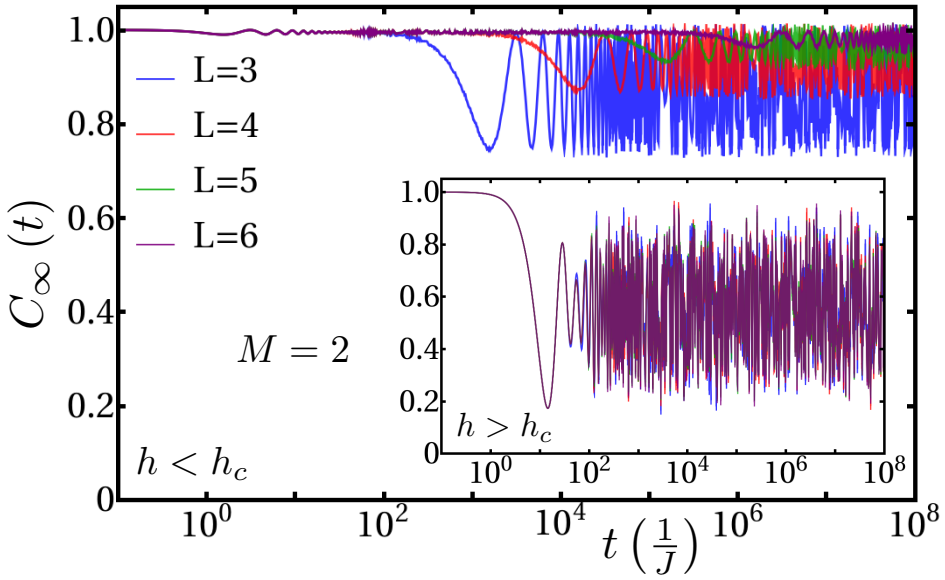


Figure 3.5: Infinite temperature edge autocorrelation from exact diagonalization for M even. In this case we have considered $J = 1$ and $h = 0.05$ and compared the behavior of the infinite temperature time correlation functions for the edge spin operator Z_1 [*cf.* Eq. (3.14)] in the ladder model with $M = 2$ for different system sizes. The value of the autocorrelator is not decaying to zero but actually saturates to a finite value. For the chosen parameters ($\alpha < 1$), the remaining oscillations around this value decrease for increasing system sizes. In the inset we display the behavior of the infinite temperature time correlation functions when $J = 0.05$, $h = 0.05$ (resulting in $\alpha = 2$) and L as in the main figure. In this case, the autocorrelator saturates to a smaller value than in the previous case and the oscillations around this value are not affected by increasing the size of the system. In the plot time is represented on a log-scale.

is given by

$$\frac{1}{\dim_{\vec{\omega}}} \mathrm{Tr}\left(e^{it\tilde{H}_{\vec{\omega}}}\tau_1^z e^{-it\tilde{H}_{\vec{\omega}}}\tau_1^z\right) \approx \cos\left(t\,\Omega_{\vec{\omega}}\right) , \tag{3.31}$$

where

$$\Omega_{\vec{\omega}} = 2J\prod_{k=1}^{L}\left(h_k/J\right) \tag{3.32}$$

is a frequency (exponentially small in the system size) that depends on the profile of the transverse field. In the M odd case, this frequency is never zero for finite systems, and the sum of all possible sectors can be understood as an average over the possible realizations of the transverse field profile. One therefore expects a flat behavior of the total autocorrelator up to time-scales of the order α^{-L} followed by a decay due to the average over all sectors. Indeed, after this time scale, one expects the oscillations due to the different frequencies of all the sectors to eventually become dephased. This trend is shown in Fig. 3.4(a): even if the considered system sizes are small, we see how the edge spins correlation times increase with the system size. After staying almost constant for times of order α^{-L}, the

autocorrelator, rather than displaying stable oscillations as in the TFIM, decays to zero.

In Fig. 3.4(b) we display the same curves for a different value of the ladder transverse field h. In particular, we choose a value of h for which there is no SZM Ψ for the whole ladder system, i.e., the sum in Eq. (3.11) diverges. However, we consider a h small enough such that it is possible to obtain, in some symmetry sector, the SZMs $\Psi_{\vec{\omega}}$ (3.29). This has non-trivial consequences: while the absence of the SZM Ψ would imply that the full information stored in the boundary spins is rapidly lost, $\Psi_{\vec{\omega}}$ has the capability of preserving some of this information—namely the amount assigned to its sector—for long times. In some parameter regimes this can lead to long coherence times arising from the contribution to the full autocorrelator in Eq. (3.30) of the sectors manifesting SZMs $\Psi_{\vec{\omega}}$. Given that not all sectors contribute, the correlator $C_\infty(t)$ stabilizes for long times around values smaller than those of the case $\alpha < 1$, and then eventually decays for finite systems. Also in this regime, decay times show an exponential dependence on the number of rungs L in the ladder. On the other hand Fig. 3.4(c) shows that, for values of the ladder transverse field h for which none of the sectors can sustain a SZM, the edge spins coherence time has no dependence on the system size and decay is fast.

A different behavior is observed when M is even. In this case, the fact that in many sectors $\Omega_{\vec{\omega}} = 0$ prevents the autocorrelator to fully decay to zero and converging instead to a finite value. When $\alpha \ll 1$, the SZM has a large overlap with the edge operator Z_1 and the saturation value of the autocorrelator to be very close to 1, as shown in Fig. 3.5. Furthermore, even when $\alpha > 1$, because of the presence of exactly conserved SZMs in several sectors, the autocorrelator does not decay to zero either, but in contrast to $\alpha < 1$ the decay to the asymptotic value is fast and size independent. Compare also the amplitude of the oscillations around the asymptotic value which seem to decrease with size for $\alpha < 1$, *cf.* Fig. 3.5 and its Inset.

The mapping of Eq. (3.24) can be used to investigate the features of the correlation functions for larger system sizes than those shown in Figs. 3.4 and 3.5 obtained by exact diagonalization. Figure 3.6 shows the correlation functions of the boundary spin operator τ_1^z {*cf.* Eq. (17) in [32]} from sampling Ising models with random transverse fields compatible with the distribution of $M = 3$, *cf.* (3.27). In Fig. 3.6(a) one can observe - in addition to the features already discussed in Fig. 3.4 - what appears to be plateaus due to the distinct lifetimes of the SZMs in the various symmetry sectors. Figure 3.6(b) shows that for a larger value of h ($h_i = h|s_i^x|$), the infinite temperature time correlation functions still have a system size dependence. In this case rather than via plateaus they appear to decay logarithmically: this would correspond to the fact that in this regime not all sectors have SZMs (3.29) and their lifetimes are shorter than those in the regime of Fig. 3.6(a). Lastly, Fig. 3.6(c) shows the autocorrelation in a regime similar to that of Fig. 3.4(c). Here none of the sectors have SZMs and decay to zero is fast and size independent, as expected.

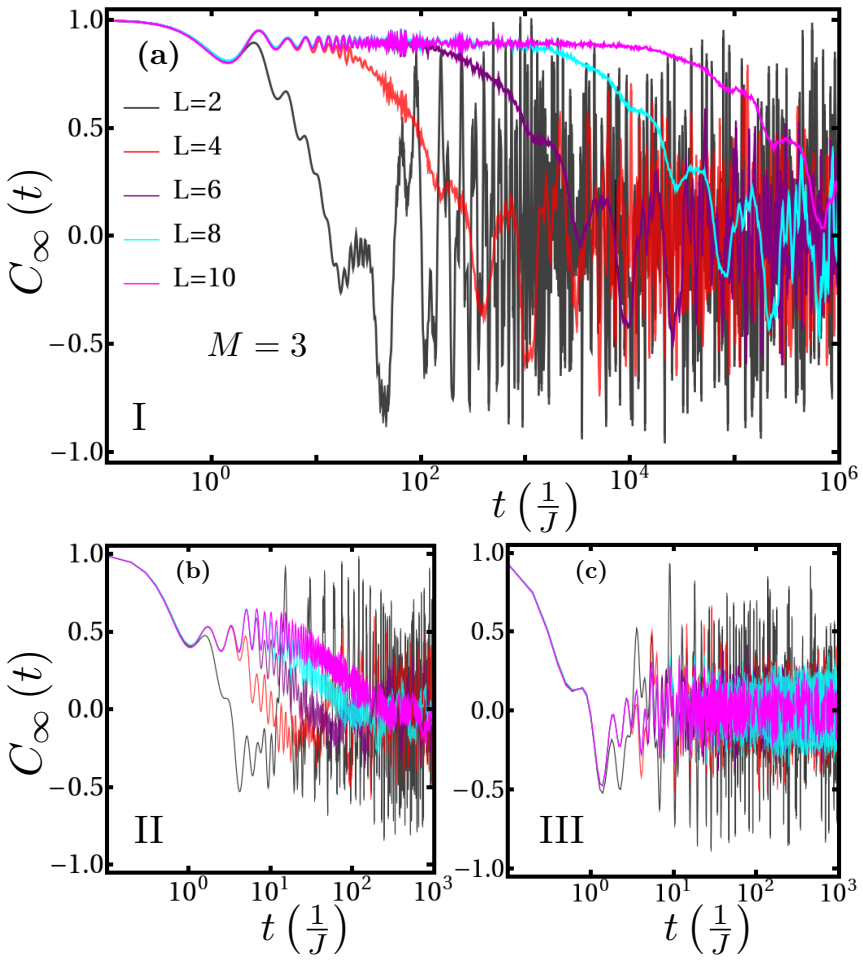


Figure 3.6: Infinite temperature edge autocorrelation from sampling from sector sampling for $M = 3$. **(a)** Also in this case we have taken $J = 1$ and $h = 0.2$ ($h_i = h|s_i^x|$) and compared the behavior of the infinite temperature time correlation functions for the edge spin operator τ_1^z [*cf.* Eq. (3.24)] for different system sizes. For this choice of the parameters, where all the Ising models with random magnetic field over which the sampling is carried out have a SZM, by increasing system size it becomes more and more apparent the formation of a staircase like function. **(b)** For $J = 1$, $h = 0.5$ and same L as in **(a)**, a logarithmic decay of the infinite temperature time correlators can be observed which might be due to the fact that the above staircase like function shrinks. **(c)** When $J = 1$, $h = 1.1$ and L as in **(a)** none of the Ising models with random magnetic field has SZM and the correlation functions which decay almost immediately do not display any size dependence. Sectors I, II, III, correspond to those of Fig. 3.2. In the plot time is represented on a log-scale.

3.7 Discussion

In this chapter we have studied strong zero modes in a class of spin ladders with plaquette interactions. Like in other models, the presence of SZM implies long coherence times for boundary degrees of freedom, and thus provide a general mechanism for long timescales in quantum many-body systems. Our results here are an addition to the growing list of findings in this area [32–34, 36, 37, 40, 54, 78, 86]. We were able to obtain the explicit form of the SZM operators - and understand the behaviour of edge correlators - because the models we consider, while appearing complex superficially, can be brought to simple and (almost) solvable forms by exploiting the large number of symmetries they possess.

Chapter 4

Trajectory phase transitions in non-interacting spin systems

This chapter contains the results of the second part of the thesis which deals with large deviations. In this chapter we show that a collection of independent Ising spins evolving stochastically can display surprisingly large fluctuations towards ordered behaviour, as quantified by certain types of time-integrated plaquette observables, despite the underlying dynamics being non-interacting. In the large deviation (LD) regime of long times and large system size, this can give rise to a phase transition in trajectory space. As a non-interacting system we consider a collection of spins undergoing single spin-flip dynamics at infinite-temperature. For the dynamical observables we study, the associated tilted generators have an exact and explicit spin-plaquette duality. Such setup suggests the existence of a transition (in the large size limit) at the self-dual point of the tilted generator. The nature of the LD transition depends on the observable. We consider explicitly two situations: (i) for a pairwise bond observable the LD transition is continuous, and equivalent to that of the transverse field Ising model; (ii) for a higher order plaquette observable, in contrast, the LD transition is first order. Case (i) is easy to prove analytically, while we confirm case (ii) numerically via an efficient trajectory sampling scheme that exploits the non-interacting nature of the original dynamics. The work discussed in this chapter appeared in the publication:

"Trajectory phase transitions in non-interacting spin systems"
L. M. Vasiloiu, T. Oakes, F. Carollo and J. P. Garrahan
Physical Review E **101**, 042115 (2020).

4.1 Introduction

Phase transitions [1,87–91] occur when a physical system undergoes a sudden structural change as a reaction to an infinitesimal variation of a suitable control parameter across a critical value. The abrupt modification of the macroscopic properties of the system is reflected in a non-analytic behaviour of an order parameter [87–89]. In classical equilibrium

the parameter driving the phase transition is an intensive field conjugate to the order parameter, such as the inverse temperature or a chemical potential, while in quantum phase transitions it is a coupling constant in the Hamiltonian, such as the strength of an external field or of the interactions. More recently, the notion of phase transition has been extended to include also critical phenomena taking place in large fluctuations of nonequilibrium processes, e.g. [24, 26, 30, 92–101] (see [20–22, 28] for reviews). In this scenario, sudden changes in the spatio-temporal structures of the system (trajectories) are witnessed by a non-analytic behaviour in free-energy or entropy-like functionals describing the statistics of an appropriate time-integrated observable.

Similarly to what happens in equilibrium statistical mechanics, where the emergence of a phase transition is more likely expected in the presence of interactions and of an infinite number of degrees of freedom, one would expect to observe these large deviation (dynamical) phase transitions uniquely in many-body interacting dynamics. However, there are noticeable counterexamples to this paradigm provided by several recently investigated single-particle models where a dynamical phase transition occurs without the need of infinitely many degrees of freedom [18, 31, 102–105].

In this thesis, we consider a complementary setting: we show that it is possible to observe large deviation phase transitions, from a disordered phase to an ordered one, in systems of many, but independent, degrees of freedom. We focus specifically on the case of independently evolving Ising spins. This rather counterintuitive result says that the probability of observing an ordered dynamical fluctuation, in a system evolving in a non-interacting manner, can be surprisingly large. This is a statement about the spontaneous dynamical synchronization of the independent elementary constituents at the fluctuation level.

In this chapter we present examples of these LD transitions by exploring fluctuations in a class of dynamical observables that correspond to time-integrated plaquette operators. For these, the associated tilted generators that encode their LD behaviour (see section 4.2 for definitions) have an explicit Kramers-Wannier duality. In the LD formulation, this duality is an exact mapping between weak tilting (corresponding to close to typical behaviour) and strong tilting (corresponding to far from typical behaviour), cf. weak-strong coupling in the more standard context of dualities. The dualities are very informative, as they can help to locate the critical point (at the self-dual point) in the presence of a phase transition, something we exploit in the examples we consider.

We study two cases in detail. In the first one, the transition to the ordered dynamical phase is continuous and the critical behaviour of the dynamical order parameter is of Ising type. This can be shown analytically as the calculation reduces to solving the transverse field Ising model. In the second example we consider the transition is discontinuous (first-order). Here we can demonstrate the duality analytically, and thus determine the self-dual point at which the transition occurs exactly, but we confirm the existence of a LD transition numerically. We achieve this by devising an efficient trajectory sampling scheme which relies on the non-interacting nature of the dynamics.

The dynamical phase transitions discussed here seem to point to the existence of a far more general class of trajectory transitions in the large size and long-time arising not due

to the complexity of the underlying dynamics but of the properties of the time-integrated observable that is probed.

This chapter is organised as follows. In section 4.2 we define the model and dynamical observables we consider. In section 4.3 we prove the duality of one of the cases we consider. Sections 4.4 and 4.5 presents the main results of this chapter. Finally, in section 4.6 we give our conclusions.

4.2 Model and Observables

In this section we introduce the specific class of models that we study in this chapter. We consider systems which consist of N non-interacting Ising spins. For each spin, the state space is spanned by two configurations: an up state $|\uparrow\rangle$ indicating the spin has a positive magnetisation and a down state $|\downarrow\rangle$ indicating instead a negative local magnetisation. The magnetisation operator for each spin is the Pauli matrix σ^z, i.e. $\sigma^z |\uparrow\rangle = |\uparrow\rangle$ and $\sigma^z |\downarrow\rangle = -|\downarrow\rangle$. The basis state $|C\rangle$ for a configuration C of the whole system can thus be written as a tensor product of the state of each individual spin.

The probability vector $|P_t\rangle$ evolves according to a non-interacting thermal dynamics

$$\mathbb{W} = \gamma_+ \sum_{i=1}^{N} \left[\sigma_i^+ - (\mathbf{1} - n_i)\right] + \gamma_- \sum_{i=1}^{N} \left(\sigma_i^- - n_i\right) , \tag{4.1}$$

where $\sigma_i^{+/-}$ is the ladder operator flipping the i-th spin up/down. The operator n is the number operator, defined as $n = \sigma^+\sigma^-$, taking values 0 or 1 for a spin down or up, respectively. We denote the rate for the up transition $|\downarrow\rangle \to |\uparrow\rangle$ by γ_+ and the rate for the down transition $|\uparrow\rangle \to |\downarrow\rangle$ by γ_-. The shape of the generator, which is a separate sum over spins without any interaction terms, makes explicit the fact that the spins evolve in a completely independent way. The dynamics (4.1) is "thermal" as it obeys detailed balance. The stationary state is therefore an equilibrium state, which given the non-interacting nature of the dynamics takes the form of a product state,

$$|\mathrm{eq}_T\rangle = \otimes_{i=1}^{N} \left(\frac{\gamma_+}{\gamma_+ + \gamma_-} |\uparrow\rangle_i + \frac{\gamma_-}{\gamma_+ + \gamma_-} |\downarrow\rangle_i \right) , \tag{4.2}$$

where the "temperature" is defined in terms of the ratio of the rates, $T = 1/\log(\gamma_-/\gamma_+)$ (assuming $\gamma_+ < \gamma_-$). That is, this corresponds to the equilibrium state of a collection of non-interacting spins in a magnetic field of unit strength at temperature T.

When $\gamma_+ = \gamma_- = \gamma$, up and down transitions have the same probability. In this case, which is the one we consider below, the generator further simplifies to

$$\mathbb{W} = \gamma \sum_{i=1}^{N} (\sigma_i^x - \mathbf{1}) , \tag{4.3}$$

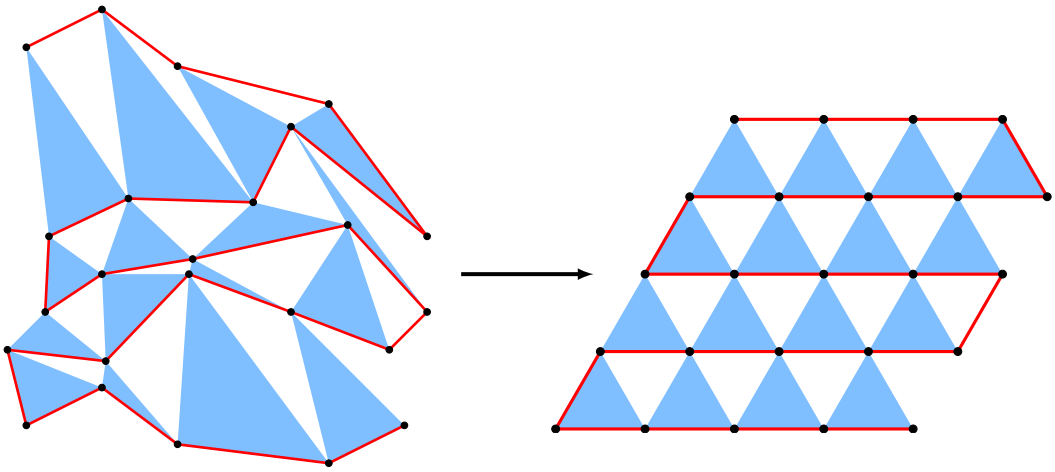


Figure 4.1: Left: Geometrical illustration of 24 non-interacting spins. We represent them as randomly distributed in space as without interactions there is no notion of a geometrical arrangement. Their dynamics is described by the generator of Eq. (4.3). Right: When considering an observable we induce a particular geometry. For Eq. (4.10) this corresponds to one dimensional sequence, corresponding to the red solid lines connecting the spins. For Eq. (4.11) it is that of a triangular lattice geometry where triplets of spins defining the local plaquettes sit on the vertices of upward-pointing triangles (shaded blue). Here we are representing only a subsection of these lattices therefore we do not describe their corresponding boundary conditions.

where $\sigma_i^x = \sigma_i^+ + \sigma_i^-$ is the first Pauli matrix acting on the i-th spin. For this case, the equilibrium state of the system is an equal superposition of all states, i.e. the $T = \infty$ state

$$|\mathrm{eq}_\infty\rangle = \otimes_{i=1}^N \left(\frac{1}{2} |\uparrow\rangle_i + \frac{1}{2} |\downarrow\rangle_i \right) = 2^{-N} \, |-\rangle \, . \tag{4.4}$$

We term the dynamics generated by (4.3) an infinite temperature dynamics. Note that in this case the generator is Hermitian and the left and right eigenvectors coincide (up to normalisation).

For a collection of independently evolving Ising spins, as expected, typical trajectories are uncorrelated and lack of any structure. We are interested in studying large fluctuations of time-integrated observables which represent a measure of "order" in the spin configuration. We will consider what we call in general a plaquette operator over the spins, of the general form

$$O_{\mathrm{plaquette}}(C) = \sum_\mu p_\mu(C) \, . \tag{4.5}$$

Here p_μ are N operators (we always consider periodic boundary conditions)

$$p_\mu(C) = \sigma^z_{i_{\mu_1}} \sigma^z_{i_{\mu_2}} \cdots \sigma^z_{i_{\mu_m}} \, , \tag{4.6}$$

formed by the product of m spins. We call the product (4.6) a plaquette. Each spin in the system belongs to m plaquettes. This means the following: for each configuration of spins

$C = \{\sigma_i^z\}_{i=1}^N$ there is a corresponding set of values of the plaquettes $\{p_\mu\}_{\mu=1}^N$ which is unique (or almost unique, up to symmetries) and therefore a 1-to-1 correspondence between spins and plaquettes. The corresponding dynamical order parameters that we consider then take the form,

$$\mathcal{O}_{\text{plaquette}} = \int_0^t dt' \sum_\mu p_\mu(C(t')). \tag{4.7}$$

We consider in detail two specific plaquette operators, as they illustrate the range of behaviour that we expect to see more generally. The first one corresponds to $m = 2$ and we call it a bond operator. It is a sum of the simplest plaquettes formed by the product of two spins,

$$O_{\text{bond}} = \sum_{i=1}^{N-1} \sigma_i^z \sigma_{i+1}^z + \sigma_N^z \sigma_1^z \,. \tag{4.8}$$

It measures the degree of ordering between consecutive spins. The last term is a "boundary condition" connecting the first and last spins. Each term in (4.8) is a local plaquette p_μ, and the set of them obeys the conditions above: there are N plaquettes; each plaquette is composed of $m = 2$ spins and each spin belongs to exactly $m = 2$ plaquettes; for each arrangement of the plaquettes there is a unique arrangement of spins, up to a global up-down symmetry in the spins (a consequence of m being even).

The second operator we consider below is the sum of plaquettes with $m = 3$ formed by triplets of spins, or triangular plaquettes

$$O_{\text{TP}} = \sum_{i,j,k \in \triangle} \sigma_i^z \sigma_j^z \sigma_k^z \,, \tag{4.9}$$

where the sum is over triplets of sites (i, j, k) involved in the triangular plaquette $\triangle$, chosen such that the 1-to-1 condition above is obeyed. Note that by defining the observables we are introducing a certain geometrical arrangement of the otherwise unstructured ensemble of N spins. For O_{bond} the corresponding arrangement is that of a one dimensional chain with periodic boundaries, where the observable is defined in terms of the bonds between nearest neighbouring spins. For O_{TP}, it is that of a two-dimensional triangular lattice, and the plaquettes are upward pointing triangles of nearest neighbours (as in the classical triangular plaquette model, see Refs. [106–109]). For O_{TP} we also obey the conditions above: there are as many upward pointing triangles as spins, and since there is no up-down symmetry, plaquette arrangements and spin configurations are 1-to-1 (for periodic boundary conditions in at least one direction, see e.g. [108]). The arrangements for the two observables are illustrated in Fig. 4.1.

The corresponding dynamical order parameters are

$$\mathcal{O}_{\text{bond}} = \int_0^t dt' \sum_{i=1}^N \sigma_i^z(t') \sigma_{i+1}^z(t') \,, \tag{4.10}$$

where i runs through the spins and we identify site $N+1$ with site 1, and

$$\mathcal{O}_{\mathrm{TP}} = \int_0^t dt' \sum_{i,j,k\in\triangle} \sigma_i^z(t')\sigma_j^z(t')\sigma_k^z(t')\,. \tag{4.11}$$

These trajectory observables probe spontaneous fluctuations in the dynamics displaying the two different kinds of order in the spin patterns.

The associated tilted generators $\mathbb{W}_s$, cf. (1.75), which encode the LD statistics of these observables, are

$$\mathbb{W}_{s,\mathrm{bond}} = \sum_{i=1}^N (\sigma_i^x - \mathbf{1}) + s\sum_{i=1}^N \sigma_i^z\sigma_{i+1}^z\,, \tag{4.12}$$

and

$$\mathbb{W}_{s,\mathrm{TP}} = \sum_{i=1}^N (\sigma_i^x - \mathbf{1}) + s\sum_{i,j,k\in\triangle} \sigma_i^z\sigma_j^z\sigma_k^z\,, \tag{4.13}$$

These two deformed operators look respectively like (up to a sign and an additive constant N) the 1D Transverse Field Ising Model (TFIM) with periodic boundary conditions (PBC) [1, 6] [*cf.* (1.6)]

$$H_{\mathrm{TFIM}} = -J\sum_{i=1}^N \sigma_i^z\sigma_{i+1}^z - h\sum_{i=1}^N \sigma_i^x\,, \tag{4.14}$$

and the 2D Quantum Triangular Plaquette Model (QTPM) [109–111], *cf.* Fig. 4.1

$$H_{\mathrm{QTPM}} = -J\sum_{i,j,k\in\triangle} \sigma_i^z\sigma_j^z\sigma_k^z - h\sum_{i=1}^N \sigma_i^x\,. \tag{4.15}$$

The identification being

$$\mathbb{W}_{s,\mathrm{bond}} = -H_{\mathrm{TFIM}} - N\,, \tag{4.16}$$

$$\mathbb{W}_{s,\mathrm{TP}} = -H_{\mathrm{QTPM}} - N\,, \tag{4.17}$$

with

$$J = s \;\text{ and }\; h = 1\,. \tag{4.18}$$

These two models have an exact Kramers-Wannier duality. This duality is well known for the TFIM [1] (see section 1.1.2), and we prove it for the QTPM in section 4.3. Duality symmetries like this one are very informative. They often help to locate the critical point at which a phase transition occurs in the large size limit. For the models above, the self-dual point is at $J = |h|$. This is known to be the phase transition point of the TFIM and, as we show below, also a transition point for the QTPM. As we discuss below, the duality has important consequences for the scaled cumulant generating function (SCGF) $\theta(s)$ (1.70) that is the largest eigenvalue associated with the deformation of the original stochastic generator $\mathbb{W}$ (4.3) and therefore for the statistics of trajectories of the non-interacting spin system.

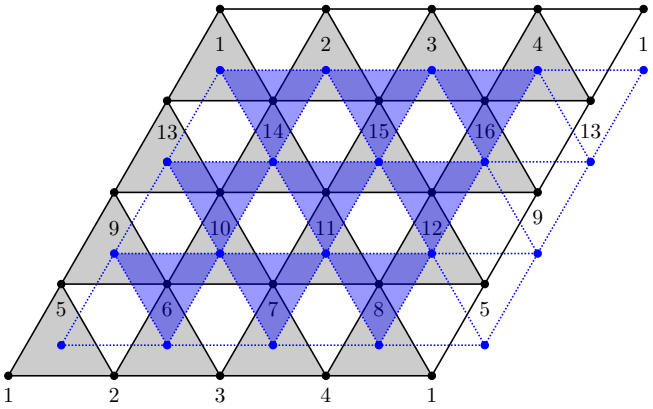


Figure 4.2: Geometrical illustration of the QTPM with periodic boundary conditions for 16 spins (grey triangles). The spins σ_i^β are positioned at the vertices of upward-pointing triangles $\triangle$ of the original lattice. In the dual problem (blue triangles), the dual spins τ_i^β are located at the vertices of downward-pointing triangles $\triangledown$, which are at the centers of the original plaquettes, on the dual lattice.

4.3 Duality of the Quantum Triangular Plaquette Model

In this section we prove the duality of the Quantum Triangular Plaquette Model (QTPM). To do this we make use of the generalization in higher dimensions of the Kramers-Wannier duality [7] of the classical Ising model in $2D$ [112]. This method uses the mapping between the D-dimensional classical statistical mechanical models and the d-dimensional quantum Ising models where $D = d + 1, D > 1$ [1] (see appendix D); this technique allows us to show the duality of the QTPM in its classical form for simplicity.

The $2d$ QTPM is described by a plaquette spin model, defined in terms of Ising spins, on a regular triangular lattice, with Hamiltonian

$$H_{\mathrm{QTPM}} = -J \sum_{\triangle} \sigma_1^z \sigma_2^z \sigma_3^z - h \sum_i \sigma_i^x \,, \tag{4.19}$$

where σ_i^β, with $\beta = x, y, z$, are the local Pauli matrices in the direction β acting on the $i-$th site. The interaction, embodied in the parameter J, occurs between triplets of spins, which for simplicity we denote as $\sigma_1^z, \sigma_2^z, \sigma_3^z$, positioned at the vertices of upward-pointing triangles $\triangle$, while h is a transverse magnetic field in the x direction. We consider a system whose linear size is an integer power of two and periodic boundary conditions [108, 109, 113, 114], *cf.* Fig. 4.2.

The energy function of the corresponding $3D$ classical model has the form

$$\beta E = -K \sum_{\triangle} s_1^{\triangle} s_2^{\triangle} s_3^{\triangle} - J_z \sum_b s_1^b s_2^b \,, \tag{4.20}$$

where $s_i^\alpha = \pm 1$, with $\alpha = \triangle, b$ are Ising variables corresponding to the $i-$th site. The first sum in the right-hand side of (4.20) is over all triangular plaquettes $\triangle$ in the xy

plane, where K represents the magnetic interaction among the dynamic variables $s_i^{\triangle}$, while the second sum is over all the bonds b in the z direction with coupling constant J_z, *cf.* Fig. 4.3. The mapping relations between classical and quantum coupling constants are the conventional ones [1, 112]: $K = aJ$, $e^{-2J_z} = \tanh(ah)$ and $T = 1/(Ma)$, where a is the lattice spacing, M is the number of sites in the z direction of the classical model, and T is the temperature in the quantum model. The mapping between the quantum and the classical model becomes exact in the scaling limits: $a \to 0$, $M \to \infty$ and $T \to 0$. The partition function of the $3D$ classical model is

$$\begin{aligned} Z &= \sum_{\{s\}} e^{-\beta E} \\ &= \sum_{\{s\}} e^{K \sum_{\triangle} s_1^{\triangle} s_2^{\triangle} s_3^{\triangle} + J_z \sum_b s_1^b s_2^b} \\ &= \sum_{\{s\}} \left[\prod_{\triangle} \left(\cosh K + s_1^{\triangle} s_2^{\triangle} s_3^{\triangle} \sinh K \right) \right. \\ &\left. \times \prod_b \left(\cosh J_z + s_1^b s_2^b \sinh J_z \right) \right]. \end{aligned} \tag{4.21}$$

By defining the face variables $k_{\triangle} = 0, 1$, the bond variables $k_b = 0, 1$ and the constants $c_0 = \cosh K$, $c_1 = \sinh K$, $d_0 = \cosh J_z$ and $d_1 = \sinh J_z$, we can express the partition function as

$$Z = \sum_{\{s\}} \sum_{k_{\triangle}} \sum_{k_b} \left\{ \left[\prod_{\triangle} c_{k_{\triangle}} \left(s_1^{\triangle} s_2^{\triangle} s_3^{\triangle} \right)^{k_{\triangle}} \right] \times \left[\prod_b d_{k_b} \left(s_1^b s_2^b \right)^{k_b} \right] \right\}. \tag{4.22}$$

We can note that if an Ising variable s_i^{α} is raised to an even power then we obtain a factor 2 in the partition function Z, originated from the sum over all the spin configurations, otherwise we get a factor 0. This can be expressed in formulae by rewriting the partition function Z as a constrained sum $\sum'$ over the k variables

$$Z = 2^N \sum_{k_{\triangle}, k_b}{}' \left(\prod_{\triangle} c_{k_{\triangle}} \right) \left(\prod_b d_{k_b} \right), \tag{4.23}$$

where N is the total number of sites. Since every site of the original lattice belongs to 3 triangular face terms and to 2 bond terms, the restriction on the partition function is equivalent to ask that the sum of all 5 $k_{\triangle/b}$ variables has to be an even number for each site. In order to solve this constraint dual variables are introduced. The dual spins s^* are positioned at the centers of the triangular prisms of the original prismatic lattice, *cf.* Fig. 4.3. For each site i, belonging to the original lattice, 3 vertical bonds, of the dual lattice, bisect the 3 neighboring spacelike faces $\triangle$ of the site i. Thus, each bisecting bond b of the dual lattice is given by the relation $k_{\triangle} = \frac{1}{2}\left(1 - s^{*b}_1 s^{*b}_2\right)$. Each spacelike face $\triangledown$ of

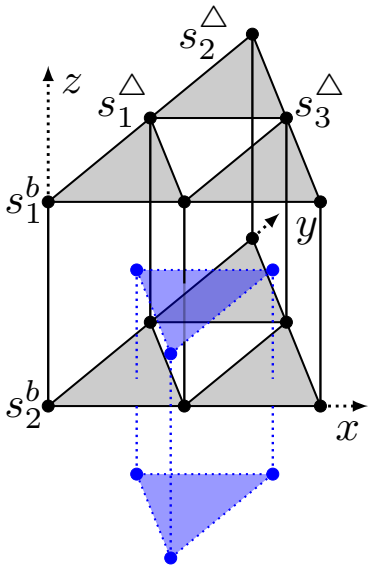


Figure 4.3: Geometrical illustration of plaquette $\triangle = s_1^{\triangle} s_2^{\triangle} s_3^{\triangle}$ and bond $b = s_1^b s_2^b$ interactions on the original lattice (gray triangles) in the classical $3D$ model. In the dual problem (blue triangles), the spins are located on the dual lattice at the vertices of downward-pointing triangles $\triangledown$. The blue prism is the geometrical illustration of the plaquette and bond interactions on the dual lattice in the classical $3D$ model.

the dual lattice is pierced by a vertical bond b between two spins of the original lattice, thus the plaquette on the dual lattice is set by $k_b = \frac{1}{2}(1 - s^{*\triangledown}_1 s^{*\triangledown}_2 s^{*\triangledown}_3)$, *cf.* Fig. 4.3. The constraint on the variables $k_{\triangle/b}$ is fulfilled since the 6 dual lattice sites around one site on the original lattice meet the condition

$$\begin{aligned} k_{\triangle_1} + k_{\triangle_2} + k_{\triangle_3} + k_{b_1} + k_{b_2} = \\ \frac{1}{2}\left(1 - s^{*b}_1 s^{*b}_4\right) + \frac{1}{2}\left(1 - s^{*b}_2 s^{*b}_5\right) + \\ \frac{1}{2}\left(1 - s^{*b}_3 s^{*b}_6\right) + \frac{1}{2}\left(1 - s^{*\triangledown}_1 s^{*\triangledown}_2 s^{*\triangledown}_3\right) \\ + \frac{1}{2}\left(1 - s^{*\triangledown}_4 s^{*\triangledown}_5 s^{*\triangledown}_6\right) \equiv 0 \pmod 2. \end{aligned} \tag{4.24}$$

In order to calculate the dual constant couplings $(\tilde{K}, \tilde{J}_z)$ it is useful to rewrite $c_k = k \sinh K + (1-k)\cosh K$ by using the fact that c_k has been defined for a face $\triangle$ of the original lattice that is pierced by a Ising bond b in the dual problem

$$\begin{aligned} c_{k_\triangle} &= \frac{1 + s^{*b}_1 s^{*b}_2}{2} \cosh K + \frac{1 - s^{*b}_1 s^{*b}_2}{2} \sinh K \\ &= \frac{1}{2} e^K \left(1 + s^{*b}_1 s^{*b}_2\, e^{-2K}\right) \\ &= \frac{1}{\sqrt{2 \sinh 2\tilde{J}_z}} e^{\tilde{J}_z s^{*b}_1 s^{*b}_2}, \end{aligned} \tag{4.25}$$

with $\tilde{J}_z$ determined by $e^{-2K} = \tanh \tilde{J}_z$. By defining $\tanh \tilde{K} = e^{-2J_z}$ we obtain

$$\begin{aligned} d_{k_b} &= k_b \sinh J_z + (1 - k_b) \cosh J_z \\ &= \frac{1}{\sqrt{2 \sinh 2\tilde{K}}} e^{\tilde{K} s^{*\triangledown}_1 s^{*\triangledown}_2 s^{*\triangledown}_3}. \end{aligned} \tag{4.26}$$

Using the results of equations (4.25) and (4.26), we can write, for the $3D$ classical model, the relation between the partition function of the original lattice $Z(K, J_z)$ and dual lattice $Z(\tilde{K}, \tilde{J}_z)$

$$\begin{aligned} &Z(K, J_z) = \\ &\frac{1}{\mathrm{Vol}(G)} \left(\sinh 2\tilde{J}_z\right)^{-\frac{N}{2}} \left(\sinh 2\tilde{K}\right)^{-\frac{N}{2}} Z(\tilde{K}, \tilde{J}_z), \end{aligned} \tag{4.27}$$

and the duality relation for the coupling constants

$$\sinh 2J_z \sinh 2K = 1, \tag{4.28}$$

where the size of the gauge group $\mathrm{Vol}(G) = 1$ because if the linear size of the system is an integer power of two and the system has periodic boundary conditions in at least one direction of the lattice, the ground state is unique, thus one dual spin configuration corresponds to one spin configuration in the original lattice [108].
The corresponding $2d$ quantum model has the same duality

$$\begin{aligned} H_{\mathrm{QTPM}} &= -J \sum_{\triangle} \sigma^z_1 \sigma^z_2 \sigma^z_3 - h \sum_i \sigma^x_i \\ &= -J \sum_i \tau^x_i - h \sum_{\triangledown} \tau^z_1 \tau^z_2 \tau^z_3, \\ &\sinh 2J \sinh 2h = 1, \end{aligned} \tag{4.29}$$

where τ^β_i, with $\beta = x, y, z$, are the dual Ising spins.
This Kramers-Wannier duality shows that if the QTPM has a phase transition at zero temperature then the transition should take place at the self dual point $J/h = 1$.

4.4 Large deviations of the bond order parameter

The one dimensional spin-1/2 TFIM is one of the most studied models in physics. It allows for amenable analytical considerations and it has direct experimental realisations [1, 55]. One of its prominent features is an exact duality between an ordered and a disordered phase, which has been proved in [7,8]. Here we discuss the consequences of this duality in the TFIM with PBC for the SCGF $\theta(s)$. We denote as $E_0(J, h)$ the ground state energy of the TFIM Hamiltonian with PBC $H_{\mathrm{TFIM}}(J, h)$ [5,6] (*cf.* (1.24)), where

$$E_0(J, h) = -J \sum_{\substack{m=0 \\ m \,\mathrm{odd}}}^{2N-1} \left[\left(1 - \frac{h}{J}\right)^2 + 4 \frac{h}{J} \sin^2 \left(\frac{m\pi}{2N}\right) \right]^{1/2}, \tag{4.30}$$

and perform the duality transformation introduced in section 1.1.2

$$\begin{aligned} H_{\mathrm{TFIM}}(J,h) &= H_{\mathrm{TFIM}}(h,J) \\ &= J\, H_{\mathrm{TFIM}}(h/J,1)\,, \end{aligned} \tag{4.31}$$

which for the ground state energy means

$$E_0(J,h) = J\, E_0(h/J,1)\,. \tag{4.32}$$

As seen in the previous section, the associated tilted operator describing the statistics of the observable $\mathcal{O}_{\mathrm{bond}}$ is given by (4.16). The SCGF is therefore

$$\theta(s) = -E_0(s,1) - N\,, \tag{4.33}$$

and the duality relation (4.32) gives

$$\theta(s) = s\,\theta(1/s) + N(s-1)\,. \tag{4.34}$$

If we take the derivative with respect to s of (4.33) we get the average of the order parameter, $\langle \mathcal{O}_{\mathrm{bond}} \rangle / t$, *cf.* Eq.(4.10). In Fig. 4.4(left) we plot it for a range of system sizes. We observe a second order phase transition at the self dual points, which are $s = 1$ and, because of a $\mathbb{Z}_2$ symmetry, also $s = -1$. Finite size effects are present for the smaller sizes shown, $N = 6, 10$, but for $N = 50$ and beyond the SCGFs show convergence, with the exception of points close to the transition, as expected.

Using the relation between the SCGF and the rate function as defined by Eq. (1.73) we plot the rate function in Fig. 4.4(right). The transitions that can be seen in the observables appear as a broadening of the rate function. This broadening is due to the transition between two different dynamical phases of the model. The rate function being broader than the corresponding Gaussian (dashed line), with variance given by the second scaled cumulant of the observable, shows that the fluctuations associated with the order detected by (4.10) are more pronounced that one could have anticipated from the non-interacting nature of the dynamics.

4.5 Large deviations of the triangular plaquette order parameter

4.5.1 Sampling LDs with transition path sampling

The same relation as in Eq. (4.34) holds also for the SCGF of the TPM, but unlike the TFIM, this model is not exactly solvable. In order to numerically access the statistics of the triangular plaquette observable (4.11) in the trajectories of the non-interacting spin system we employ the method of transition path sampling (TPS) [115], as adapted for the study of LDs, see e.g. [27, 98, 116]. The basic idea behind TPS is similar to that of Markov chain Monte Carlo but applied to trajectories rather than configurations [115].

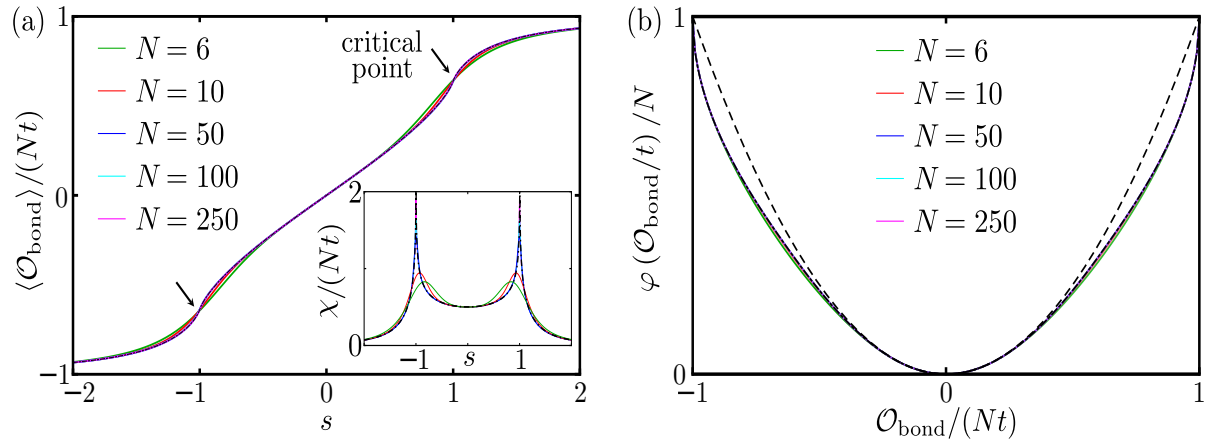


Figure 4.4: Continuous LD transition for bond observable. (a) Order parameter $\langle o \rangle_s = \langle \mathcal{O}_{\rm bond} \rangle / (Nt) = \theta'(s)/N$ as a function of the counting field s, *cf.* Eqs. (1.74) and (4.10). There is a continuous transition of the 2D Ising type at the self-dual points $s = 1$ (to a ferromagnetic phase with finite positive magnetization) and $s = -1$ (to an antiferromagnetic phase with finite negative magnetization). Around $s = 0$ we observe a linear trend in $\langle o \rangle_s$, while for $s > 1$ ($s < 1$) it saturates asymptotically to its minimum and maximum values. Here we display $\langle o \rangle_s$ with appropriate scaling for different system sizes by means of Eq.(4.30). Inset, susceptibility as a function of s illustrating a finite size scaling around the critical points $s = 1$ and $s = -1$. The hydrodynamic limit, given by $\theta(s) \simeq \int_0^1 dx \left[\sqrt{1 - 2s\cos(2\pi x) + s^2} - 1 \right]$, is represented by the dot-dashed black lines. (b) Rate function $\varphi(o)$ for the observable $\mathcal{O}_{\rm bond}$ (4.10) for different system sizes. We compare this function with the Gaussian LD rate function accounting for the Gaussian fluctuations of the noninteracting spin system. This has zero mean and variance $\sigma^2 = \theta''(0) = 0.5$ (back dashed curve). The existence of a singularity of this observable is manifested in the broadening of $\varphi(o)$, with respect to the Gaussian distribution, as well as in the existence of non-analytic points in the higher derivatives of $\varphi(o)$, indicating that fluctuations of the order parameter are correlated. Also in this case the hydrodynamic limit is represented by the dot-dashed black line.

For the case of LDs, it amounts to an importance sampling method that helps overcome some of the exponential (in size and time) cost of sampling the rare event. TPS is well suited for dynamics that is reversible - like the infinite temperature dynamics we study here - for reasons we explain below. Other numerical methods for LDs include sampling exponentially rare trajectories via "cloning" (also known as splitting) [117], variational approximations to rate functions [118], or tensor network methods to directly estimate SCGFs [119, 120].

TPS [27, 98, 115] does a biased random walk in trajectory space (just like normal Monte Carlo does in configuration space) by starting from a seed trajectory and updating it by proposing modifications to it. These are accepted or rejected according a Metropolis rule, that is, with probability of acceptance $\min\left(1, e^{s\Delta\mathcal{O}}\right)$, where $\Delta\mathcal{O}$ is the change in the observable of interest in the case of LD studies, cf. Eq. (1.70). A key aspect of TPS is how to propose trajectories. In two commonly used approaches, such as "shooting" or "shifting" [115], the proposed update to the trial trajectory begins by selecting a given

time τ_{cut} during the previous trajectory. Starting from the configuration at τ_{cut} in the old trajectory, a new section of trajectory is produced ending at either the end of the trajectory $t_{\max} = t$ (in the case of forward dynamics) or at the start of the trajectory $t = 0$ (in the case of reversible dynamics). In either case, the new section of trajectory is bounded only by configuration at τ_{cut}, since the configurations at either $t = 0$ or $t_{\max}$ can be changed. This is a desired property of TPS methods, since the initial and final configurations will typically be sampled using the original dynamics, i.e. they will be representative of the $s = 0$ distribution of trajectories.

The drawback of the above ways of proposing trajectories comes in the convergence (in terms of TPS iterations) of the bulk of the trajectory. Since the acceptance rule is exponential in the change $\Delta\mathcal{O}$, smaller updates are accepted exponentially (in time) more frequently. The consequence is that the ends of the trajectories converge more quickly that its bulk, which gets updated very rarely. This means that the decorrelation of TPS moves takes a number of iterations that increases exponentially both in time and system size.

4.5.2 Improvement to TPS trajectory proposal and acceptance

To sample the desired trajectory ensemble $\langle \mathcal{O}(\omega) e^{-s\mathcal{O}(\omega)} \rangle$ we use a modified form of the TPS method that takes advantage of the non-interacting nature of our spin dynamics. We do two things that allow to overcome the exponential in time and size cost of TPS equilibration.

First, since the dynamics is non-interacting we can propose a new trajectory from an old one by only changing the dynamics of a single spin. This guarantees that the change $\Delta\mathcal{O}$ will be of order 1 in terms of system size, rather than order N as usual (while still for the moment extensive in time). This obvious trick already represents a significant speed up to the acceptance of TPS moves. Of course, this is only possible in a non-interacting case as the one we are considering.

The second improvement is to propose only changes in a single spin trajectory which are localised in time. Specifically, rather than using τ_{cut} as the only point along the spin trajectory defining the change, we also introduce a window of variable time for the new section of trajectory, whose maximum is $\tau_{\text{window}} = \tau_{\text{cut}} + \tau_{\text{lim}}$, where τ_{lim} is uniformly sampled from $1 \leq \tau_{\text{lim}} \leq 0.2\,\tau_{\max}$. The boundary conditions imposed at the two edges of the window are dictated by the orientation of the spins at the times τ_{cut} and τ_{window}. That is, the orientation of the spin in the new trajectory at $\tau_{\text{cut}}(\tau_{\text{window}})$ has to match up with the orientation that it had at $\tau_{\text{cut}}(\tau_{\text{window}})$ in the old trajectory. Since each spin can take only one of two values, this limitation does not impose too much of an extra computational cost. This cost of discarding trajectories that do not satisfy the boundary conditions of the time window is compensated by the ability of these windows to equilibrate (in the TPS sense) the whole trajectory faster. The reason is that between the two improvements $\Delta\mathcal{O}$ becomes order 1 in both the space and time extent.

Fig. 4.5 shows a schematic of how a new trajectory is produced by modifying only the chosen window τ_{window} of the selected spin trajectory rather than the usual update to part of the trajectory for the whole system as used in other typical TPS methods [115].

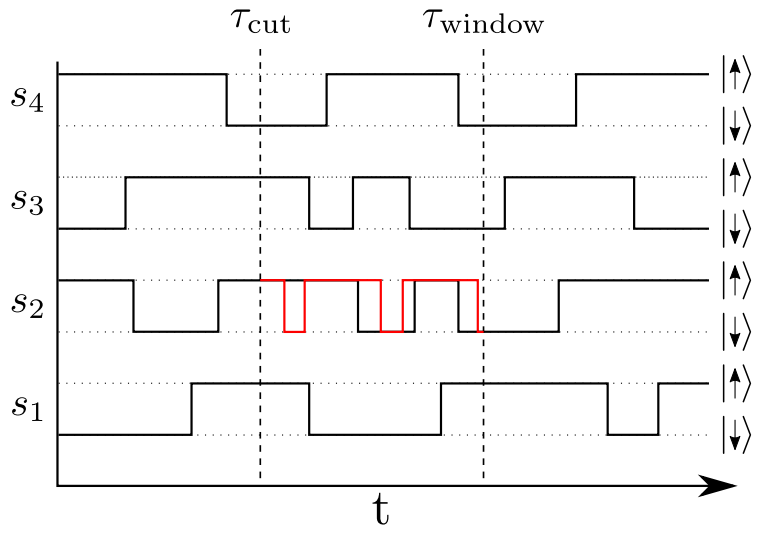


Figure 4.5: WTPS trajectory proposal scheme. This schematic shows a system of four spins s_i, where $i = 1, 2, 3, 4$. The many-body trajectory is composed of four individual spin trajectories which are independent due to the non-interacting underlying dynamics (black solid lines indicate the original trajectory). Each spin is either up or down. The proposed trajectory changes a single spin only, $i = 2$ in the sketch. The change starts at time τ_{cut} and ends at τ_{window} as described in the main text. Only for the selected spin a new part of the trajectory is created between τ_{cut} and τ_{window} (red solid line).

4.5.3 Trajectory umbrella sampling and choice of alternative dynamics

In order to efficiently sample trajectories for value of s across the LD transition, expected to occur at the self-dual points $s = \pm 1$, we need further enhancements to the efficiency of the TPS scheme. We achieve this by means of umbrella sampling in trajectory space [27, 121–124].

We are trying to calculate quantities like

$$\langle \mathcal{A}(\omega) e^{s\mathcal{O}(\omega)} \rangle = \sum_{\omega} \mathcal{P}(\omega)\, \mathcal{A}(\omega)\, e^{s\mathcal{O}(\omega)}\,, \tag{4.35}$$

by sampling trajectories in the exponential tilted ensemble, where TPS deals with the exponential factor in the expression above. The idea of umbrella sampling is to exploit the identity,

$$\begin{aligned} \langle \mathcal{A}(\omega) e^{s\mathcal{O}(\omega)} \rangle &= \sum_{\omega} \mathcal{P}(\omega)\, \mathcal{A}(\omega)\, e^{s\mathcal{O}(\omega)} \\ &= \sum_{\omega} \mathcal{P}_{\text{ref}}(\omega)\, \frac{\mathcal{P}(\omega)}{\mathcal{P}_{\text{ref}}(\omega)}\, \mathcal{A}(\omega)\, e^{s\mathcal{O}(\omega)} \\ &= \langle \mathcal{A}(\omega) e^{s\mathcal{O}(\omega)} e^{\mathcal{G}(\omega)} \rangle_{\text{ref}}\,, \end{aligned} \tag{4.36}$$

where

$$\mathcal{G}(\omega) = \log \mathcal{P}(\omega) - \log \mathcal{P}_{\text{ref}}(\omega)\,. \tag{4.37}$$

Equation (4.36) means that we can estimate (4.35) by means of a "reference" dynamics different from the original dynamics and adjusting through the exponential of $\mathcal{G}$ to account for the change in measure over the trajectories [27, 121–124]. Chosen judiciously, the reference dynamics may reduce the sampling error due to the exponential weighting in (4.36). There is an optimal choice for this reference, that of the dynamics obtained via a generalised Doob transformation [99, 125, 126]. This optimal choice is in general impossible to implement explicitly (as it requires the diagonalisation of the tilted generator) and one has to resort to tractable approximations.

For the specific model we are investigating, we choose dynamics to maintain the interesting nature of a collective phase transition for a set of stochastic independently evolving spins. The plaquette observable we are considering, cf. (4.6), may suggest a reference dynamics that contains interactions. But to really emphasise that this collective behaviour emerges from the non-interacting nature, we chose a reference dynamics which is also non-interacting.

Specifically, we choose dynamics generated by (4.1), where the reference dynamics differs from the original one in that $\gamma_+ \neq \gamma_-$. That is, we use "temperature" as the control parameters of the trajectory umbrella sampling. The exponent $\mathcal{G}$ of the reweighing factor is easy to calculate in terms of the original dynamics rate, γ, and those of the reference, $\gamma_\pm$. In order to sample (4.36) we ran TPS with the reference dynamics, under the proposal rules described in the previous subsection, and with acceptance criterion where $s\Delta\mathcal{O}$ is replaced by $s\Delta\mathcal{O} + \Delta\mathcal{G}$ [27, 121–124].

4.5.4 First order transition in triangular plaquette order

In Fig. 4.6(left) we show the results of sampling the average of the observable (4.11) using the TPS scheme described above for system sizes $N = 8, 16, 32, 64, 128, 256$ (full lines). For comparison we also show the results from exact diagonalisation (E.D.) of small sizes, $L = 8, 16$ (dashed lines). For increased system size it is clear that the order parameter tends towards becoming discontinuous at the self-dual points $s = 1$ and $s = -1$. This indicates that the trajectory transition is of the first-order kind, between a dynamically disordered phase for $|s| < 1$, and dynamical phases with triangular plaquette order for $|s| > 1$.

In Fig. 4.6(right) we show the corresponding rate function. We observe that the latter has broader tails than as compared to a Gaussian rate function (i.e., a parabola) with the same average and variance. We see that the first-order nature of the transition is reflected in a linear behaviour of the rate function for values of the observable which lie in between the extreme values across the discontinuous jumps of the SCGF at $s = \pm 1$. The linear behaviour of the rate function correspond to a Maxwell construct for the first-order transitions of the SCGF. This becomes exact in the $N \to \infty$ limit, and the slope which coincides with the critical s-field values ($s = -1$ and $s = 1$), shown for comparison in

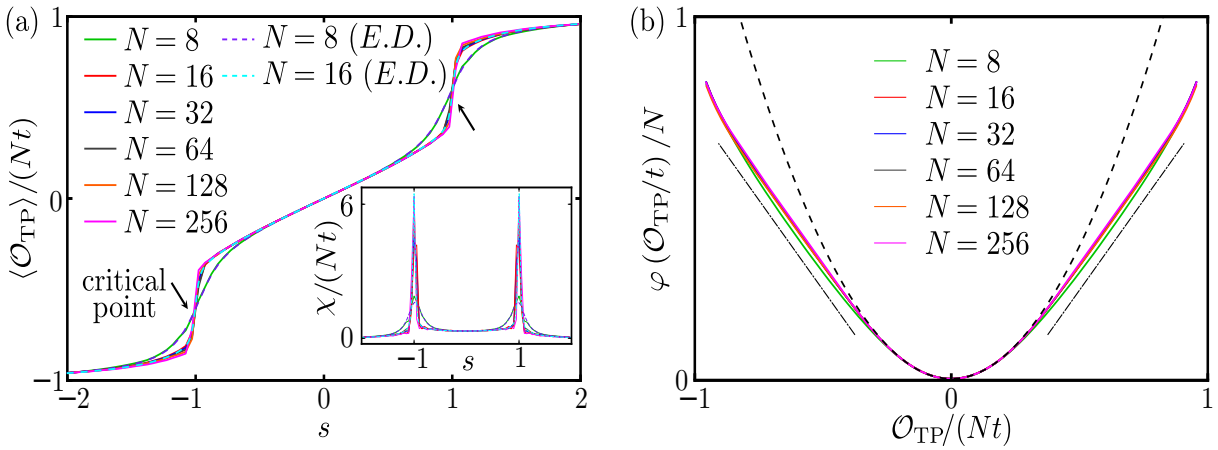


Figure 4.6: LD transition for the triangular plaquette observable. (a) Discontinuous phase transition of time-averaged value of the TPM-like plaquette observable at $s = 1$ and $s = -1$. Data obtained by utilizing the method discussed in Sec. 4.5 are shown for various system sizes. As a further numerical tool to improve the analysis of the data we used multistate Bennett acceptance ratio (MBAR) [127, 128]. Also for this model we observe linear regime around $s = 0$ and asymptotic behavior beyond the critical point $s > 1$ and $s < -1$. Inset, susceptibility as a function of s illustrating a finite size scaling around the critical points $s = 1$ and $s = -1$. (b) Rate function $\varphi(o)$ for the observable $\mathcal{O}_{\rm TP}$ (4.11) for different system sizes. This is also compared with the Gaussian fluctuations of the noninteracting spin system. In this case such Gaussian LD rate function has zero mean and variance $\sigma^2 = \theta''(0) \approx 0.34$ (back dashed curve). The existence of a first-order phase transition is manifested in the linear behaviour of $\varphi(o)$ in the region delimited by the values across the first-order jumps in the SCGF of the left panel. The rate function is thus much broader than the corresponding Gaussian, indicating the higher likelihood of trajectories with plaquette order. The slope of the linear parts is given by the critical values $s = \pm 1$, shown as the dot-dashed lines for comparison.

Fig. 4.6(right) as the dot-dashed lines. The broadness of the rate function indicates the enhanced probability of the triangular plaquette order in the dynamics.

Operators similar to (4.13) have been considered before in the context of quantum codes [110] and of "fractons" [111]. The first order transition we find numerically at the self-dual point via our augmented TPS scheme is also compatible with the results of Ref. [110].

4.6 Discussion

In this chapter we have investigated the dynamical fluctuations of a collection of independent spins evolving stochastically. We have shown that despite the non-interacting nature of their dynamics, the statistics of time-integrated interacting observables can be non trivial, and give rise to correlated behaviour at the fluctuation level. We considered two examples of a general class of plaquette observables, showing that in the large number of spins limit they give rise to both continuous and first order LD transitions.

Our findings here fit with recent results for few body problems [18, 102] where singularities in long-time trajectory ensembles were not a consequence of interactions in the dynamics in the large size limit (like in most other systems displaying LD transitions [20, 28]) but of the properties of the dynamical observables probed. We focused on spin systems and observables where tilted generators displayed a duality symmetry, which we exploited to identify precisely the location of the dynamical transitions. Our approach here directly generalises to other plaquette observables for which their tilted generators will have dualities. These cases will display similar dynamical transitions at their self-dual points.

We expect the kind of behaviour we uncovered in this chapter to be more widespread. Our results suggest that a large collection of non-interacting degrees of freedom can have atypical fluctuations where the system dynamically synchronises and behaves cooperatively for long times. Furthermore, such rare events would correspond to dynamical singularities in the ensemble of trajectories, making them much more likely than the non-interacting nature of the dynamics would indicate.

Conclusions

In this thesis we investigated two main topics: strong zero modes in quantum chains with open boundary conditions and large deviations in non-interacting classical spin systems.

In the first part we have seen that in certain quantum spin chains with open boundaries the emergence in the thermodynamic limit of conserved local quantities, called strong zero modes, results in infinitely long coherence times for the edge spins. In particular, we have investigated the behavior of these coherence times when the spin chain weakly interacts with a large external environment. Our main result is that, in specific dissipative settings, the correlation times of the boundary spins are significantly enhanced by the presence of the environment. This observation allowed us to generalise the notion of strong zero mode operators in systems undergoing unitary dynamics to that of strong zero maps in systems with dissipative and Markovian dynamics. Overall this result is surprising, since often dissipation suppresses the memory of initial states, and the stability of strong zero modes might be useful for applications in quantum technologies in realistic non-equilibrium settings. Next, we constructed strong zero modes for a class of closed, isolated ladder spin systems with plaquette interactions in the presence of a transverse field that are a simple generalization of the transverse field Ising model and posses an extensive set of symmetries. Precisely these symmetries are responsible for the emergence of quasirandomness in most symmetry sectors of the clean quantum ladder system. Furthermore, we observed an interesting mechanism for slow decorrelation; even in parameter regimes where the strong zero mode for the full ladder model is absent, some of the initial information stored in the edge spins can still be preserved for long times as a consequence of the existence of strong zero modes within individual symmetry sectors.

In the second part of the thesis we have shown that, by reweighing trajectories accordingly to a certain type of time-integrated observable, a collection of spins undergoing single spin-flip dynamics at infinite-temperature can display large fluctuations towards ordered behavior. In the large deviation regime of long times and large system size, this can give rise to singularities in trajectory space. We studied in detail two examples of a general class of plaquette observables that in the limit of a large number of degrees freedom give rise to both first and second order large deviation transitions. Our results suggest that the probability of observing a spontaneous dynamical synchronization of the independent elementary constituents, at the fluctuation level in trajectory space, can be surprisingly large.

The results presented in this thesis lead also to many open questions. Concerning the research presented in the first part, an interesting direction for future studies would be to explore the existence of strong zero modes or related slow operators in more complex quantum plaquette models, in particular those closer to systems with fractons [129]. In addition, it would be interesting to investigate the existence of possible classical analogous of the strong zero modes. It would be also interesting to probe that local dissipation enhances the correlation times in experiments realized by means of trapped ions or Rydberg atoms [130–134]. Regarding the research of the second part of the thesis it would be relevant to extend the investigation of the spontaneous dynamical synchronization at the fluctuation level to other systems by considering more complex time-integrated plaquette observables than the ones we considered in this thesis and for which the associated tilted operators have an explicit Kramers-Wannier duality.

Appendix A

Markovian quantum master equation

In this appendix we continue the derivation of the quantum master equation in Lindblad form [9–14] started in section 1.2. As seen in the main text, the first approximation we perform is the Born approximation (1.41) that leads to the differential equation [*cf.* (1.45)]

$$\frac{d}{dt}\rho_S(t) = -\int_0^t tr_E\Big[H(t),[H(s),\rho_S(s)\otimes\rho_E(0)]\Big]ds\,, \tag{A.1}$$

for the reduced density matrix ρ_S (1.43) under the assumption $tr_E\left[H(t),\rho_S(0)\otimes\rho_E(0)\right] = 0$ [*cf.* (1.46)]. Formally integrating both sides of the above equation from t to s we obtain

$$\rho_S(s)-\rho_S(t) = -\int_t^s tr_E\Big(\Big[H(s),\int_0^s[H(w),\rho_S(w)\otimes\rho_E(0)]\,dw\Big]\Big)ds\,, \tag{A.2}$$

showing that the difference $\rho_S(s)-\rho_S(t)$ is of the second order in H_{SE}. This observation allows us to approximate, and so to substitute, $\rho_S(s)$ in equation (A.1), without violating the Born approximation, with $\rho_S(t)$,

$$\frac{d}{dt}\rho_S(t) = -\int_0^t tr_E\Big[H(t),[H(s),\rho_S(t)\otimes\rho_E(0)]\Big]ds\,, \tag{A.3}$$

obtaining an equation for the density matrix operator that is local in time given that now the time evolution of the state of the system at time t depends only on the state of the system at time t. This form of the equation of motion is not of the Markovian type equations as it still contains a dependence of the initial state of the system at $t = 0$.

The second approximation we encounter in this perturbative approach is the so-called Markov approximation. The foundation of this approximation lies in the assumption that characteristic decay times τ_E of correlation functions in the external environment E take place on shorter timescales when compared to the timescales τ_S over which the state of the open quantum system S undergoes relevant and appreciable changes. In other words, the memory of the environment, that translates into fast decaying correlation times, is much shorter than the timescales we are interested in investigating. This assumption allows us

to substitute s with $t-s$ and send the upper limit of the integral to infinity

$$\frac{d}{dt}\rho_S(t) = -\int_0^\infty tr_E\Big[H(t),[H(t-s),\rho_S(t)\otimes\rho_E(0)]\Big]ds\,, \tag{A.4}$$

and in this way we obtain the Born-Markov quantum master equation known also as the Redfield equation. The Redfield equation does not always preserve positivity of the density matrix thus is necessary to implement a further approximation known as the secular approximation in order to neglect, as we will see below, the fast oscillating degrees of freedom.

We consider the most general form of the interaction Hamiltonian H_{SE} in the Schödinger picture

$$H_{SE} = \sum_\alpha S_\alpha \otimes E_\alpha\,, \tag{A.5}$$

where $S_\alpha = S_\alpha^\dagger$ is a general Hermitian operator acting only on the Hilbert space $\mathcal{H}_S$ while $E_\alpha = E_\alpha^\dagger$ indicates a general Hermitian operator acting only on the environment $\mathcal{H}_E$. In particular we define the operators $S_\alpha(\omega)$ that are eigenoperators of the system Hamiltonian H_S associated to the frequency ω [9, 10, 14]

$$\begin{aligned}\big[H_S, S_\alpha(\omega)\big] &= -\omega S_\alpha(\omega)\ ,\\ \big[H_S, S_\alpha^\dagger(\omega)\big] &= +\omega S_\alpha(\omega)\ ,\end{aligned} \tag{A.6}$$

and that in the interaction picture have the form

$$\begin{aligned}e^{iH_St}S_\alpha(\omega)\,e^{-iH_St} &= e^{-i\omega t}S_\alpha(\omega)\ ,\\ e^{iH_St}S_\alpha^\dagger(\omega)\,e^{-iH_St} &= e^{+i\omega t}S_\alpha^\dagger(\omega)\ ,\end{aligned} \tag{A.7}$$

whereas the environment operators in the interaction picture $E_\alpha(t)$ are related to their analogous operators in the Schödinger picture E_α by

$$E_\alpha(t) = e^{iH_Et}E_\alpha e^{-iH_Et}\,. \tag{A.8}$$

The Hamiltonian H_{SE} describing a weak interaction between the system and the environment can thus be written in the interaction picture as follows

$$H(t) = \sum_{\alpha,\omega} e^{i\omega t}S_\alpha^\dagger(\omega)\otimes E_\alpha^\dagger(t) = \sum_{\alpha,\omega} e^{-i\omega t}S_\alpha(\omega)\otimes E_\alpha(t)\,. \tag{A.9}$$

Introducing this expression of the interaction Hamiltonian in the interaction picture into

the Redfield equation (A.4) we obtain

$$\begin{aligned}\frac{d}{dt}\rho_S(t) =& -\int_0^\infty tr_E\Big(H(t)H(t-s)\left(\rho_S(t)\otimes\rho_E(0)\right) - H(t-s)\left(\rho_S(t)\otimes\rho_E(0)\right)H(t)\Big)ds + \\ & -\int_0^\infty tr_E\Big(H(t)\left(\rho_S(t)\otimes\rho_E(0)\right)H(t-s) + \left(\rho_S(t)\otimes\rho_E(0)\right)H(t-s)H(t)\Big)ds \\ =& \sum_{\alpha,\beta}\sum_{\omega,\omega'} e^{i(\omega'-\omega)t}\Gamma_{\alpha\beta}\left(\omega\right)\Big(-S_\alpha^\dagger\left(\omega'\right)S_\beta\left(\omega\right)\rho_S(t) + S_\beta\left(\omega\right)\rho_S(t)S_\alpha^\dagger\left(\omega'\right)\Big) + \\ & \sum_{\alpha,\beta}\sum_{\omega,\omega'} e^{i(\omega-\omega')t}\Gamma^*_{\alpha\beta}\left(\omega\right)\Big(+S_\alpha\left(\omega'\right)\rho_S(t)S_\beta^\dagger\left(\omega\right) - \rho_S(t)S_\beta^\dagger\left(\omega\right)S_\alpha\left(\omega'\right)\Big),\end{aligned} \tag{A.10}$$

where have defined the factors

$$\begin{aligned}\Gamma_{\alpha\beta}\left(\omega\right) &= \int_0^\infty e^{i\omega s}\,tr_E\Big(E_\alpha^\dagger\left(t\right)E_\beta\left(t-s\right)\rho_E(0)\Big)ds\,, \\ \Gamma^*_{\alpha\beta}\left(\omega\right) &= \int_0^\infty e^{-i\omega s}\,tr_E\Big(E_\alpha\left(t\right)E_\beta^\dagger\left(t-s\right)\rho_E(0)\Big)ds\,,\end{aligned} \tag{A.11}$$

with $\rho_E(0)$ a stationary state of the environment, thus such that $[H_E,\rho_E(0)]=0$. The environment correlation functions defined as

$$\langle E_\alpha^\dagger\left(t\right)E_\beta\left(t-s\right)\rangle = tr_E\Big(E_\alpha^\dagger\left(t\right)E_\beta\left(t-s\right)\rho_E(0)\Big)\,, \tag{A.12}$$

are homogeneous in time since $\rho_E(0)$ does not change with time

$$\langle E_\alpha^\dagger\left(t\right)E_\beta\left(t-s\right)\rangle = \langle E_\alpha^\dagger\left(s\right)E_\beta\left(0\right)\rangle\,, \tag{A.13}$$

meaning that the quantities $\Gamma_{\alpha\beta}\left(\omega\right)$, $\Gamma^*_{\alpha\beta}\left(\omega\right)$ are time independent.

In equation (A.10) the fast oscillating terms $e^{i(\omega'-\omega)t}$, with $\omega'\neq\omega$, can be neglected under the Markovian approximation, that is for $\tau_S \gg \tau_E$, since they oscillate very rapidly during the typical time scale of the system evolution, which leads to

$$\begin{aligned}\frac{d}{dt}\rho_S(t) =& \sum_{\alpha,\beta}\sum_{\omega}\Gamma_{\alpha\beta}\left(\omega\right)\Big(-S_\alpha^\dagger\left(\omega\right)S_\beta\left(\omega\right)\rho_S(t) + S_\beta\left(\omega\right)\rho_S(t)S_\alpha^\dagger\left(\omega\right)\Big) + \\ & \sum_{\alpha,\beta}\sum_{\omega}\Gamma^*_{\alpha\beta}\left(\omega\right)\Big(+S_\alpha\left(\omega\right)\rho_S(t)S_\beta^\dagger\left(\omega\right) - \rho_S(t)S_\beta^\dagger\left(\omega\right)S_\alpha\left(\omega\right)\Big).\end{aligned} \tag{A.14}$$

We can decompose the operators $\Gamma_{\alpha\beta}\left(\omega\right)$ into real and imaginary parts in the following way

$$\Gamma_{\alpha\beta}\left(\omega\right) = \frac{1}{2}\gamma_{\alpha\beta}\left(\omega\right) + i\eta_{\alpha\beta}\left(\omega\right)\,, \tag{A.15}$$

such that the non Hermitian part is obtained as

$$\eta_{\alpha\beta}\left(\omega\right) = \frac{1}{2i}\left(\Gamma_{\alpha\beta}\left(\omega\right) - \Gamma^*_{\alpha\beta}\left(\omega\right)\right)\,, \tag{A.16}$$

while the Hermitian part is

$$\gamma_{\alpha\beta}(\omega) = \Gamma_{\alpha\beta}(\omega) + \Gamma^{*}_{\alpha\beta}(\omega) \ . \tag{A.17}$$

Using these definitions we can separate the Hermitian part of the dynamics from the non Hermitian part and obtain

$$\frac{d}{dt}\rho_S(t) = -i\left[H_{LS}, \rho_S(t)\right] + \sum_{\alpha,\beta}\sum_{\omega}\gamma_{\alpha\beta}(\omega)\left(S_\beta(\omega)\,\rho_S(t)S^{\dagger}_{\alpha}(\omega) - \frac{1}{2}\{S^{\dagger}_{\alpha}(\omega)\,S_\beta(\omega)\,, \rho_S(t)\}\right), \tag{A.18}$$

known as the first standard form of the Lindblad generator $\mathcal{L}$. The linear superoperator $\mathcal{L}$, named this way since when acting on a operator results in a new operator, is a trace, hermiticity and positivity preserving map. It appear in the superoperator form of the local in time Markovian quantum master equation for the state of the system

$$\frac{d}{dt}\rho_S(t) = \mathcal{L}\rho_S(t)\,. \tag{A.19}$$

The operator

$$H_{LS} = \sum_{\alpha,\beta}\sum_{\omega}\eta_{\alpha\beta}(\omega)\,S^{\dagger}_{\alpha}(\omega)\,S_\beta(\omega)\ , \tag{A.20}$$

is Hermitian and since $[H_{LS}, H_S] = 0$, its role is to renormalize the system energy levels due to system interaction with the environment. This Hamiltonian contribution to the dynamics is known as Lamb shift Hamiltonian. The Schrödinger picture master equation can be obtain from the first standard form by adding the system Hamiltonian H_S to H_{LS}. In addition, it can be shown that the matrices $\gamma_{\alpha\beta}(\omega)$ are always positive meaning that they can be diagonalised by means of an unitary trasformation $\mathcal{U}$ [9]

$$\mathcal{U}\gamma_{\alpha\beta}(\omega)\mathcal{U}^{\dagger} = \begin{pmatrix} d_1(\omega) & 0 & \cdots & 0 \\ 0 & d_2(\omega) & \cdots & 0 \\ 0 & 0 & \ddots & 0 \\ 0 & 0 & \cdots & d_N(\omega) \end{pmatrix}. \tag{A.21}$$

Finally the diagonal form of the master equation is

$$\frac{d}{dt}\rho_S(t) = -i\left[H_S + H_{LS}, \rho_S(t)\right] + \sum_{\alpha,\omega}\left(L_\alpha(\omega)\,\rho_S(t)L^{\dagger}_{\alpha}(\omega) - \frac{1}{2}\left\{L^{\dagger}_{\alpha}(\omega)\,L_\alpha(\omega)\,, \rho_S(t)\right\}\right). \tag{A.22}$$

In some physical systems of interest there will be only one frequency ω that is relevant, so in these cases the quantum master equation can be written as

$$\frac{d}{dt}\rho_S(t) = -i\left[H_S + H_{LS}, \rho_S(t)\right] + \sum_{\alpha}\left(L_\alpha\rho_S(t)L^{\dagger}_{\alpha} - \frac{1}{2}\left\{L^{\dagger}_{\alpha}L_\alpha, \rho_S(t)\right\}\right), \tag{A.23}$$

where the operators L_α are referred to as jump operators. The first term on the right side of the equation describes the coherent part of the evolution, that is the Hamiltonian dynamics, whereas the terms in the sum represent the dissipator of the master equation which encodes the consequences of the existence of the environment and its effect on the system.

The Lindblad superoperator is not Hermitian therefore left and right eingenmatrices do not coincide [52, 56]. In particular, its eigenvalues λ_m are in general complex with $Re(\lambda_m) \leq 0$, with at least one zero eigenvalue $\lambda_0 = 0$. The corresponding right eigenmode to the zero eigenvalue is the stationary state ρ_{ss} of the time evolution

$$\mathcal{L}\rho_{ss} = 0\,, \tag{A.24}$$

while the other eigenmatrices with $Re(\lambda_m) \neq 0$ are decaying modes for which

$$tr\big(\mathcal{L}\rho(t)\big) = tr\Big([H_S + H_{LS}, \rho(t)] + \sum_\alpha \big(L_\alpha \rho(t) L_\alpha^\dagger - \frac{1}{2}\big\{L_\alpha^\dagger L_\alpha, \rho(t)\big\}\big)\Big) = 0\,. \tag{A.25}$$

The statement of the probability conservation is given in terms of the left eigenmatrix associated to the zero eigenvalue $\lambda_0 = 0$,

$$\mathcal{L}^\dagger(\mathbf{1}) = i\,[H_S + H_{LS}, \mathbf{1}] + \sum_\alpha \Big(L_\alpha L_\alpha^\dagger - \frac{1}{2}\big\{L_\alpha^\dagger L_\alpha, \mathbf{1}\big\}\Big) = 0\,, \tag{A.26}$$

where $\mathcal{L}^\dagger$ is the dual of the superoperator $\mathcal{L}$ and $\mathbf{1}$ is the identity operator.

Appendix B

Examples for the Clebsch−Gordan decomposition series

In this appendix we present two explicit examples, one for M odd and one for M even, for the Clebsch−Gordan decomposition series.
For $M = 3$ spin-1/2 systems the series is

$$\begin{aligned}\mathbf{2}^{\otimes 3} &= \bigoplus_{k=0}^{\lfloor 1 \rfloor} \left(\frac{4-2k}{4} \binom{4}{k} \right) (\mathbf{4-2k}) \\ &= 1\,(\mathbf{4}) + 2\,(\mathbf{2})\,,\end{aligned}$$

which means that by composing three spins 1/2 we will obtain one irreducible representation of dimension 4 (i.e., $s_i^2 = 4\ell(\ell+1)$ where $\ell = 3/2$ and $s_i^x = -3, -1, 1, 3$) and one irreducible representation of dimension 2 (i.e., $\ell = 1/2, s_i^x = -1, 1$) with multiplicity 2. In terms of the quantum numbers $(s_i^2, (s_i^x)^2)$ associated to the conserved quantities we will obtain 4 doublets.

When composing $M = 4$ spins 1/2 the decomposition series gives

$$\begin{aligned}\mathbf{2}^{\otimes 4} &= \bigoplus_{k=0}^{\lfloor 2 \rfloor} \left(\frac{5-2k}{5} \binom{5}{k} \right) (\mathbf{5-2k}) \\ &= 1(\mathbf{5}) + 3\,(\mathbf{3}) + 2\,(\mathbf{1}),\end{aligned}$$

one irreducible representation of dimension 5 (i.e., $s_i^2 = 4\ell(\ell+1)$ where $l = 2$ and $s_i^x = -4, -2, 0, 2, 4$), one irreducible representation of dimension 3 (i.e., $\ell = 1, s_i^x = -2, 0, 2$) with multiplicity 3 and one irreducible representation of dimension 1 (i.e., $l = 0, s_i^x = 0$) with multiplicity 2. In terms of the quantum numbers $(s_i^2, (s_i^x)^2)$ associated with the conserved quantities we will obtain 5 doublets and 6 singlets.

Appendix C

Probability for the random transverse field

In appendix B we provided the multiplicities and dimension of all irreducible representations one can obtain when combining M spin 1/2 systems for both M even and M odd cases. Here we want to explicitly write all possible values of $|s_i^x| = M - 2k$ and their multiplicities ν_{M-2k} [*cf.* Eq. (3.25)] for $M = 3$ and $M = 4$.
When composing $M = 3$ spins 1/2 the values that $|s_i^x| = M - 2k$ can assume are $|s_i^x| = 3$ with multiplicity $\nu_3 = 1$ and $|s_i^x| = 1$ with multiplicity $\nu_1 = 3$.
For $M = 4$ the values assumed by $|s_i^x| = M - 2k$ with their multiplicities are $|s_i^x| = 4$ with $\nu_4 = 1$, $|s_i^x| = 2$ with $\nu_2 = 4$ and $|s_i^x| = 0$ with $\nu_0 = 6$. This information allows one to calculate the probability for the random transverse magnetic field. For instance for $M = 3$ [*cf.* Eq. (3.27)]

$$P[h_i = 3\,h] = \frac{1}{4}, \quad P[h_i = h] = \frac{3}{4},$$

there is probability 1/4 to have the value $3h$ and probability 3/4 to have the value h while for $M = 4$

$$P[h_i = 4\,h] = \frac{1}{11}, \quad P[h_i = 2\,h] = \frac{4}{11},$$
$$P[h_i = 0] = \frac{6}{11},$$

there is probability 1/11 to have the value $4h$, 4/11 to have the value $2h$ and 6/11 to have the value 0 for h_i.

Appendix D

Mapping from 1d TFIM to 2D classical Ising model

In this appendix we discuss the mapping between the two-dimensional classical Ising model and the one dimensional quantum transverse field Ising chain. Using the transfer matrix method it can be shown that classical model in the time continuum limit is equivalent to the quantum model [1, 112, 135]. This mapping can be generalized to higher dimensions, that is, D-dimensional classical statistical mechanical models can be mapped into d-dimensional quantum Ising models where $D = d + 1, D > 1$ and vice versa and is the one used in section 4.3. As seen in section 1.1.1 the one-dimensional transverse field Ising model is described by the Hamiltonian

$$H_{\text{TFIM}} = -J \sum_{i=1}^{L} \sigma_i^z \sigma_{i+1}^z - h \sum_{i=1}^{L} \sigma_i^x \,. \tag{D.1}$$

The classical Ising model is defined on a two-dimensional lattice illustrated in figure D.1, where to each site $\vec{n} = (i, l)$ is associated a dynamical variable $s^z(\vec{n}) = \pm 1$ and it has the partition function

$$Z = \sum_{\{s^z(\vec{n})=\pm 1\}} \exp\left(\sum_{i=1}^{N_x} \sum_{l=1}^{N_\tau} \left[K_x s^z(i,l) s^z(i+1,l) + K_\tau s^z(i,l) s^z(i,l+1) \right] \right) , \tag{D.2}$$

where the first sum is over all possible configurations of the spins, the spatial K_x and temporal K_τ coupling constants are different and each site interacts only with nearest neighbors.

Defining the length $L_\tau = M_\tau a = 1/T$, with a the lattice spacing, M_τ the number of sites in the τ direction and T temperature of the quantum model, we can write the quantum partition function of the transverse field Ising model with periodic boundary conditions as a transfer matrix associated with imaginary time evolution over a temporal lattice spacing a

$$Z = \text{Tr}\left(\exp\left(-H_{\text{TFIM}}/T\right)\right) = \text{Tr}\left(\exp\left(-aH_{\text{TFIM}}\right)\right)^{M_\tau} \tag{D.3}$$

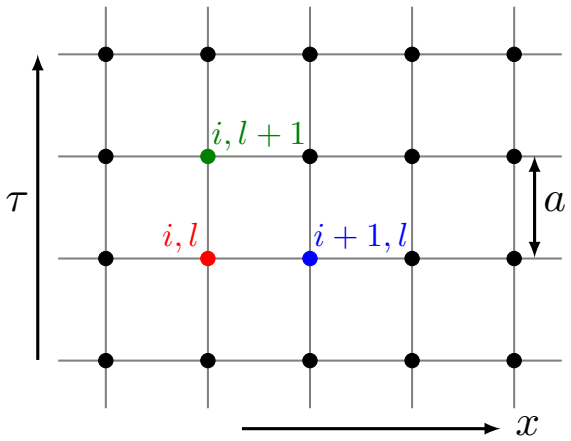


Figure D.1: Schematic of the two-dimensional lattice on which the classical Ising model is defined. The x coordinate is a schematic of the one dimensional direction on which is defined the transverse field Ising model, while the τ direction represents an imaginary time. The operator $e^{-aH_{\text{TFIM}}}$ is the transfer matrix from one row to the next, where a is the lattice spacing. We denote with i the coordinates of a site along the x direction while we denote with l the coordinates along the τ direction.

We are interested in the scaling limit for which $a \to 0$ and $M_\tau \to \infty$ at fixed $M_\tau a = 1/T$. In this limit we can write the above exponential of the transverse field Ising Hamiltonian (using Lie-Trotter product formula [11]) as

$$\exp\left(-aH_{\text{TFIM}}\right) = T_1 T_2 + \mathcal{O}(a^2) \tag{D.4}$$

with

$$T_1 = \exp(ah \sum_{i=1}^{L} \sigma_i^x)\,, \tag{D.5}$$

and

$$T_2 = \exp(aJ \sum_{i=1}^{L} \sigma_i^z \sigma_{i+1}^z)\,. \tag{D.6}$$

By inserting a resolution of the identity $\mathbf{1}$ in the basis of σ_i^z,

$$\mathbf{1} = \sum_{\{\varphi_i\}} |\{\varphi_i\}\rangle \langle\{\varphi_i\}|\,, \quad \sigma_i^z |\{\varphi_i\}\rangle = \varphi_i |\{\varphi_i\}\rangle\,, \quad \varphi_i = \pm 1\,, \tag{D.7}$$

between each $T_1 T_2$ term in (D.3), we transform the transfer operators T_1 and T_2 into transfer matrices. In particular we have

$$T_2 |\{\varphi_i\}\rangle = \exp\left(aJ \sum_{i=1}^{L} \varphi_i \varphi_{i+1}\right) |\{\varphi_i\}\rangle\,, \tag{D.8}$$

since T_2 is diagonal in the σ_i^z basis. We label the M_τ time steps in the partition function (D.3) by the index l and thus we can rewrite it as

$$Z = \sum_{\{\varphi_i(l)\}} \prod_{l=1}^{M_\tau} \langle \{\varphi_i(l)\} | \, T_1 T_2 \, | \{\varphi_i(l+1)\} \rangle \ , \tag{D.9}$$

where we rewrote the states $|\{\varphi_i\}\rangle$ as $|\{\varphi_i(l)\}\rangle$. The transfer operator T_1 is off-diagonal in the σ_i^z basis

$$\langle \{\varphi_i(l)\} | \, T_1 \, | \{\varphi_i(l+1)\} \rangle = \prod_{i=1}^{L} \langle \{\varphi_i(l)\} | \exp\left(ah\sigma_i^x\right) | \{\varphi_i(l+1)\} \rangle \ , \tag{D.10}$$

but we can note that the right side of the above equation consists in a product of terms where the operator σ_i^x acts only on a single Ising subspace at site i thus

$$\langle \varphi | \exp\left(ah\sigma_i^x\right) | \varphi' \rangle = A \exp\left(B\varphi\varphi'\right) \ , \tag{D.11}$$

where $\varphi, \varphi' = \pm 1$ with

$$A^2 = \cosh\left(ah\right) \sinh\left(ah\right) \ , \tag{D.12}$$

and

$$e^{-2B} = \tanh\left(ah\right) \ , \tag{D.13}$$

that leads to

$$Z = \sum_{\{\varphi_i(l)\}} \exp\left(\sum_{i=1}^{L} \sum_{l=1}^{M_\tau} \left[aJ\varphi_i(l)\varphi_{i+1}(l) + B\varphi_i(l)\varphi_i(l+1) \right] \right) . \tag{D.14}$$

In the last step we neglected an overall normalization factor associated with powers of A^{LM_τ}. This partition function has the same structure as the one of the classical model (D.2) with $aJ = K_x$, $B = K_\tau$, $L = N_x$ and $M_\tau = N_\tau$ and is anisotropic as the coupling constants are different in the x and τ directions. This is not an issue since the mapping from the one dimensional quantum Ising model to the two dimensional classical model becomes quantitatively precise at the critical point $J = h$ where the coupling B in the τ direction can be absorbed in a rescaling of the spatial directions.

Bibliography

[1] S. Sachdev, *Quantum Phase Transitions*. Cambridge University Press, 2nd ed., 2011.

[2] S. Suzuki, J.-i. Inoue, and B. K. Chakrabarti, *Quantum Ising Phases and Transitions in Transverse Ising Models*. (Springer-Verlag Berlin Heidelberg, 2nd ed., 2013).

[3] M.-w. Xiao, "Theory of transformation for the diagonalization of quadratic Hamiltonians," *arXiv:0908.0787*, 2009.

[4] E. Lieb, T. Schultz, and D. Mattis, "Two soluble models of an antiferromagnetic chain," *Annals of Physics*, vol. 16, no. 3, pp. 407 – 466, 1961.

[5] Y. He and H. Guo, "The boundary effects of transverse field ising model," *J. Stat. Mech.: Theory Exp.*, vol. 2017, no. 9, p. 093101, 2017.

[6] G. G. Cabrera and R. Jullien, "Role of boundary conditions in the finite-size ising model," *Phys. Rev. B*, vol. 35, pp. 7062–7072, May 1987.

[7] H. A. Kramers and G. H. Wannier, "Statistics of the two-dimensional ferromagnet. part i," *Phys. Rev.*, vol. 60, pp. 252–262, Aug 1941.

[8] J. B. Kogut, "An introduction to lattice gauge theory and spin systems," *Rev. Mod. Phys.*, vol. 51, pp. 659–713, Oct 1979.

[9] H. P. Breuer and F. Petruccione, *The Theory of Open Quantum Systems*. Oxford University Press, 2007.

[10] C. Gardiner and P. Zoller, *Quantum Noise*. Springer-Verlag Berlin Heidelberg, 3rd ed., 2004.

[11] A. Rivas and S. F. Huelga, *Open Quantum Systems*. Springer Berlin Heidelberg, 2012.

[12] G. Lindblad, "On the generators of quantum dynamical semigroups," *Comm. Math. Phys.*, vol. 48, no. 2, pp. 119–130, 1976.

[13] V. Gorini, A. Kossakowski, and E. C. G. Sudarshan, "Completely positive dynamical semigroups of n-level systems," *J. Math. Phys.*, vol. 17, no. 5, pp. 821–825, 1976.

[14] D. Manzano, "A short introduction to the lindblad master equation," *AIP Advances*, vol. 10, no. 2, p. 025106, 2020.

[15] C. A. Brasil, F. F. Fanchini, and R. d. J. Napolitano, "A simple derivation of the Lindblad equation," *Revista Brasileira de Ensino de Física*, vol. 35, pp. 01 – 09, 03 2013.

[16] N. Shibata and H. Katsura, "Dissipative spin chain as a non-hermitian kitaev ladder," *Phys. Rev. B*, vol. 99, p. 174303, May 2019.

[17] B. Derrida and T. Sadhu, "Large deviations conditioned on large deviations ii: Fluctuating hydrodynamics," *Journal of Statistical Physics*, vol. 177, pp. 151–182, Oct 2019.

[18] P. T. Nyawo and H. Touchette, "A minimal model of dynamical phase transition," *EPL*, vol. 116, p. 50009, dec 2016.

[19] A. Budini, "Large deviations of ergodic counting processes: A statistical mechanics approach," *Phys. Rev. E*, vol. 84, p. 011141, July 2011.

[20] R. L. Jack, "Ergodicity and large deviations in physical systems with stochastic dynamics," 2019.

[21] H. Touchette, "The large deviation approach to statistical mechanics," *Phys. Rep.*, vol. 478, no. 1, pp. 1 – 69, 2009.

[22] H. Touchette, "A basic introduction to large deviations: Theory, applications, simulations," 2011.

[23] D. Ruelle, *Thermodynamic Formalism: The Mathematical Structure of Equilibrium Statistical Mechanics*. Cambridge Mathematical Library, Cambridge University Press, 2 ed., 2004.

[24] J. P. Garrahan, R. L. Jack, V. Lecomte, E. Pitard, K. van Duijvendijk, and F. van Wijland, "First-order dynamical phase transition in models of glasses: an approach based on ensembles of histories," *J. Phys. A: Mathematical and General*, vol. 42, p. 075007, jan 2009.

[25] V. Gurarie, "The equivalence between the canonical and microcanonical ensembles when applied to large systems," *American Journal of Physics*, vol. 75, no. 8, pp. 747–751, 2007.

[26] V. Lecomte, C. Appert-Rolland, and F. van Wijland, "Thermodynamic formalism for systems with markov dynamics," *J. Stat. Phys.*, vol. 127, pp. 51–106, Apr 2007.

[27] T. Oakes, S. Powell, C. Castelnovo, A. Lamacraft, and J. P. Garrahan, "Phases of quantum dimers from ensembles of classical stochastic trajectories," *Phys. Rev. B*, vol. 98, p. 064302, Aug 2018.

[28] J. P. Garrahan, "Aspects of non-equilibrium in classical and quantum systems: Slow relaxation and glasses, dynamical large deviations, quantum non-ergodicity, and open quantum dynamics," *Physica A*, vol. 504, pp. 130–154, 2018.

[29] R. Chetrite and H. Touchette, "Nonequilibrium microcanonical and canonical ensembles and their equivalence," *Phys. Rev. Lett.*, vol. 111, p. 120601, Sep 2013.

[30] B. Derrida and T. Sadhu, "Large deviations conditioned on large deviations i: Markov chain and langevin equation," *J. Stat. Phys.*, vol. 176, pp. 773–805, Aug 2019.

[31] N. Tizón-Escamilla, V. Lecomte, and E. Bertin, "Effective driven dynamics for one-dimensional conditioned langevin processes in the weak-noise limit," *J. Stat. Mech.: Theory Exp.*, vol. 2019, p. 013201, jan 2019.

[32] J. Kemp, N. Y. Yao, C. R. Laumann, and P. Fendley, "Long coherence times for edge spins," *J. Stat. Mech.*, vol. 2017, no. 6, p. 063105, 2017.

[33] P. Fendley, "Strong zero modes and eigenstate phase transitions in the xyz/interacting majorana chain," *J. Phys. A: Math. Theor.*, vol. 49, no. 30, p. 30LT01, 2016.

[34] P. Fendley, "Parafermionic edge zero modes in Z_n-invariant spin chains," *J. Stat. Mech.*, vol. 1211, p. P11020, 2012.

[35] S. D. Sarma, M. Freedman, and C. Nayak, "Majorana zero modes and topological quantum computation," *npj Quantum Information*, vol. 1, no. 15001, 2015.

[36] J. Alicea and P. Fendley, "Topological phases with parafermions: Theory and blueprints," *Annu. Rev. Condens. Matter Phys.*, vol. 7, no. 1, pp. 119–139, 2016.

[37] D. V. Else, P. Fendley, J. Kemp, and C. Nayak, "Prethermal strong zero modes and topological qubits," *Phys. Rev. X*, vol. 7, p. 041062, 2017.

[38] L. Mazza, M. Rizzi, M. D. Lukin, and J. I. Cirac, "Robustness of quantum memories based on majorana zero modes," *Phys. Rev. B*, vol. 88, p. 205142, 2013.

[39] S. Bravyi and R. Konig, "Disorder-assisted error correction in majorana chains," *Comm. Math. Phys.*, vol. 316, no. 3, p. 641692, 2012.

[40] M. Ippoliti, M. Rizzi, V. Giovannetti, and L. Mazza, "Quantum memories with zero-energy majorana modes and experimental constraints," *Phys. Rev. A*, vol. 93, p. 062325, 2016.

[41] F. Benatti, F. Carollo, and R. Floreanini, "Dissipative entanglement of quantum spin fluctuations," *J. Math. Phys.*, vol. 57, no. 6, p. 062208, 2016.

[42] M. B. Plenio, S. F. Huelga, A. Beige, and P. L. Knight, "Cavity-loss-induced generation of entangled atoms," *Phys. Rev. A*, vol. 59, pp. 2468–2475, 1999.

[43] D. Braun, "Creation of entanglement by interaction with a common heat bath," *Phys. Rev. Lett.*, vol. 89, p. 277901, 2002.

[44] M. S. Kim, J. Lee, D. Ahn, and P. L. Knight, "Entanglement induced by a single-mode heat environment," *Phys. Rev. A*, vol. 65, p. 040101, 2002.

[45] S. Schneider and G. J. Milburn, "Entanglement in the steady state of a collective-angular-momentum (dicke) model," *Phys. Rev. A*, vol. 65, p. 042107, 2002.

[46] A. M. Basharov, "Decoherence and entanglement in radiative decay of a diatomic system," *J. Exp. Theor. Phys.*, vol. 94, no. 6, pp. 1070–1079, 2002.

[47] L. Jakobczyk, "Entangling two qubits by dissipation," *J. Phys. A: Math. Gen.*, vol. 35, no. 30, p. 6383, 2002.

[48] F. Benatti, R. Floreanini, and M. Piani, "Environment induced entanglement in markovian dissipative dynamics," *Phys. Rev. Lett.*, vol. 91, p. 070402, 2003.

[49] F. Benatti and R. Floreanini, "Entangling oscillators through environment noise," *J. Phys. A: Math. Gen.*, vol. 39, no. 11, p. 2689, 2006.

[50] B. Kraus, H. P. Büchler, S. Diehl, A. Kantian, A. Micheli, and P. Zoller, "Preparation of entangled states by quantum markov processes," *Phys. Rev. A*, vol. 78, p. 042307, 2008.

[51] S. Lieu, D. K. K. Lee, and J. Knolle, "Disorder protected and induced local zero-modes in longer-range kitaev chains," *Phys. Rev. B*, vol. 98, p. 134507, 2018.

[52] J. P. Garrahan, "Aspects of non-equilibrium in classical and quantum systems: Slow relaxation and glasses, dynamical large deviations, quantum non-ergodicity, and open quantum dynamics," *Physica A*, vol. 504, pp. 130 – 154, 2018.

[53] S. Diehl, E. Rico, M. A. Baranov, and P. Zoller, "Topology by dissipation in atomic quantum wires," *Nat. Phys.*, vol. 7, pp. 971–977, 2011.

[54] A. Carmele, M. Heyl, C. Kraus, and M. Dalmonte, "Stretched exponential decay of majorana edge modes in many-body localized kitaev chains under dissipation," *Phys. Rev. B*, vol. 92, p. 195107, 2015.

[55] R. J. Baxter, *Exactly Solved Models in Statistical Mechanics*. Dover Publications, 2008.

[56] M. van Caspel and V. Gritsev, "Symmetry-protected coherent relaxation of open quantum systems," *Phys. Rev. A*, vol. 97, p. 052106, 2018.

[57] B. Buča, J. Tindall, and D. Jaksch, "Non-stationary coherent quantum many-body dynamics through dissipation," *Nat. Commun.*, vol. 10, no. 1, 2019.

[58] C. Beenakker, "Search for majorana fermions in superconductors," *Annu. Rev. Condens. Matter Phys.*, vol. 4, no. 1, pp. 113–136, 2013.

[59] J. Alicea, "New directions in the pursuit of majorana fermions in solid state systems," *Rep. Prog. Phys.*, vol. 75, no. 7, p. 076501, 2012.

[60] F. H. L. Essler, S. Kehrein, S. R. Manmana, and N. J. Robinson, "Quench dynamics in a model with tuneable integrability breaking," *Phys. Rev. B*, vol. 89, p. 165104, Apr 2014.

[61] D. Abanin, W. De Roeck, W. W. Ho, and F. Huveneers, "A rigorous theory of many-body prethermalization for periodically driven and closed quantum systems," *Commun. Math. Phys.*, vol. 354, pp. 809–827, Sep 2017.

[62] H. Kim, M. C. Bañuls, J. I. Cirac, M. B. Hastings, and D. A. Huse, "Slowest local operators in quantum spin chains," *Phys. Rev. E*, vol. 92, p. 012128, Jul 2015.

[63] A. Y. Kitaev, "Unpaired majorana fermions in quantum wires," *Phys.-Uspekhi*, vol. 44, no. 10S, p. 131, 2001.

[64] R. Nandkishore and D. A. Huse, "Many body localization and thermalization in quantum statistical mechanics," *Annu. Rev. Condens. Matter Phys.*, vol. 6, p. 15, June 2015.

[65] D. A. Huse, R. Nandkishore, V. Oganesyan, A. Pal, and S. L. Sondhi, "Localization-protected quantum order," *Phys. Rev. B*, vol. 88, p. 014206, Jul 2013.

[66] B. Bauer and C. Nayak, "Area laws in a many-body localized state and its implications for topological order," *J. Stat. Mech. Theory Exp.*, vol. 2013, no. 09, p. P09005, 2013.

[67] Y. Bahri, R. Vosk, E. Altman, and A. Vishwanath, "Localization and topology protected quantum coherence at the edge of hot matter," *Nat. Commun.*, vol. 6, 2015.

[68] D. Basko, I. Aleiner, and B. Altshuler, "Metal–insulator transition in a weakly interacting many-electron system with localized single-particle states," *Ann. Phys.*, vol. 321, no. 5, pp. 1126 – 1205, 2006.

[69] M. Žnidarič, T. Prosen, and P. Prelovšek, "Many-body localization in the heisenberg xxz magnet in a random field," *Phys. Rev. B*, vol. 77, p. 064426, Feb 2008.

[70] A. Pal and D. A. Huse, "Many-body localization phase transition," *Phys. Rev. B*, vol. 82, p. 174411, Nov 2010.

[71] J. M. Deutsch, "Quantum statistical mechanics in a closed system," *Phys. Rev. A*, vol. 43, pp. 2046–2049, Feb 1991.

[72] M. Srednicki, "Chaos and quantum thermalization," *Phys. Rev. E*, vol. 50, pp. 888–901, Aug 1994.

[73] V. Oganesyan and D. A. Huse, "Localization of interacting fermions at high temperature," *Phys. Rev. B*, vol. 75, p. 155111, Apr 2007.

[74] J. Eisert, M. Friesdorf, and C. Gogolin, "Quantum many-body systems out of equilibrium," *Nat. Phys.*, vol. 11, no. February, p. 7, 2014.

[75] K. Macieszczak, M. Guţă, I. Lesanovsky, and J. P. Garrahan, "Towards a theory of metastability in open quantum dynamics," *Phys. Rev. Lett.*, vol. 116, p. 240404, Jun 2016.

[76] D. C. Rose, K. Macieszczak, I. Lesanovsky, and J. P. Garrahan, "Metastability in an open quantum ising model," *Phys. Rev. E*, vol. 94, p. 052132, Nov 2016.

[77] F. M. Gambetta, F. Carollo, M. Marcuzzi, J. P. Garrahan, and I. Lesanovsky, "Discrete time crystals in the absence of manifest symmetries or disorder in open quantum systems," *Phys. Rev. Lett.*, vol. 122, p. 015701, Jan 2019.

[78] M. McGinley, A. Nunnenkamp, and J. Knolle, "Slow growth of out-of-time-order correlators and entanglement entropy in integrable disordered systems," *Phys. Rev. Lett.*, vol. 122, p. 020603, Jan 2019.

[79] A. Smith, J. Knolle, D. L. Kovrizhin, and R. Moessner, "Disorder-free localization," *Phys. Rev. Lett.*, vol. 118, p. 266601, Jun 2017.

[80] A. Smith, J. Knolle, R. Moessner, and D. L. Kovrizhin, "Dynamical localization in F_2 lattice gauge theories," *Phys. Rev. B*, vol. 97, p. 245137, Jun 2018.

[81] G. Vidal, "Efficient classical simulation of slightly entangled quantum computations," *Phys. Rev. Lett.*, vol. 91, p. 147902, Oct 2003.

[82] G. Vidal, "Efficient simulation of one-dimensional quantum many-body systems," *Phys. Rev. Lett.*, vol. 93, p. 040502, Jul 2004.

[83] G. Vidal, "Classical simulation of infinite-size quantum lattice systems in one spatial dimension," *Phys. Rev. Lett.*, vol. 98, p. 070201, Feb 2007.

[84] R. N. C. Pfeifer, G. Evenbly, S. Singh, and G. Vidal, "NCON: A tensor network contractor for MATLAB," *arXiv:1402.0939*, 2014.

[85] C. Zachos, "Altering the symmetry of wave functions in quantum algebras and supersymmetry," *Mod. Phys. Lett. A*, vol. 07, no. 18, pp. 1595–1600, 1992.

[86] L. M. Vasiloiu, F. Carollo, and J. P. Garrahan, "Enhancing correlation times for edge spins through dissipation," *Phys. Rev. B*, vol. 98, p. 094308, Sep 2018.

[87] D. Chandler, *Introduction to Modern Statistical Mechanics*. Oxford University Press, Oxford, 1987.

[88] J. J. Binney, N. J. Dowrick, A. J. Fisher, and M. Newman, *The Theory of Critical Phenomena: An Introduction to the Renormalization Group*. New York: Oxford University Press, Inc., 1992.

[89] J. Zinn-Justin, *Quantum Field Theory and Critical Phenomena*. Oxford: Clarendon Press, 2002.

[90] C. Pérez-Espigares and P. I. Hurtado, "Sampling rare events across dynamical phase transitions," *Chaos*, vol. 29, no. 8, p. 083106, 2019.

[91] T. Bodineau and B. Derrida, "Distribution of current in nonequilibrium diffusive systems and phase transitions," *Phys. Rev. E*, vol. 72, p. 066110, Dec 2005.

[92] L. Bertini, A. De Sole, D. Gabrielli, G. Jona-Lasinio, and C. Landim, "Current fluctuations in stochastic lattice gases," *Phys. Rev. Lett.*, vol. 94, p. 030601, Jan 2005.

[93] L. Bertini, A. De Sole, D. Gabrielli, G. Jona-Lasinio, and C. Landim, "Macroscopic fluctuation theory," *Rev. Mod. Phys.*, vol. 87, pp. 593–636, Jun 2015.

[94] S. M. Dammer, S. R. Dahmen, and H. Hinrichsen, "Yang-Lee zeros for a nonequilibrium phase transition," *J. Phys. A: Mathematical and General*, vol. 35, pp. 4527–4539, may 2002.

[95] R. Blythe and M. Evans, "The Lee-Yang theory of equilibrium and nonequilibrium phase transitions," *Braz. J. Phys.*, vol. 33, pp. 464 – 475, 09 2003.

[96] M. Merolle, J. P. Garrahan, and D. Chandler, "Space-time thermodynamics of the glass transition," *Proc. Natl. Acad. Sci. USA*, vol. 102, no. 31, p. 10837, 2005.

[97] J. P. Garrahan, R. L. Jack, V. Lecomte, E. Pitard, K. van Duijvendijk, and F. van Wijland, "Dynamical first-order phase transition in kinetically constrained models of glasses," *Phys. Rev. Lett.*, vol. 98, p. 195702, May 2007.

[98] L. O. Hedges, R. L. Jack, J. P. Garrahan, and D. Chandler, "Dynamic order-disorder in atomistic models of structural glass formers," *Science*, vol. 323, no. 5919, p. 1309, 2009.

[99] R. L. Jack and P. Sollich, "Large Deviations and Ensembles of Trajectories in Stochastic Models," *Prog. Theor. Phys. Supp.*, vol. 184, pp. 304–317, 03 2010.

[100] T. Speck, A. Malins, and C. P. Royall, "First-order phase transition in a model glass former: Coupling of local structure and dynamics," *Phys. Rev. Lett.*, vol. 109, no. 19, p. 195703, 2012.

[101] R. L. Jack, I. R. Thompson, and P. Sollich, "Hyperuniformity and phase separation in biased ensembles of trajectories for diffusive systems," *Phys. Rev. Lett.*, vol. 114, p. 060601, Feb 2015.

[102] F. Angeletti and H. Touchette, "Diffusions conditioned on occupation measures," *J. Math. Phys.*, vol. 57, no. 2, p. 023303, 2016.

[103] J. Mehl, T. Speck, and U. Seifert, "Large deviation function for entropy production in driven one-dimensional systems," *Phys. Rev. E*, vol. 78, p. 011123, Jul 2008.

[104] T. Speck, A. Engel, and U. Seifert, "The large deviation function for entropy production: the optimal trajectory and the role of fluctuations," *J. Stat. Mech.: Theory Exp.*, vol. 2012, p. P12001, dec 2012.

[105] K. Proesmans and B. Derrida, "Large-deviation theory for a brownian particle on a ring: a WKB approach," *J. Stat. Mech.: Theory Exp.*, vol. 2019, p. 023201, feb 2019.

[106] M. Newman and C. Moore, "Glassy dynamics and aging in an exactly solvable spin model," *Phys. Rev. E*, vol. 60, no. 5, p. 5068, 1999.

[107] J. P. Garrahan and M. Newman, "Glassiness and constrained dynamics of a short-range nondisordered spin model," *Phys. Rev. E*, vol. 62, pp. 7670–7678, 2000.

[108] J. P. Garrahan, "Glassiness through the emergence of effective dynamical constraints in interacting systems," *J. Phys. Condens. Matter*, vol. 14, pp. 1571–1579, 2002.

[109] R. M. Turner, R. L. Jack, and J. P. Garrahan, "Overlap and activity glass transitions in plaquette spin models with hierarchical dynamics," *Phys. Rev. E*, vol. 92, p. 022115, Aug 2015.

[110] B. Yoshida and A. Kubica, "Quantum criticality from ising model on fractal lattices," *arXiv:1404.6311*, 2014.

[111] T. Devakul, Y. You, F. J. Burnell, and S. L. Sondhi, "Fractal Symmetric Phases of Matter," *SciPost Phys.*, vol. 6, p. 7, 2019.

[112] C. Xu and J. E. Moore, "Strong-weak coupling self-duality in the two-dimensional quantum phase transition of $p+ip$ superconducting arrays," *Phys. Rev. Lett.*, vol. 93, p. 047003, Jul 2004.

[113] O. Martin, A. M. Odlyzko, and S. Wolfram, "Algebraic properties of cellular automata," *Commun. Math. Phys.*, vol. 93, pp. 219–258, Jun 1984.

[114] J. P. Garrahan, "Transition in coupled replicas may not imply a finite-temperature ideal glass transition in glass-forming systems," *Phys. Rev. E*, vol. 89, p. 030301, Mar 2014.

[115] P. G. Bolhuis, D. Chandler, C. Dellago, and P. L. Geissler, "Transition path sampling: Throwing ropes over rough mountain passes, in the dark," *Annu. Rev. Phys. Chem.*, vol. 53, no. 1, pp. 291–318, 2002.

[116] T. Mora, A. M. Walczak, and F. Zamponi, "Transition path sampling algorithm for discrete many-body systems," *Phys. Rev. E*, vol. 85, p. 036710, Mar 2012.

[117] C. Giardina, J. Kurchan, V. Lecomte, and J. Tailleur, "Simulating rare events in dynamical processes," *J. Stat. Phys.*, vol. 145, p. 787, 2011.

[118] D. Jacobson and S. Whitelam, "Direct evaluation of dynamical large-deviation rate functions using a variational ansatz," *Phys. Rev. E*, vol. 100, p. 052139, Nov 2019.

[119] M. C. Bañuls and J. P. Garrahan, "Using matrix product states to study the dynamical large deviations of kinetically constrained models," *Phys. Rev. Lett.*, vol. 123, p. 200601, Nov 2019.

[120] P. Helms, U. Ray, and G. K.-L. Chan, "Dynamical phase behavior of the single- and multi-lane asymmetric simple exclusion process via matrix product states," *Phys. Rev. E*, vol. 100, p. 022101, Aug 2019.

[121] U. Ray, G. K.-L. Chan, and D. T. Limmer, "Importance sampling large deviations in nonequilibrium steady states. i," *J. Chem. Phys.*, vol. 148, no. 12, p. 124120, 2018.

[122] U. Ray, G. K.-L. Chan, and D. T. Limmer, "Exact fluctuations of nonequilibrium steady states from approximate auxiliary dynamics," *Phys. Rev. Lett.*, vol. 120, p. 210602, May 2018.

[123] T. Nemoto, F. Bouchet, R. L. Jack, and V. Lecomte, "Population-dynamics method with a multicanonical feedback control," *Phys. Rev. E*, vol. 93, p. 062123, Jun 2016.

[124] K. Klymko, P. L. Geissler, J. P. Garrahan, and S. Whitelam, "Rare behavior of growth processes via umbrella sampling of trajectories," *Phys. Rev. E*, vol. 97, p. 032123, Mar 2018.

[125] R. Chetrite and H. Touchette, "Nonequilibrium markov processes conditioned on large deviations," in *Annales Henri Poincaré*, vol. 16, pp. 2005–2057, Springer, 2015.

[126] F. Carollo, J. P. Garrahan, I. Lesanovsky, and C. Pérez-Espigares, "Making rare events typical in markovian open quantum systems," *Phys. Rev. A*, vol. 98, p. 010103, Jul 2018.

[127] M. R. Shirts and J. D. Chodera, "Statistically optimal analysis of samples from multiple equilibrium states," *J. Chem. Phys.*, vol. 129, no. 12, p. 124105, 2008.

[128] C. H. Bennett, "Efficient estimation of free energy differences from monte carlo data," *J. Comput. Phys.*, vol. 22, no. 2, pp. 245 – 268, 1976.

[129] R. M. Nandkishore and M. Hermele, "Fractons," *Annu. Rev. Condens. Matter Phys.*, vol. 10, no. 1, pp. 295–313, 2019.

[130] J. G. Bohnet, B. C. Sawyer, J. W. Britton, M. L. Wall, A. M. Rey, M. Foss-Feig, and J. J. Bollinger, "Quantum spin dynamics and entanglement generation with hundreds of trapped ions," *Science*, vol. 352, no. 6291, pp. 1297–1301, 2016.

[131] K. Kim, S. Korenblit, R. Islam, E. E. Edwards, M.-S. Chang, C. Noh, H. Carmichael, G.-D. Lin, L.-M. Duan, C. C. J. Wang, J. K. Freericks, and C. Monroe, "Quantum simulation of the transverse ising model with trapped ions," *New J. Phys.*, vol. 13, no. 10, p. 105003, 2011.

[132] P. Schauss, M. Cheneau, M. Endres, T. Fukuhara, S. Hild, A. Omran, T. Pohl, C. Gross, S. Kuhr, and I. Bloch, "Observation of spatially ordered structures in a two-dimensional rydberg gas," *Nature*, vol. 491, no. 7422, pp. 87–91, 2012.

[133] H. Bernien, S. Schwartz, A. Keesling, H. Levine, A. Omran, H. Pichler, S. Choi, A. S. Zibrov, M. Endres, M. Greiner, V. Vuletić, and M. D. Lukin, "Probing many-body dynamics on a 51-atom quantum simulator," *Nature*, vol. 551, pp. 579–584, 2017.

[134] H. Labuhn, D. Barredo, S. Ravets, S. de Léséleuc, T. Macrì, T. Lahaye, and A. Browaeys, "Tunable two-dimensional arrays of single Rydberg atoms for realizing quantum Ising models," *Nature*, vol. 534, pp. 667–670, 2016.

[135] T. D. Schultz, D. C. Mattis, and E. H. Lieb, "Two-dimensional ising model as a soluble problem of many fermions," *Rev. Mod. Phys.*, vol. 36, pp. 856–871, Jul 1964.